THE KINEMATIC STRUCTURE OF A PREFRONTAL CONVECTIVE RAINBAND REVEALED BY TAMEX DOPPLER RADAR DATA

Michael Joseph Miglioranzi, BS

A Thesis Presented to the Faculty of the
Graduate School of Saint Louis University in
Partial Fulfillment of the Requirements for the
Degree of Master of Science (Research)

1992

128pk

REPORT DOCUMENTATION PAGE

Form Approved
OMB No. 0704-0188

1. AGENCY USE ONLY *(Leave blank)*

2. REPORT DATE
1992

3. REPORT TYPE AND DATES COVERED
THESIS/~~DISSERTATION~~

4. TITLE AND SUBTITLE
The Kinematic Structure of a Prefrontal Convective Rainband Revealed by Tamex Doppler Radar Data

5. FUNDING NUMBERS

6. AUTHOR(S)
Michael Joseph Miglioranzi, Captain

7. PERFORMING ORGANIZATION NAME(S) AND ADDRESS(ES)
AFIT Student Attending: St. Louis University

8. PERFORMING ORGANIZATION REPORT NUMBER
AFIT/CI/CIA-92-107

9. SPONSORING/MONITORING AGENCY NAME(S) AND ADDRESS(ES)
AFIT/CI
Wright-Patterson AFB OH 45433-6583

10. SPONSORING/MONITORING AGENCY REPORT NUMBER

11. SUPPLEMENTARY NOTES

12a. DISTRIBUTION/AVAILABILITY STATEMENT
Approved for Public Release IAW 190-1
Distributed Unlimited
ERNEST A. HAYGOOD, Captain, USAF
Executive Officer

12b. DISTRIBUTION CODE

13. ABSTRACT *(Maximum 200 words)*

14. SUBJECT TERMS

15. NUMBER OF PAGES
110

16. PRICE CODE

17. SECURITY CLASSIFICATION OF REPORT

18. SECURITY CLASSIFICATION OF THIS PAGE

19. SECURITY CLASSIFICATION OF ABSTRACT

20. LIMITATION OF ABSTRACT

THE KINEMATIC STRUCTURE OF A PREFRONTAL CONVECTIVE RAINBAND REVEALED BY TAMEX DOPPLER RADAR DATA

Michael Joseph Miglioranzi, BS

A Digest Presented to the Faculty of the
Graduate School of Saint Louis University in
Partial Fulfillment of the Requirements for the
Degree of Master of Science (Research)

1992

DIGEST

In this study, the kinematic features of a subtropical convective rainband in association with the Mei-Yu front on 25 June 1987 over northern Taiwan is investigated. This front caused heavy rainfall due to its slow movement (2.5 m s^{-1}) and orientation. CP-4 Doppler radar was used to collect information about this storm during TAMEX IOP-13. Fields of reflectivity, winds, radial velocity, vertical velocity, and divergence are displayed over six time periods during a 40-minute time span.

Results show that the depth of the cool air associated with the Mei-Yu front is less than 2.2 km in depth. The front moved very slowly and its orientation (ENE) caused increased low-level convergence due to the N-S orientation of the Central Mountain Range in Taiwan. The convection in the warm sector ahead of the front was moderate within a broad area ahead of the front. A narrow, weak line of stratiform precipitation was found nearly parallel to the front in the postfrontal area. The low-level southwest monsoon advected warm, moist air into the region. The cells grew in this unstable environment ahead of the front. Mid-level northwest winds caused the elongation of the convective cells to the southeast where the precipitation fell, but allowed the continued growth of new cells. Precipitation at the surface caused a strong region of divergence which in turn created areas of convergence that created upward vertical motion and allowed the growth of new cells along the

periphery.

A comparison of single-Doppler radar versus dual-Doppler radar analysis revealed that the simplified continuity equation can be used to obtain realistic vertical velocities of this quasi two-dimensional convective rainband.

THE KINEMATIC STRUCTURE OF A PREFRONTAL CONVECTIVE RAINBAND REVEALED BY TAMEX DOPPLER RADAR DATA

Michael Joseph Miglioranzi, BS

A Thesis Presented to the Faculty of the
Graduate School of Saint Louis University in
Partial Fulfillment of the Requirements for the
Degree of Master of Science (Research)

1992

COMMITTEE IN CHARGE OF CANDIDACY:

Professor Yeong-Jer Lin,
Chairperson and Advisor

Associate Professor Robert W. Pasken

Associate Professor James T. Moore

ACKNOWLEDMENTS

I would like to express my deepest appreciation to my advisor Dr. Yeong-Jer Lin for his support, guidance, and encouragement throughout the completion of this thesis. I would also like to thank Dr. Robert W. Pasken for his development of software, expertise, and patience in helping me with this project. Many thanks to Dr. James T. Moore for assistance, suggestions, and friendship while attending St. Louis University. Also, special thanks to the United States Air Force for allowing me to pursue this challenging degree.

I would like to acknowledge the help of fellow students and friends to include Tim Lambert, Tim Hutchison, Chris Buonanno, Sepi Yalda, Hsiu-Wu Chang, Andrea Hardy, and Pam Heinselman. I would like to thank my parents for their neverending support. A final thanks go to my wife Julie and son Anthony for their patience, support, and understanding that enabled me to work on and complete this degree.

TABLE OF CONTENTS

LIST OF TABLES

LIST OF FIGURES

Figure Page

Chapter 1: Introduction

Flash floods and heavy rain in Taiwan are a serious concern to that country. Three rainfall events between 1981 and 1984 caused $400-600 million each in property damage to this rapidly growing country (Chen and Kuo, 1991). In 1982, the National Science Council (NSC) of the Republic of China in Taiwan realized that heavy rain was damaging the economic growth of their country. The NSC established the Multiple Mitigation Hazards Project in light of the flooding rains that occurred mainly in late spring and early summer. A subprogram called the Meteorological Hazards Mitigation was developed to improve heavy precipitation forecasting. From this program the Taiwan Area Mesoscale Experiment or TAMEX was borne to study and learn about the mesoscale processes that cause heavy rain (Kuo and Chen, 1990).

One of the most active monsoons in the world is found in subtropical East Asia. The north Asian continent is a source for cold, dry northeasterly air in the winter. While in the summer, a warm, moist southwesterly monsoon dominates the region (Chen and Kuo, 1990). In between these times of the year a transition takes place in late spring and early summer when a front forms between a Mongolian high to the north and the Pacific high to the south (Chen, 1977).

This front, known as the Mei-Yu front, is a climatic phenomenon found over southeast China, Taiwan, and Japan (Chen, 1983). The Mei-Yu front is seen on weather maps as a quasi-stationary front with long stratiform cloud bands, up to 1000's of kilometers in length, containing embedded thunderstorms. This front moves north or south according to the strength and position of the subtropical Pacific high (Tao and Ding, 1981).

Within these large cloud bands, mesoscale convective systems (MCSs) are found to travel from west to east, interacting with the topography of Taiwan to produce dangerous rainfall amounts (Kuo and Chen, 1990). Due to a lack of mesoscale observations, the Mei-Yu front has not been well understood.

TAMEX was a very successful field operation that began on 1 May and ended on 29 June 1987 and included thirteen Intensive Observing Periods (IOPs) or periods of increased frequency of observations due to a meteorological phenomenon. Scientists from both Taiwan and the United States monitored an array of meteorological instruments and observing sites that included: 1) 12 rawinsonde sites; 2) 10 pibal sites; 3) 75 surface stations; 4) 126 rain guages; 5) 21 wind towers; 6) three research ships; 7) three Doppler radars and five conventional radars; 8) one satellite station that received information from three meteorological satellites-GMS-3, NOAA-9, and NOAA-10, and 9) one P-3 research aircraft (Kuo and Chen, 1990).

The information gathered has been used to study the following three objectives (Kuo and Chen, 1990):

(1) Mesoscale circulation associated with the Mei-Yu front.

(2) Evolution of the MCSs in the vicinity of the Mei-Yu front, and

(3) Effects of orography on the Mei-Yu front and on MCSs.

This study will take an in-depth look at the prefrontal convective rainband that passed through northern Taiwan during IOP-13 on 24-25 June 1987. This rainband was the result of a Mei-Yu front that slowly moved through Taiwan in an east-northeasterly (ENE) through west-southwesterly (WSW) alignment. This storm dropped the heaviest amount of precipitation on Taiwan during the entire TAMEX period.

The Mei-Yu front is a unique weather system with many different factors affecting its performance. Notice that Taiwan is surrounded by water and has the north-south aligned Central Mountain Range (CMR) that splits the island into two sections (Fig. 1.1). The body of water and mountains both play a major role in determining the Taiwan weather.

Chen and Chi (1980) analyzed eight years of Mei-Yu fronts from 15 May to 15 June and found that they formed in southeast China and usually were slow-moving and produced heavy rain. Ninety-five percent of these fronts affected the weather in Taiwan. Chen and Tsay (1978) concluded that the Mei-Yu front

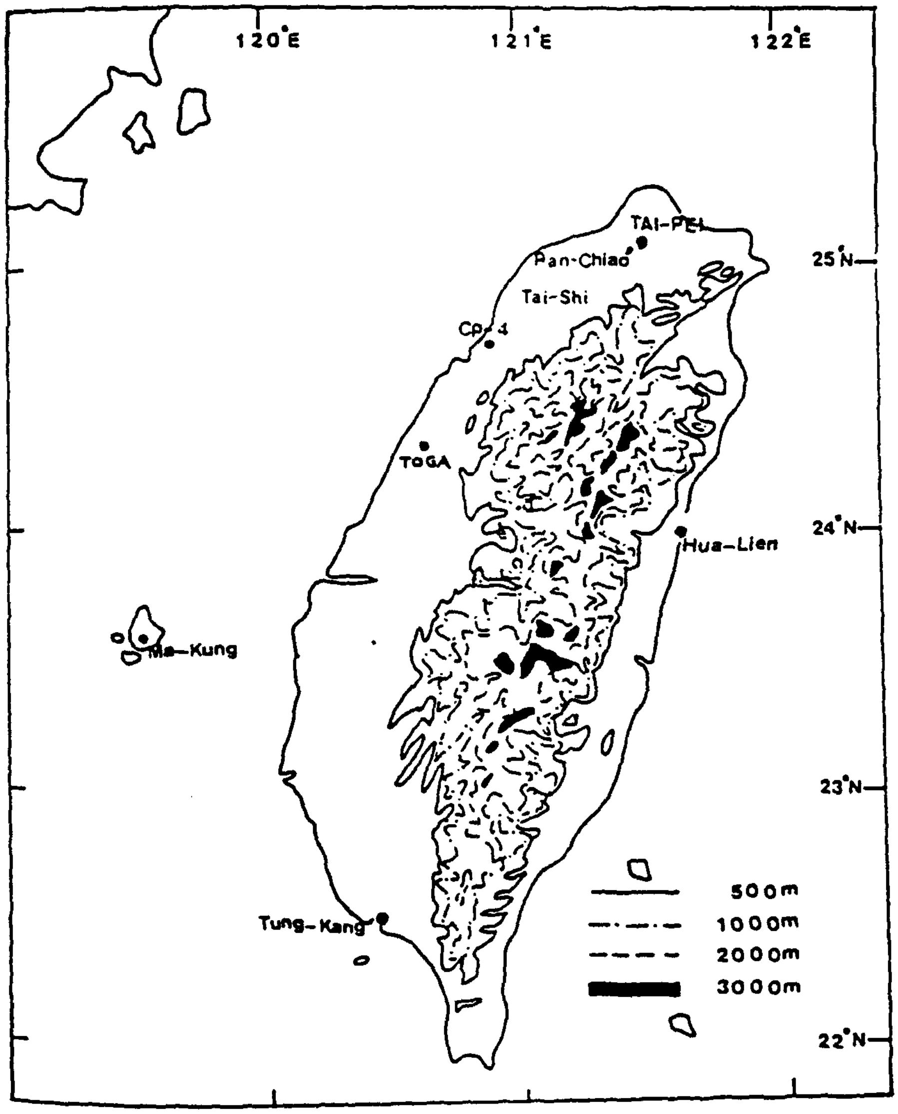

Fig. 1.1 Topography of Taiwan. Units are in meters (adopted from Trier, Parsons, and Matejka, 1990).

generally had low-level convergence and vorticity, weak temperature contrast, and weak baroclinicity associated with it. The only major contrast was in the moisture field across the front.

The CMR plays an important role in moderating weather systems as they pass through Taiwan. The CMR can split the front into two sections, one to the east of the mountains, and the other to the west (Chen, 1978; Wang, 1986; etc.). The eastern segment of the split front moves much faster than the western segment. Chen (1978, 1980) discovered that mesolows form in the northwest due to the CMR. Chen (1978) concluded that higher rainfall values occurred on the windward side of the mountain compared to the leeward side. Bell and Bosart (1988) and Forbes et al. (1987) discussed an interesting analogy between the CMR and eastern United States Appalachian Mountains. They concluded that strong ridging behind the cold air due to the blocking effects of the mountains on the east side of the CMR is similar to the cold air damming on the eastern slopes of the Appalachian Mountains.

Mannouji and Kurihara (1990) performed a numerical experiment to study the CMR presence by employing the limited area spectral model of the Japan Meteorological Agency. Using data from IOP-13, the experiment was run twice: once using a model with a simulated mountain height of 1859 meters; the other time using a model with the entire height of Taiwan equal to ten meters. Results show that the model with mountains causes the following:

1) precipitation area shifts 90 km further north;

2) rainfall amount increases 200-300% more than with no CMR;

3) mountains cause a non-continuous wind shear line across Taiwan, and

4) mesolow occurred in southeastern Taiwan. Further CMR results will follow when other TAMEX IOPs are discussed.

A low-level jet (LLJ) has been found to be another contributor or piece of the puzzle that leads to heavy precipitation. Chen and Yu (1988) studied 35 cases of the Mei-Yu heavy rain events for the months of May and June over 20 years in time. The findings point out that there is an 84% chance of a 700 mb LLJ with speeds equal to or greater than 12.5 m s^{-1} at least 12 hours before a rainfall event. From 1980-84 studies, Chen and Yu (1988) discovered that when a LLJ was in place, there was a 91% chance that it was raining or that rain would fall within 24 hours. Finally, they noticed a startling decrease in frequency and intensity of the LLJ over an area that had a heavy rainfall previously.

From observational studies by Chen and Chang (1980) and Tsay and Chen (1980), and numerical studies by Kuo and Anthes (1982), showed that latent heat release is important to maintain the front. South of the front there is a convectively unstable environment (decreasing θ_e with height) that enables MCSs to thrive and develop.

Since MCSs are found within the front, a discussion about its characteristics is needed. Houze et al. (1989) described the typical MCS to be from tens of kilometers to hundreds of kilometers horizontally at maturity with lifetimes averaging 3-12 hours. Convective cells and lines occur within the MCS with a horizontal scale from 1-50 kilometers.

Lin and Lin (1990) discussed some characteristics of MCS formation and dissipation during IOPs 1,2, and 8. They concluded that MCS development occurred when destabilization due to differential temperature advection caused a steepening temperature lapse rate. During IOP-2, a developing MCS area was found under a strong low-level warm advection field. Conversely, weak or cold advection field, such as in IOP-1, can slow down or destroy an MCS. They also found that mature MCSs generally experienced convergence at lower levels with upper level divergence, as in IOP-8. IOP-1 dynamics included weak low-level convergence and weak upper level divergence that led to the deterioration of the MCS. The vertical motion field showed strong upward vertical motion and large vertical extent over a developing MCS. Upward vertical motion became weak with a decrease in vertical extent over a mature MCS.

Moisture is also an important factor for MCS development. Frank (1978) found large-scale convergence precedes MCS formation causing an accumulation of mid-level moisture. This allowed convection to survive even when entrainment tended to dry up the atmosphere.

During the Mei-Yu season high moisture air is usually readily available, but Lin and Lin (1990) note that the MCS strengthened with increasing moisture flux convergence. The moisture flux convergence at 850 mb of 20-30 g kg^{-1} per day was reasonable for a developing MCS in IOP-2. On the other hand in IOP-1, there was moisture flux divergence and the MCS dissipated.

With the rich TAMEX data sets available, numerous studies of Mei-Yu fronts were undertaken. The following paragraphs discuss three specific IOP case studies. In IOP-2 a fast-moving squall line, orientated almost north-south, moved through Taiwan. The study by Wang et al. (1990) found that the squall line noticeably weakened as it encountered the CMR. The subtropical squall line in IOP-2 had similar features and environmental conditions to that of a fast-moving tropical squall line. The LLJ provided necessary strong shear. Many convective cells were seen to be embedded within the squall line. Convective downdrafts to the rear of the main updrafts were needed to carry cooler, mid-tropospheric air into lower layers. This negatively buoyant air from the rear flowed forward to collide with advancing high θ_e air to start the growth of new convective cells.

Further results of IOP-2 from Lin et al. (1990) show that convective updrafts were warmed by latent heat releases due to condensation, while convective downdrafts were cooled by evaporation. Precipitation loading increased the density of the downdraft air in the high reflectivity areas. The subtropical squall line continued to survive due to the connection of the cells cold outflow at the surface and low-level shear. Finally, the horizontal and vertical flux convergence (divergence) of horizontal momentum due to the mean and eddy motions contribute largely to the growth (decay) of the mean horizontal momentum.

IOP-8 was characterized by subtropical cold front advancing into Taiwan. The LLJ at 800 mb was southwest at 15 m s^{-1}. Moist environmental conditions prevailed in the boundary layer (BL) causing a 14 m s^{-1} vertical wind shear normal to the axis of convection (Trier and Parsons, 1990). Trier et al. (1990) performed an in-depth study of this front and concluded that the Mei-Yu front was 1-2 km in depth, moderately baroclinic with a 5-7^{o}C temperature contrast across the front, and a 3-4^{o}C moisture contrast. Doppler radar analysis of radial velocity revealed a structure similar to a density current at the leading edge of a shallow front.

The density current front can be identified by the following three phenomena: 1) wind shift occurring on the scale of one kilometer; 2) a convergent zone at the leading edge, and 3) a steep frontal slope with height followed by a horizontal frontal surface (Trier et al., 1990).

It was further noted that the warming of the BL was due to upward sensible heat flux as the front passed over the warm ocean surface, in turn reducing the temperature contrast across the front by 60-70% over the length (400 km) of the island (Trier et al., 1990).

Trier et al. (1990) also described the effects of the CMR on the synoptic conditions. The CMR decelerated the low level prefrontal westerlies, splitting the flow around the island. Shallow cold air associated with the front (1-2 km) never reached the higher elevations of central Taiwan in the CMR. The west coast of Taiwan had convection due to the lifting of moist air by the slope of topography and the southwesterly advection of moist, warm air due to the LLJ. The east coast rain was suppressed due to the CMR causing subsidence warming and drying of the air due to downslope flow, stabilizing the environment. The CMR also blocked the moist and unstable low-level southwesterly flow.

Randomly scattered precipitation distribution was related to regional variations of stability across Taiwan. These variations were due to the large scale advection of an unstable tropical air mass, terrain, and a low level wind maximum or LLJ (Trier et al., 1990).

Numerous studies have been performed on the situation that evolved on 24-25 June 1987 during IOP-13. Unlike IOP-2, where the convective rainband was aligned N-S with a fast-moving squall line that quickly weakened as it encountered the CMR, the slow-moving prefrontal convective rainband in IOP-13 was aligned ENE-WSW. This storm was the largest precipitation producer during TAMEX (Chi and Scofield, 1991) and was monitored successfully by three Doppler radars during its lifetime.

Lin, Pasken, and Chang (1992) studied IOP-13 using dual-Doppler radar and concluded that the cold air depth associated with the Mei-Yu front was approximately two kilometers. The Mei-Yu front was responsible for initiating and maintaining the convective rainband ahead of it. The deep, but moderate convection in a large area ahead of the front had vertical velocities < 10 m s^{-1}, while shallow, weak convection behind the front had vertical velocities < 4 m s^{-1}. Precipitation in the warm sector was widespread, but not intense with maximum reflectivities < 40 dBZ. The heavy rain on the northwest coast of Taiwan was due to the slow system movement, not the system intensity.

Lin et al. (1991) noted the alignment of this storm enhanced the low-level convergence of the southwest monsoon air ahead of the front. The potentially unstable air was forced upward by the slope of the CMR on the western side of the island creating an environment ideal for heavy rainfall. The LLJ during IOP-13 provided the warm, moist air at low-levels to maintain an unstable atmosphere, and sustained horizontal and vertical wind shears near the front (Jou and Deng, 1990).

Further studies by Jou and Deng (1991) using dual-Doppler radar showed that the LLJ was the main trigger for convection. The physical mechanism to maintain and organize convection along the Mei-Yu front can be tied into the deflection of the LLJ by prefrontal downward motions due to convection. In turn, these downward motions produce convergence of momentum, heat, and moisture along the front. This convergence then produced more convective activity, enhancing the intensity of convective downward motions.

Other studies on pre-frontal convective rainbands have been done in the past using Doppler radars. For instance, Browning and Harrold (1970) used single-Doppler radar to study a cold front over the British Isles. Results were interesting due to the fact that many of the environmental conditions were similar to the atmosphere in IOP-13. There was a tongue of warm air ahead of the surface cold front along with a LLJ parallel to the front in the warm sector with speeds of 25-30 knots at a height of one kilometer. However, there was strong convergence of 10^{-2} s^{-1} at low levels near the surface providing the forced lifting that led to a convection line that was two-dimensional and steady state. Carbone (1982) studied a severe frontal rainband in California with the aid of three Doppler radars. The results were similar to Browning and Harrold (1970).

This study will explore the kinematics of the pre-frontal rainband during IOP-13 using single-Doppler radar. In essence, this study extends the analysis done by Pasken and Lin (1991).

Chapter 2. Statement of the Problem

The purpose of this study is to describe the kinematic structure of a pre-frontal convective rainband that moved through northern Taiwan on 25 June 1987 during TAMEX IOP-13. This event was closely monitored by numerous meteorological instruments including Doppler radars.

This particular rainband was associated with an MCS embedded in a Mei-Yu frontal cloud band. These bands pass through Taiwan in late spring and early summer producing copious rainfall amounts that can lead to flash flooding causing millions of dollars in damage. The pre-frontal rainband in IOP-13 caused the most serious flooding during the life-span of TAMEX.

With the aid of the intensive observing network, a better understanding of MCSs and the Mei-Yu front may be obtained through research to aid in forecasting these potentially life-threatening events.

During IOP-13 the pre-frontal rainband was orientated west-southwest through east-northeast while moving very slowly to the south. Those two characteristics allowed the MCS to thrive in an unstable environment. Also, frontal alignment ensured low-level convergence and interaction with the CMP.

The environmental conditions will be examined to explain the heavy rainfall. The kinematic structure of the prefrontal convective rainband will be explored. Single-Doppler radar analysis will be used to recover features of the rainband and compared to a dual-Doppler radar analysis. Also, we wish to test whether vertical velocities can be extracted using the simplified continuity equation.

Chapter 3: Weather Conditions

Intensive Observing Period 13 (IOP-13) began at 22 LST 24 June 1987 and lasted for 25 hours. The following section points out in detail satellite and radar depictions, surface observations at three sites, upper air soundings at two stations, and the resultant observed rainfall amounts after passage of the front.

3.1 Surface Maps and Upper Air Charts

Surface maps (Fig. 3.1) for 2000 LST 24 June and 0600 LST 25 June are present in Fig. 3.1. At 2000 LST (Fig. 3.1a), a surface low pressure (996 mb) centered 65 km northeast of northern Taiwan. A trailing cold front nearly aligned east-west was poised to enter northern Taiwan. Prefrontal surface winds were predominantly southwest with a maximum of 15 m s^{-1} just east of Taiwan advecting warm, moist air into the region.

Twelve hours later (Fig. 3.1b), the upper-level low deepened at 500 mb and moved east while the trailing cold front split into two parts. The eastern portion of the front was found in the southern most part of Taiwan, while the western frontal portion became quasi-stationary over northern Taiwan. This result is backed up by findings from Chen (1978) and Wang (1986) that the eastern segment of the front, after splitting, moves at a much faster speed than the western segment.

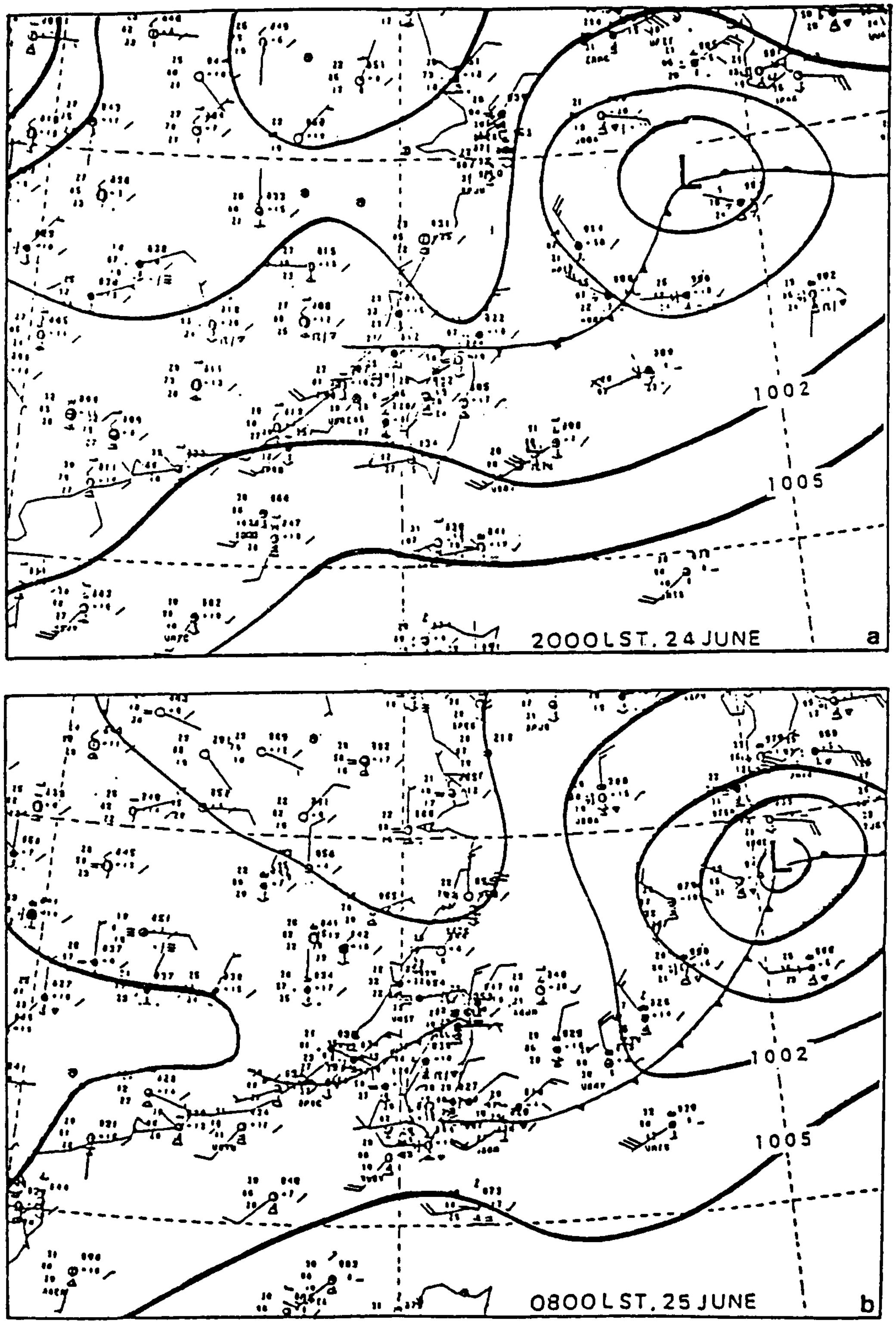

Fig. 3.1 Surface maps at (a) 20 LST (12 UTC) 24 June and (b) 08 LST (00 UTC) 25 June 1987.

Figure 3.2 shows the successive positions of the cold front from 08 LST (00 UTC) 24 June to 14 LST (08 UTC) 25 June. It is quite evident of the split in the Mei-Yu front due to the CMR (Jou and Deng, 1990).

The 850, 700, 500, and 250 mb charts (Fig. 3.3) for 20 LST (12 UTC) depict a vertically stacked low pressure system at 31^{o} N, 132^{o} E. At 850 mb the low-level jet is present over northern Taiwan with a speed of 15 m s^{-1} from the southwest continuing to advect warm, moist air into the region. The winds veer with height, a sign of large-scale warm air advection. The winds at 700 mb were roughly westerly at 18 m s^{-1}. At 500 mb, the winds decreased in strength to 12.5 m s^{-1}. The 200 mb winds were now northerly at 12-15 m s^{-1} with diffluence over a broad region south and west of Taiwan as noted by the flow.

Twelve hours later (Fig. 3.4), the upper-level low had slightly deepened at 500 mb and moved east. The winds at 850 mb decreased to 12.5 m s^{-1} and were more westerly. At 700 mb the winds increased to 20 m s^{-1} and speed divergence was occurring over northern Taiwan. Winds at 500 mb were stronger at 15 m s^{-1} from the northwest. The 200 mb winds had slowed by 2.5 m s^{-1} from the previous time period and wind directional diffluence was still in place over Taiwan resulted from numerous factors to include: An unstable environment; low-level convergence; upper-level divergence; a low-level moist environment, dry air aloft, and the veering of winds with

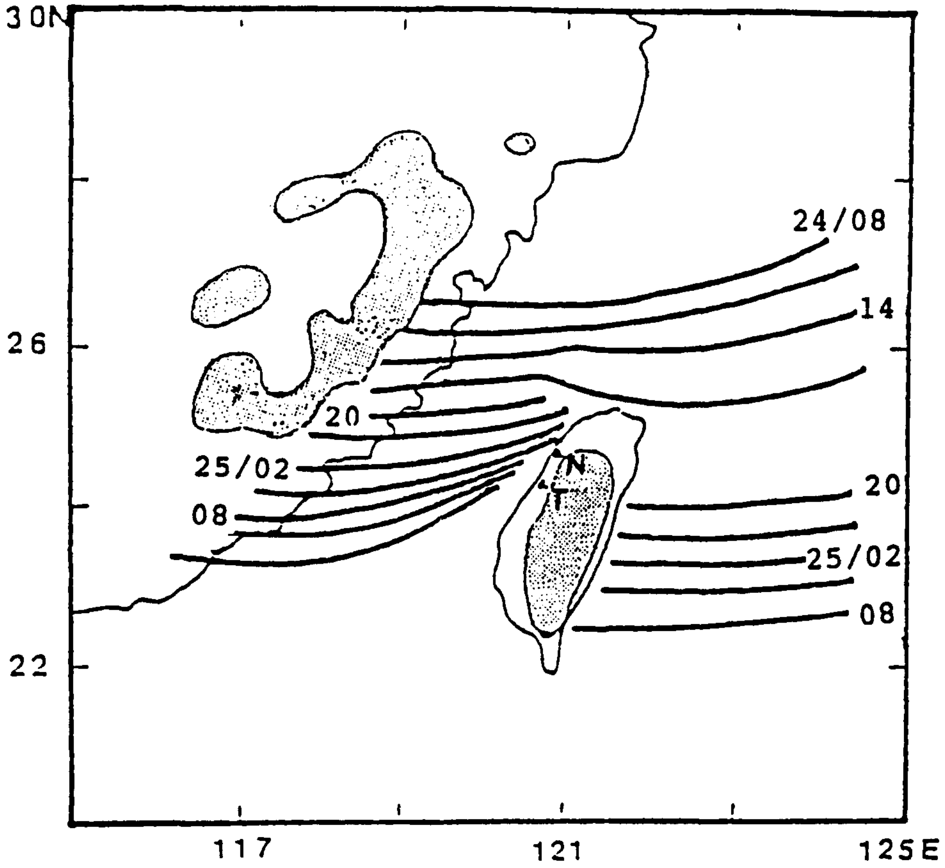

Fig. 3.2 The successive positions of the surface cold front from 08 LST (00 UTC) 24 June to 14 LST (06 UTC) 25 June 1987. Intervals are every 3 hours. Topography above 600 meters is shaded and locations of CP-4 (N) and TOGA (T) are shown (after Jou and Deng, 1990), except all times in LST.

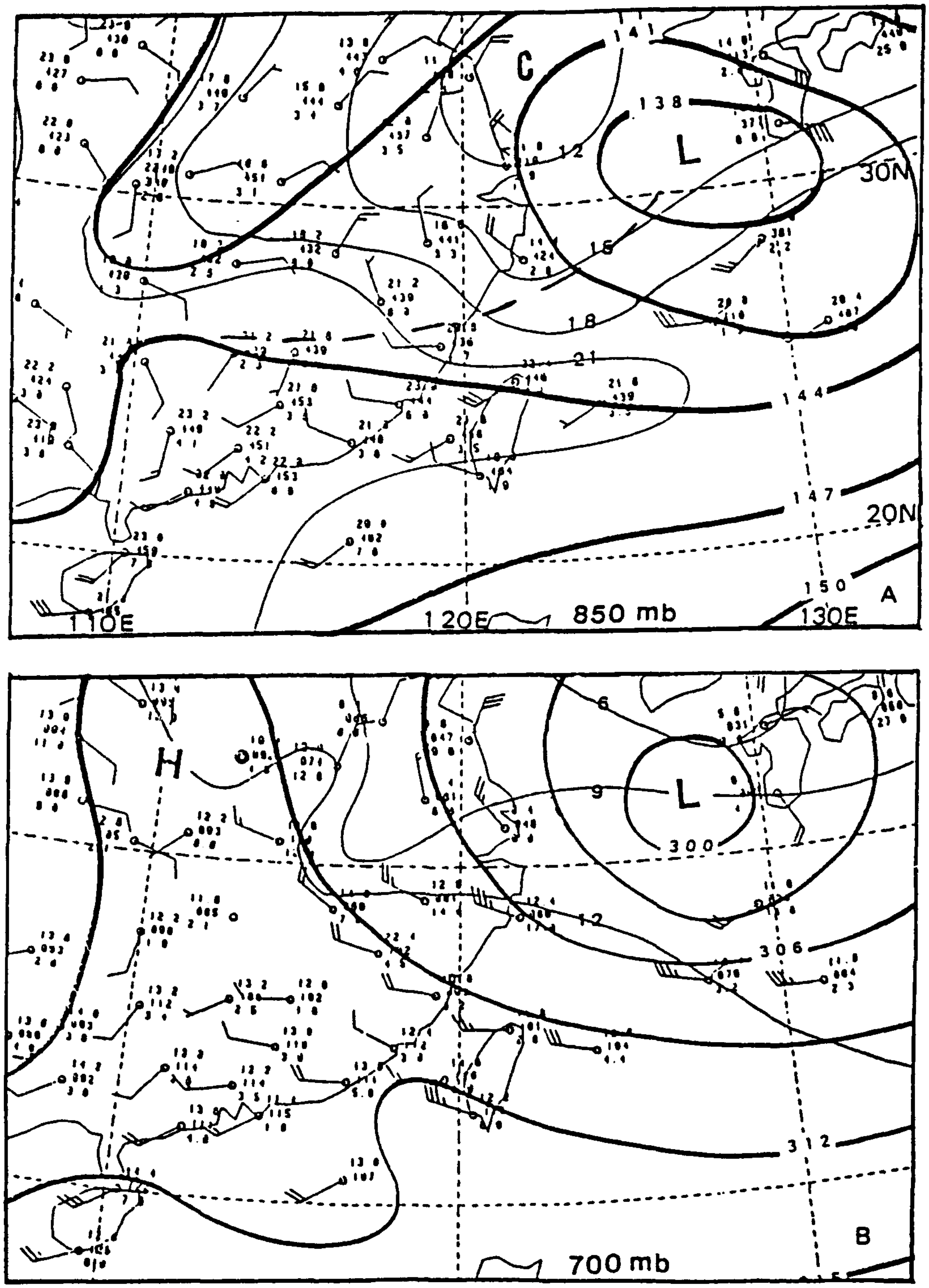

Fig. 3.3 The upper air charts at (a) 850 and (b) 700 mb for 20 LST (12 UTC) 24 June 1987.

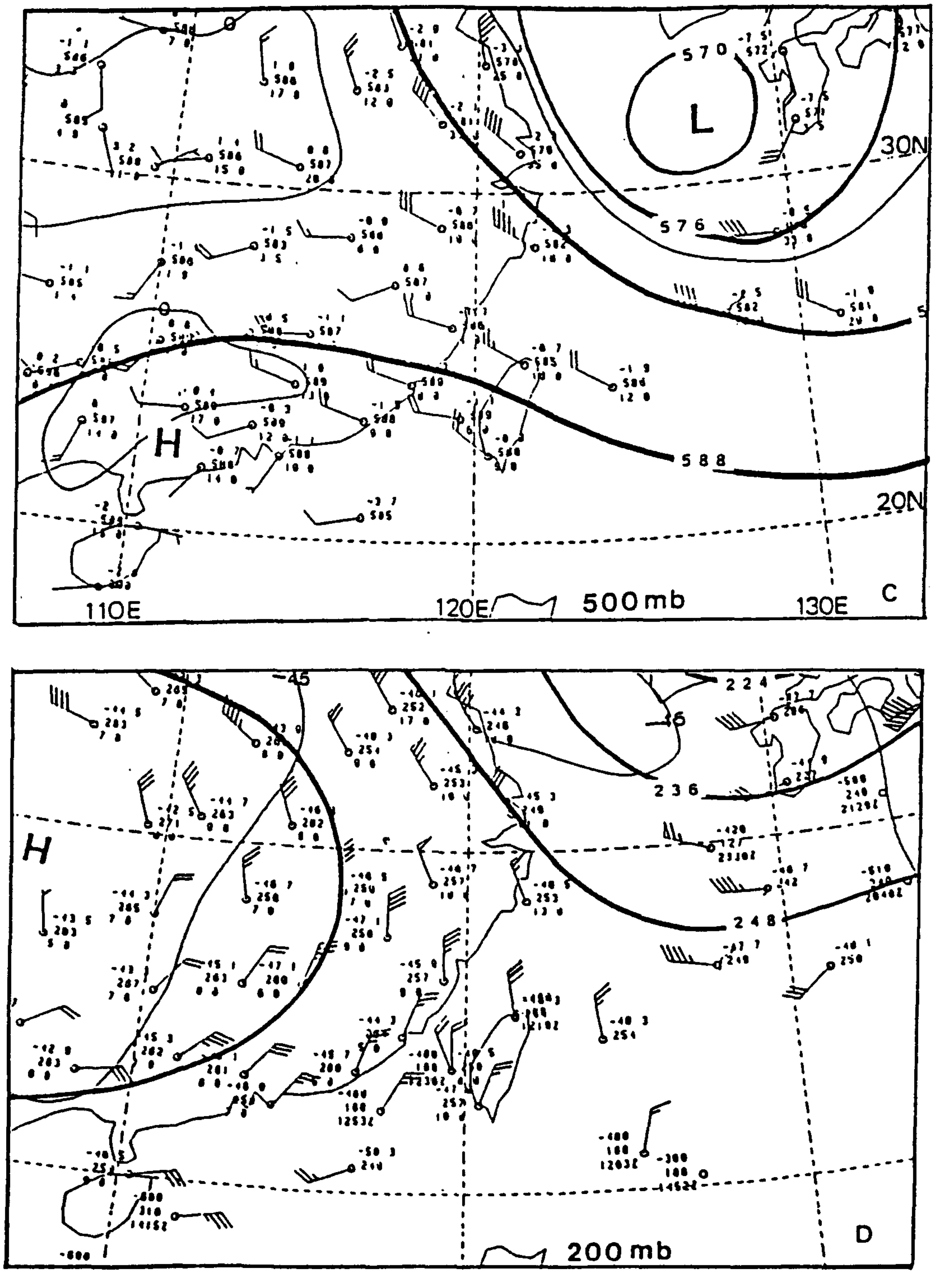

Fig. 3.3 cont. The upper air charts at (c) 500 and (d) 200 mb for 20 LST (12 UTC) 24 June 1987.

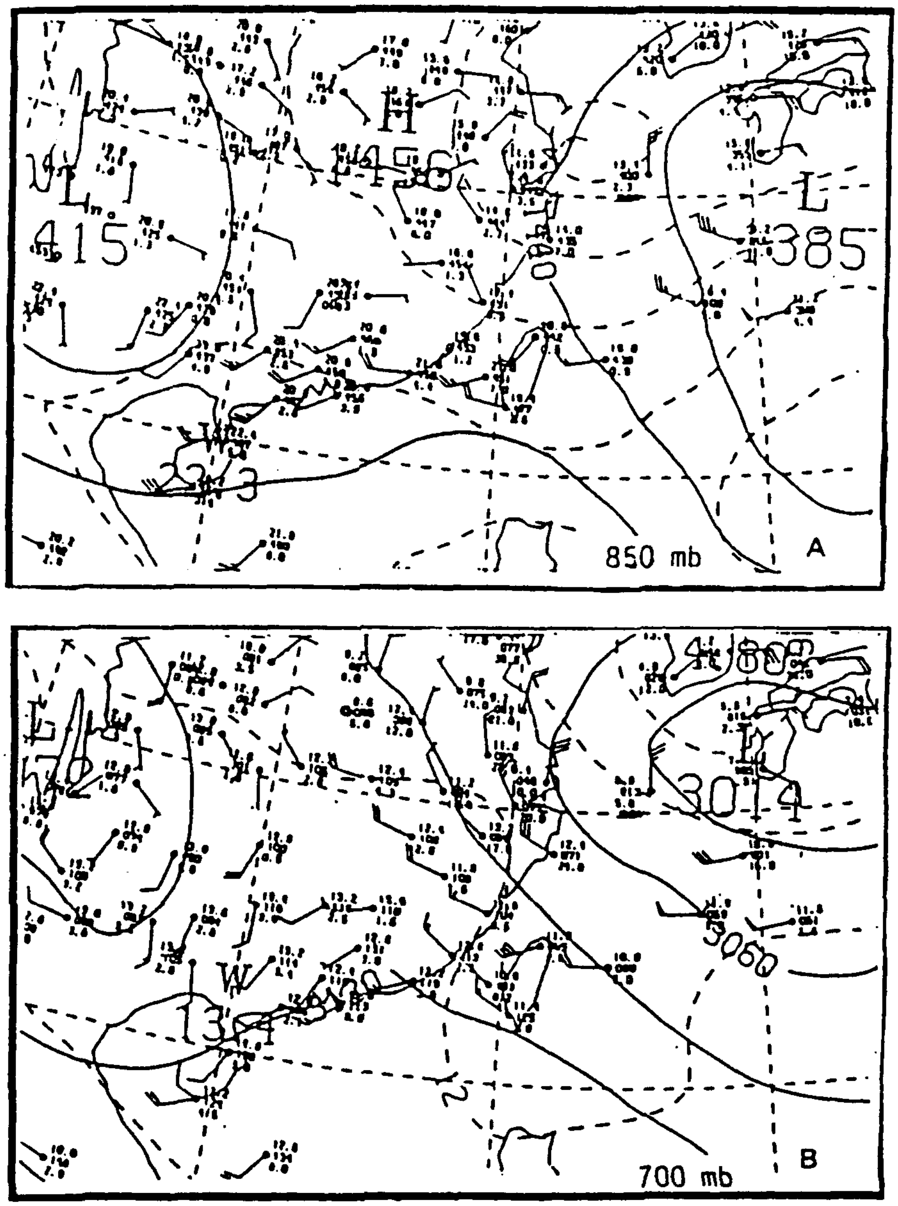

Fig. 3.4 The upper air charts at (a) 850 and (b) 700 mb for 08 LST (00 UTC) 25 June 1987.

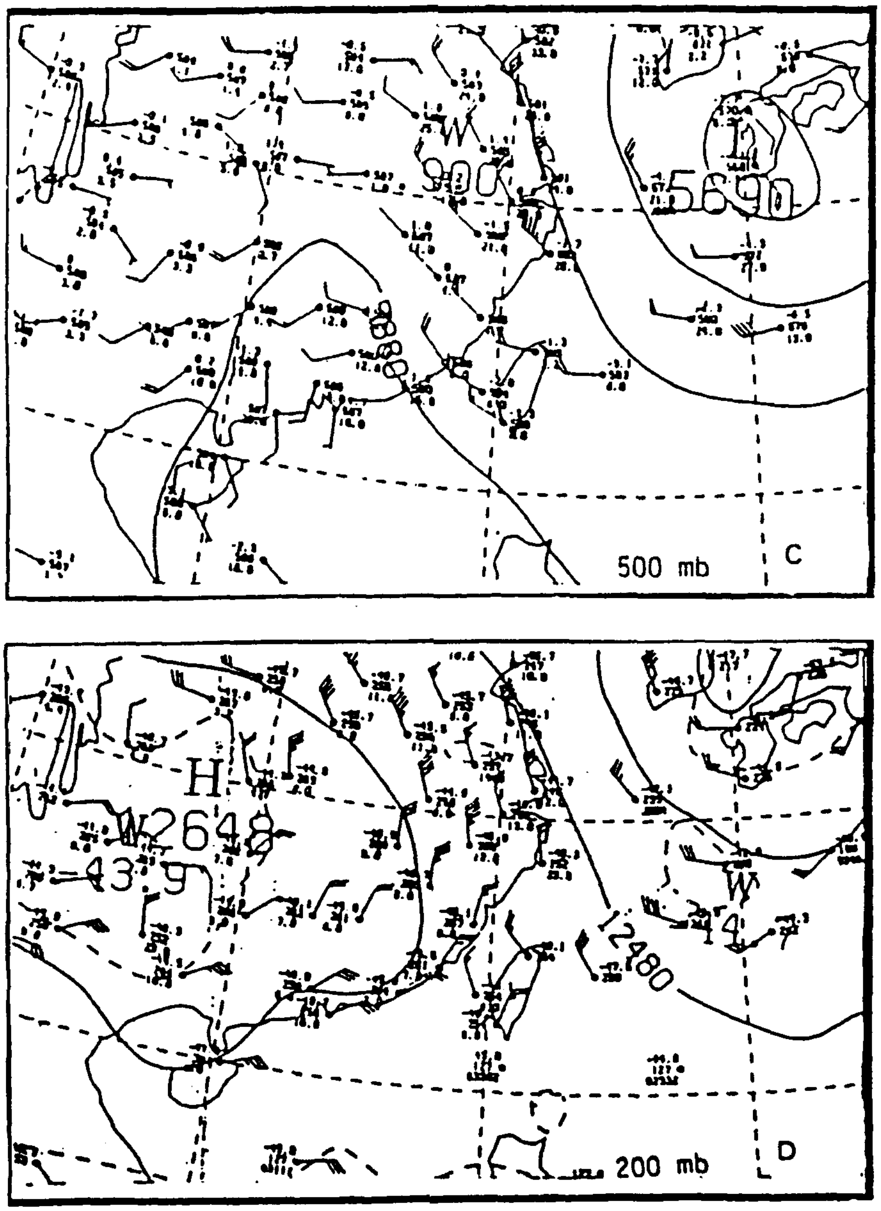

Fig. 3.4 The upper air charts at (c) 500 and (d) 200 mb for 08 LST (00 UTC) 25 June 1987.

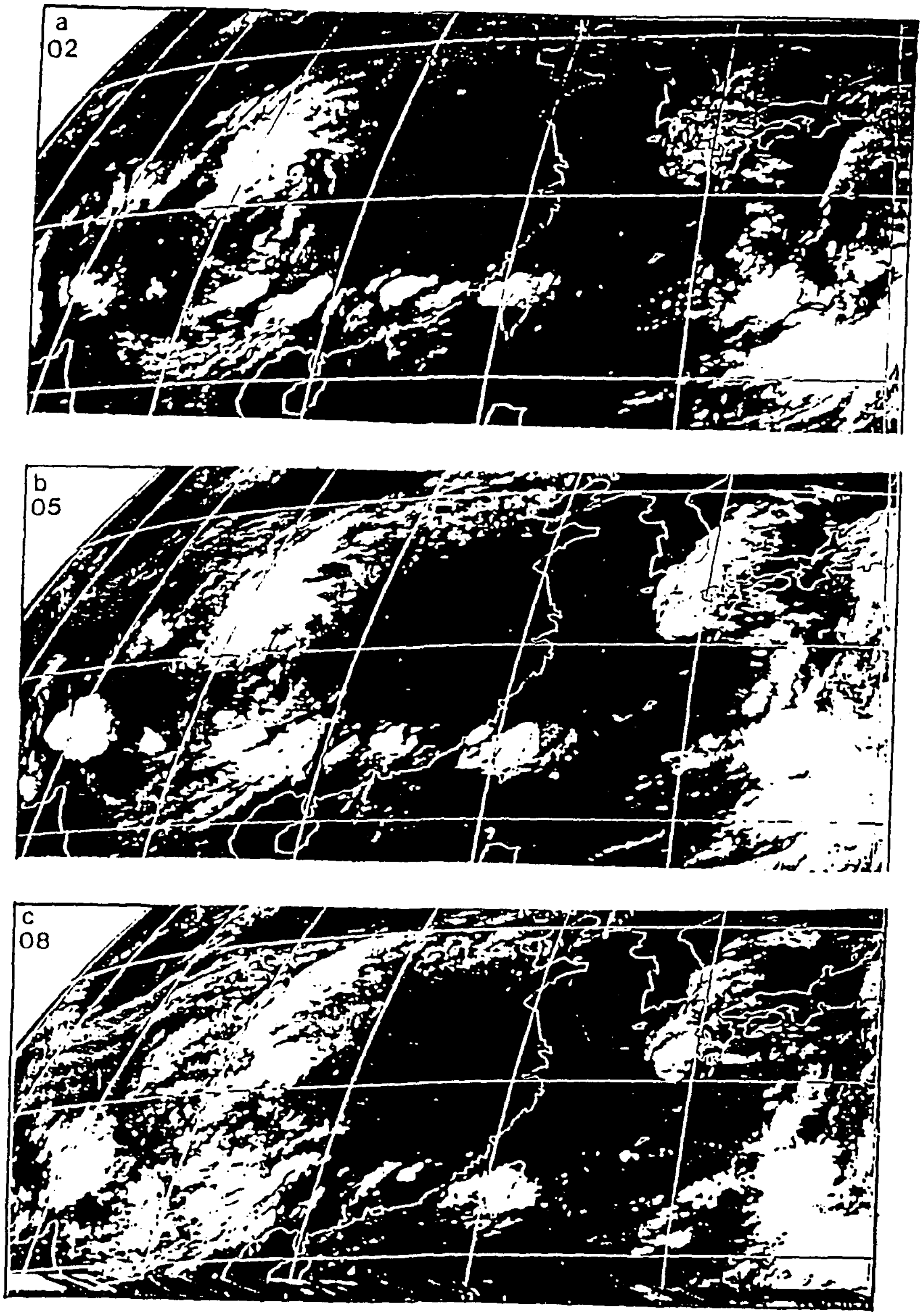

Fig. 3.5 Three GMS infra-red images for 25 June 1987 at (a) 02 LST, (b) 05 LST and (c) 08 LST.

height.

3.2 Satellite and Radar Depictions

Figure 3.5 shows a 3-hourly progression of infrared images from the Geostationary Meteorological Satellite (GMS) starting at 0200 LST 25 June. Notice the east-west band of smaller MCSs just north of Taiwan. By 08 LST (00 UTC) the MCS that earlier hugged northern Taiwan had grown and moved over the entire island of Taiwan. This caused extremely heavy rainfall (Chiou, 1990) over northern Taiwan. Chi and Scoffield (1991) observed the following satellite features. A Mei-Yu front signified the synoptic scale boundary. The coldest cloud tops were in the northern portion of the MCS with anvil debris in the southern area of the MCS. The MCS produced an outflow boundary which interacted with the surface front. Convergence was enhanced by the southerly winds at the surface. The heaviest convection occurred on the west coast of Taiwan.

The hourly plan-position indicator (PPI) scans from the Kaohsiung radar on the west coast of Taiwan are displayed in Fig. 3.6. Notice the east-northeast through west-southwest alignment of the convective rainband ahead of the superimposed Mei-Yu front. The band dropped south at 2.5 m s^{-1} over the eight-hour time sequence. Parsons and Trier (1989) reported Doppler radar reflectivities greater than 50 dBZ associated with this rainband just northwest of Taiwan in earlier hours.

The CP-4 radar site began receiving heavy rainfall by 0512

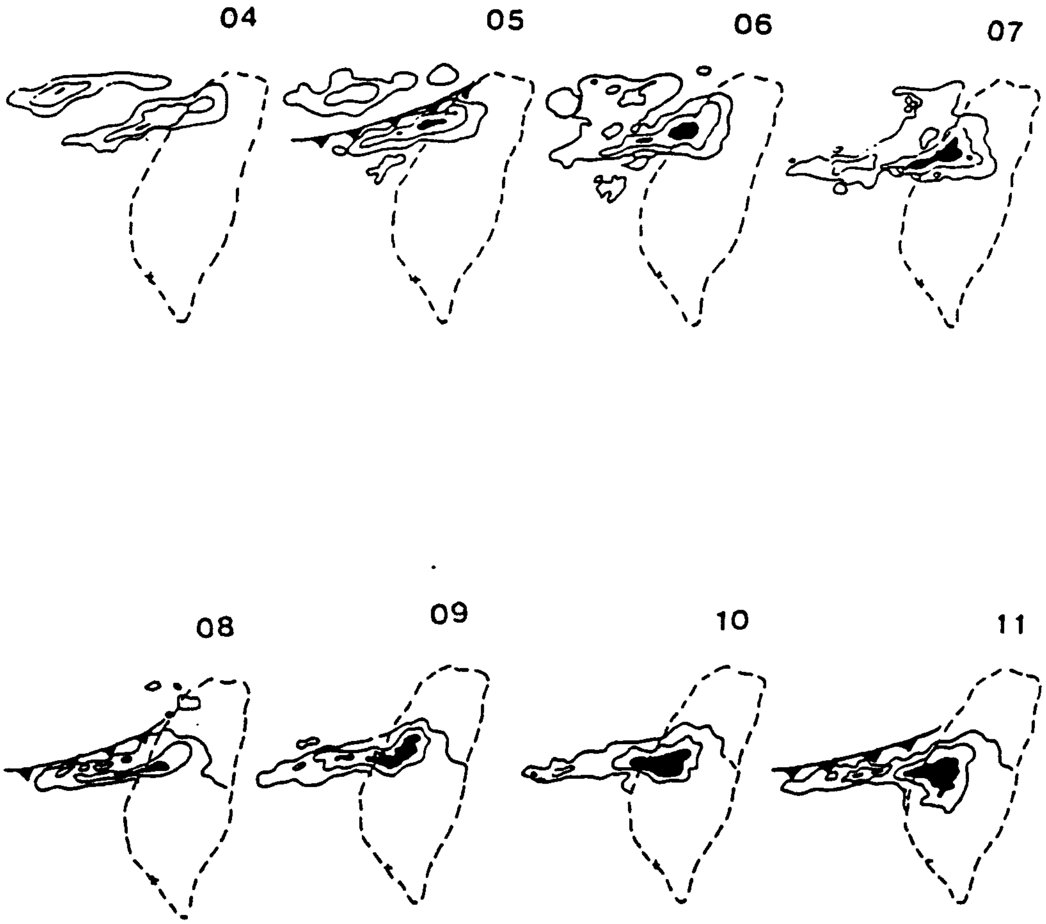

Fig. 3.6 Hourly PPI displays in LST from the 10-cm conventional Kaohsiung radar in southern Taiwan on 25 June 1987. Contour intervals are 10 dBZ starting at 15 dBZ. Dark area corresponds to reflectivity greater than 35 dBZ. Frontal positions extracted from Fig. 3.2 (after Lin et al., 1992).

LST. Nearly 2 inches of rain fell to the northeast of this site by 0600 LST. The heavy convection lasted until the prefrontal rainband passed through the site at 0748 LST. Winds continued out of the southwest to suggest that the precipitation was prefrontal. Not until 1257 LST did the cold front reach this site (Parsons and Trier, 1989).

3.3 Surface Observations

Three surface observation stations were selected to describe the wind direction and speed, pressure tendency, temperature and dewpoint distribution, and cumulative rainfall amounts. Each stations was selected to show how the front affected areas in northern Taiwan (Hsinchu), the central west coast of Taiwan (Ching-Chung-Kang, CCK), and an island station (Makung) west of central Taiwan.

The surface observations at Hsinchu for the 24-hour period on 25 June are shown in Fig. 3.7. The Mei-Yu front passed through the station around 0730 LST as depicted by the light vertical line on all four panels. Notice the wind shift and decrease in wind speed after frontal passage. The station pressure rose a few hours before frontal passage. Also, the temperature decreased slightly after passage. Notice the small temperature-dewpoint depression from 06-09 LST indicating high θ_e air near the surface (Chang, 1992). This depression increased after frontal passage due to an invasion of cooler, drier air from the mainland of China. The heaviest precipitation occurred within two and a half hours of frontal

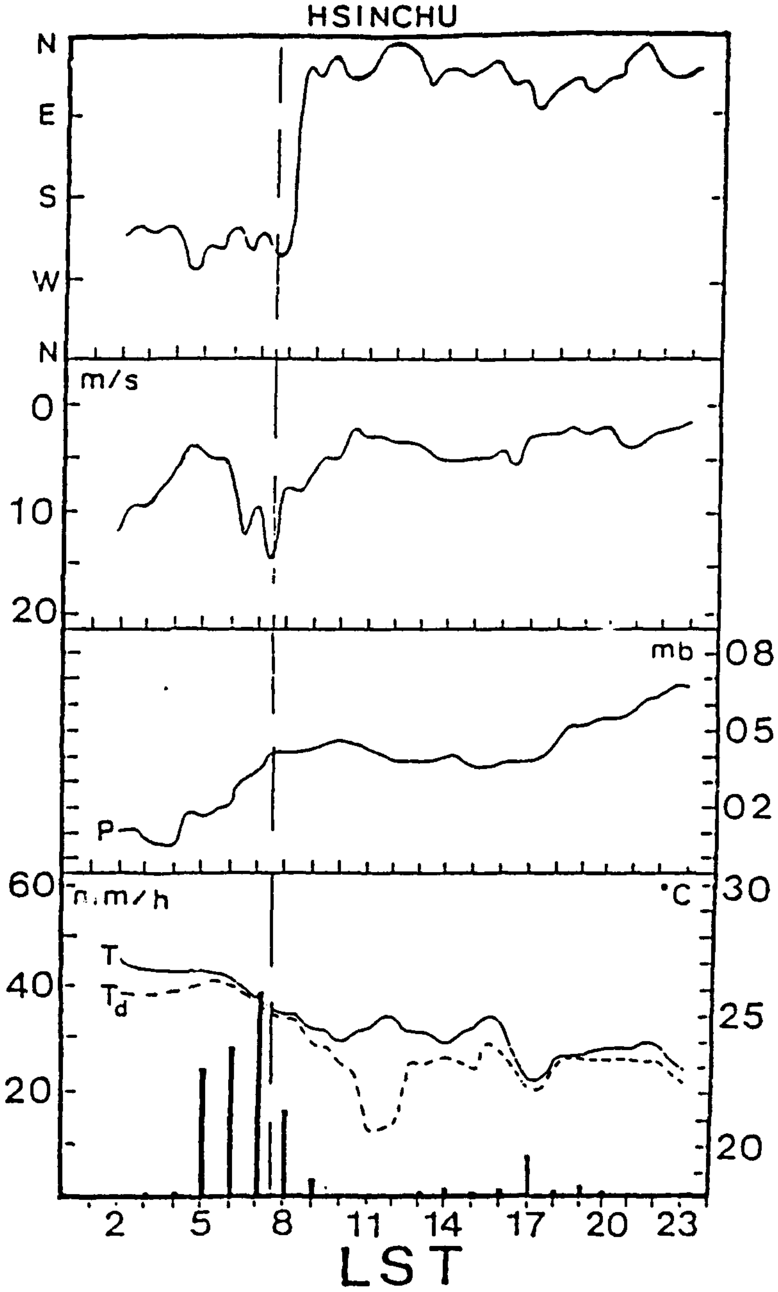

Fig. 3.7 Surface observations taken at Hsinchu on 25 June 1987. Wind direction, wind speed, pressure, temperature and dewpoint along with rainfall rate in mm/hr are shown from top to bottom, respectively. Thin vertical line represents time of frontal passage (after Chang, 1992).

passage, indicative of a prefrontal rainband. Hsinchu received 129.6 millimeters of rain from this storm, nearly 70% of its' total IOP-13 rainfall before frontal passage.

CCK (Fig. 3.8) was chosen since it was the location of the TOGA radar and was on the central west coast. Once again the winds became northerly and diminished in speed after frontal passage. The pressure rose nearly three mb within a seven hour time period leading up to frontal passage at 23 LST 25 June. Heaviest precipitation began 14 hours before frontal passage and nearly all the 168.9 mm of rain received at this station fell in conjuction with the prefrontal convective rainband. High θ_e air, reflected in the small temperature-dewpoint depression, was present throughout the entire day.

Upon frontal passage at Makung (Fig. 3.9) at 19 LST 25 June, winds decreased by 6 m s^{-1} and shifted to the north. The warm waters of the Taiwan Strait moderated the effects of the frontal passage. Pressure, temperature, and dewpoint changes were weaker than those observed at CCK and Hsinchu. Trier et al. (1990) studied the effects of the open water on a postfrontal air mass during IOP-8. The air was modified by warm water heat fluxes resulting in nearly a 70% decrease in temperature contrast across the front as it moved from the northern to southern end of Taiwan.

3.4 Upper Air Soundings

The cold front passed through Panchiao, located over north-

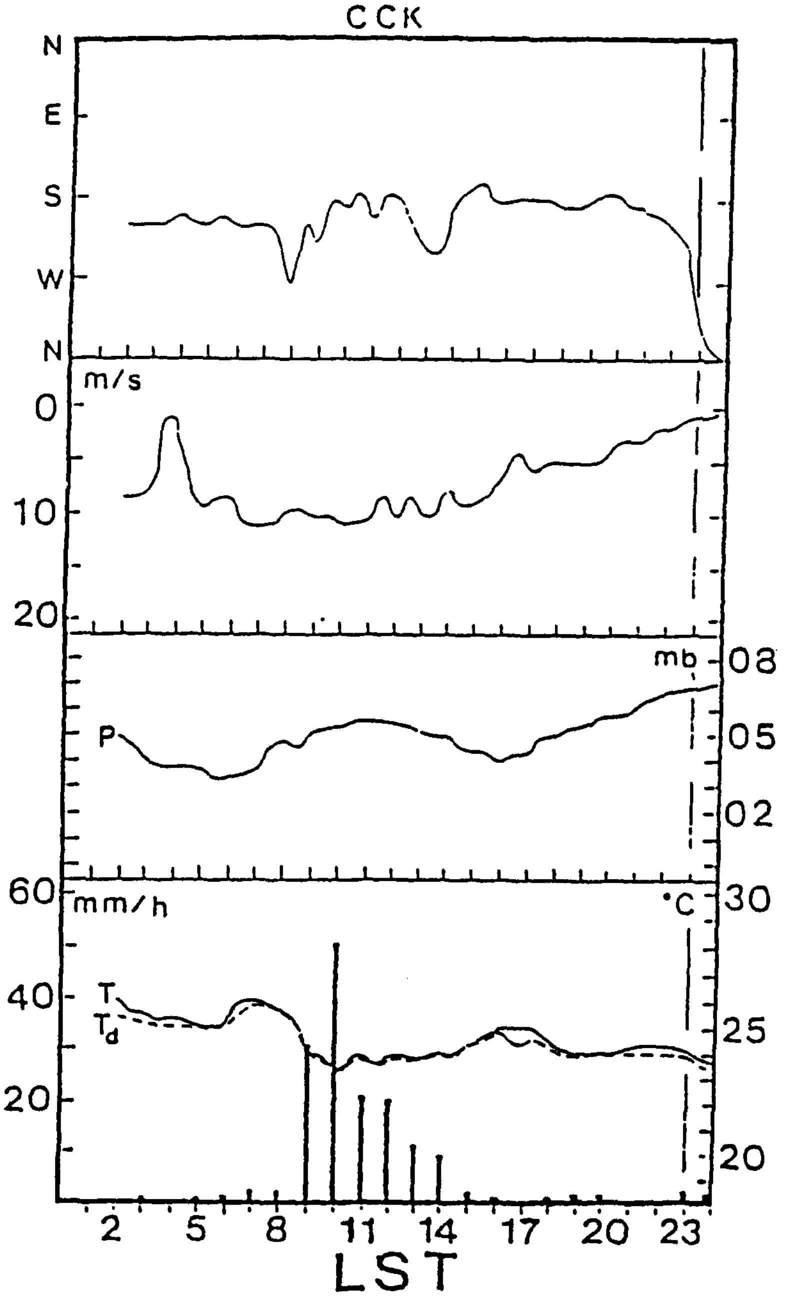

Fig. 3.8 As in Fig. 3.7 except for Ching-Chung-Kang (after Chang, 1992).

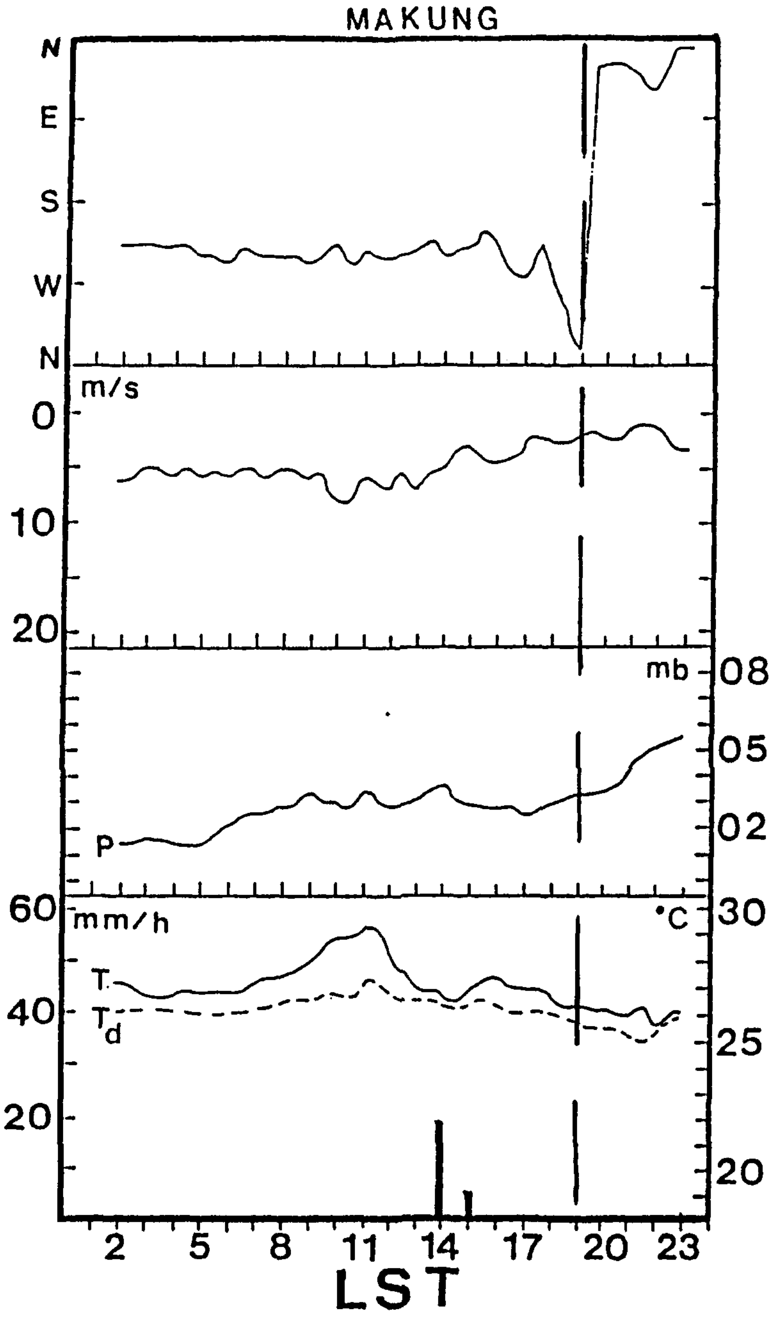

Fig. 3.9 As in Fig. 3.7 except for Makung (after Chang, 1992).

ern Taiwan, at 23 LST 24 June. Panchiao soundings before and after frontal passage are presented in Fig. 3.10. The prefrontal environment at 20 LST showed constant veering of winds with height, or warm air advection (WAA). There was a relative moist lower atmosphere up to 700 mb followed by dry air in the middle troposphere. This sounding is representative of a conditional unstable environment. If the parcel were lifted from 800 m at the lifting condensation level (LCL) to the level of free convection (LFC) at 2100 m, the parcel would ascend to nearly 13 km above ground level (ABL) along the moist adiabat (dotted line) to the equilibrium level (EL).

The Makung sounding at 02 LST 25 June is also presented to show a prefrontal environment (Fig. 3.10b). This environment is similar to the Panchiao prefrontal sounding. The value of convective available potential energy (CAPE) for IOP-13 was 1045 $m^2 s^{-2}$. CAPE is used to calculate the amount of buoyant energy able to drive the updrafts. This CAPE value suggests only weak or moderate updrafts within the rainband (Lin et al., 1991).

The postfrontal sounding (Fig. 3.11) for Panchiao at 02 LST 25 June is a good indicator of how the environment stabilized. A parcel of air would need nearly 3 km of height to reach the LFC after a forced lifting from the LCL. Then the parcel would only rise to 5.6 km before reaching the EL. Surface to 800 mb winds were light (< 5 m s^{-1}) and from the northwest, indicative of a shallow layer of cooler air.

Panchiao Prefrontal 2000 LST 24 June

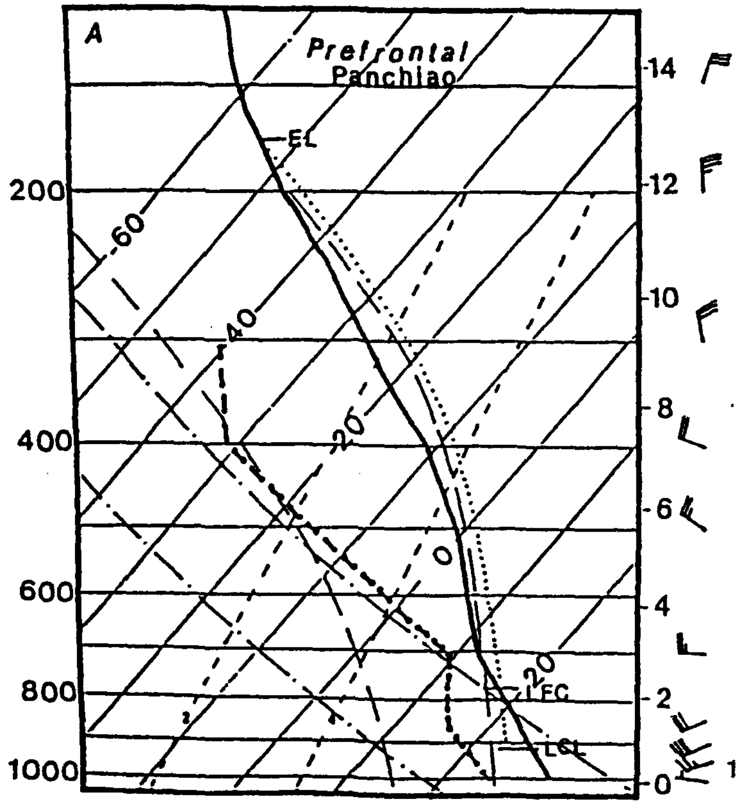

Fig. 3.10a Environmental sounding for prefrontal atmosphere at Panchiao, 20 LST on 24 June.

Makung Prefrontal 0200 LST 25 June

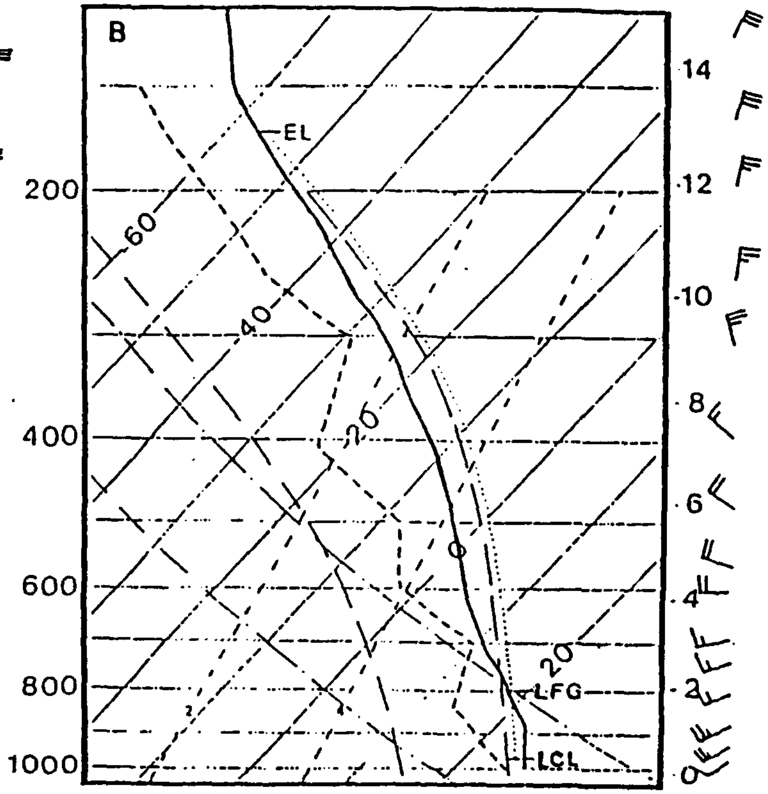

Fig. 3.10b Environmental sounding for prefrontal atmosphere at Makung, 02 LST on 25 June.

Panchiao Postfrontal 0200 LST 25 June

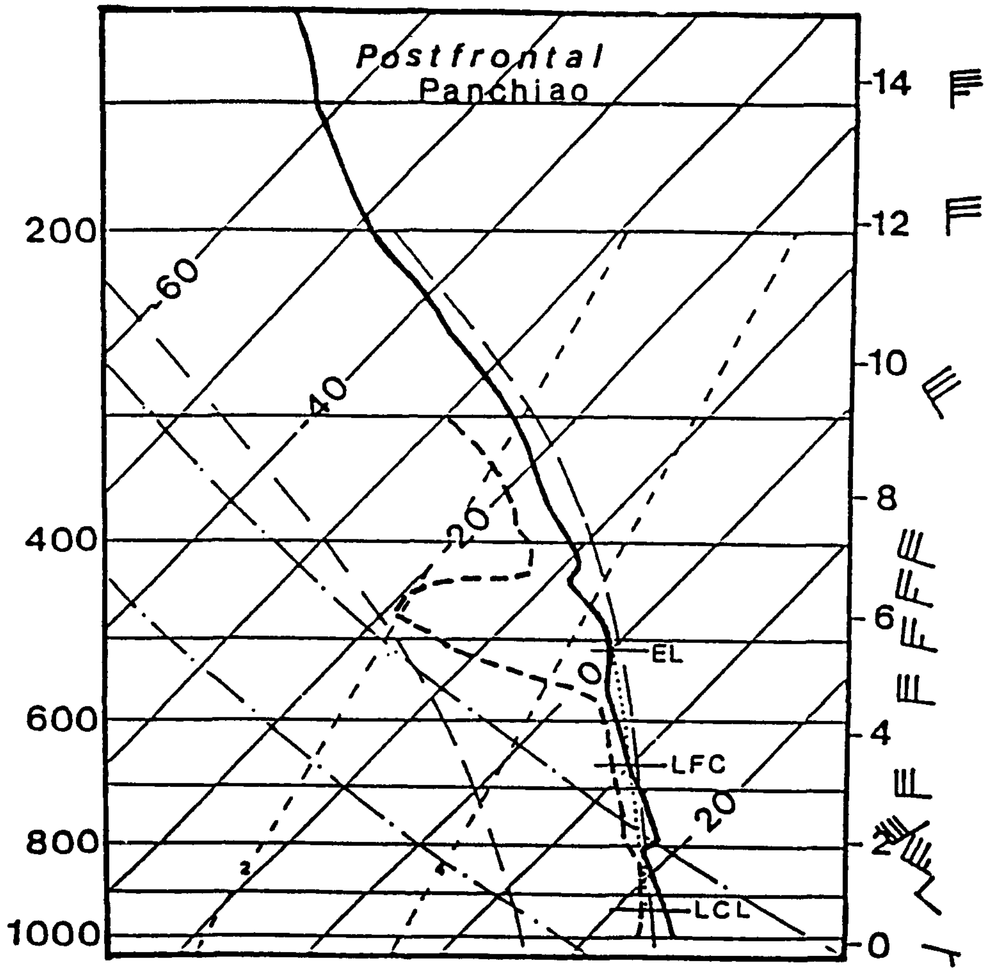

Fig. 3.11 Environmental sounding for postfrontal atmosphere at Panchiao, 02 LST on 25 June 1987.

Figure 3.12 shows the prefrontal and postfrontal environmental plots of potential temperature (Θ), equivalent potential temperature (Θ_e), and saturated equivalent potential temperature (Θ_{se}) for Panchiao. The prefrontal environment shows a decrease of equivalent and saturated potential temperature from the surface to 580 mb, indicating a convectively unstable environment (Lin et al., 1989).

The postfrontal diagram from Panchiao (Fig. 3.12b) shows equivalent and saturated equivalent potential temperature increased in value or became neutral with height, indicative of a convectively stable environment (Beeson, 1991). Also notice that at the surface equivalent potential temperature decreased by nearly 15°C, indicating cooler, drier air from the north.

Horizontal equivalent potential temperature advection and temperature advection at 850 mb are presented in Fig. 3.13. Chiou (1990) concluded that the combination of positive values (solid lines) of both maximum Θ_e advection and warm air advection lead to the development and movement of MCSs over a 12-hour period.

3.5 Time-Height Meteorological Variations

Two stations were chosen to study the wind structure of the environment over 24 hours. Panchiao was selected since it is in northern Taiwan and surrounded by mountains. Makung is a small island in the Strait of Taiwan.

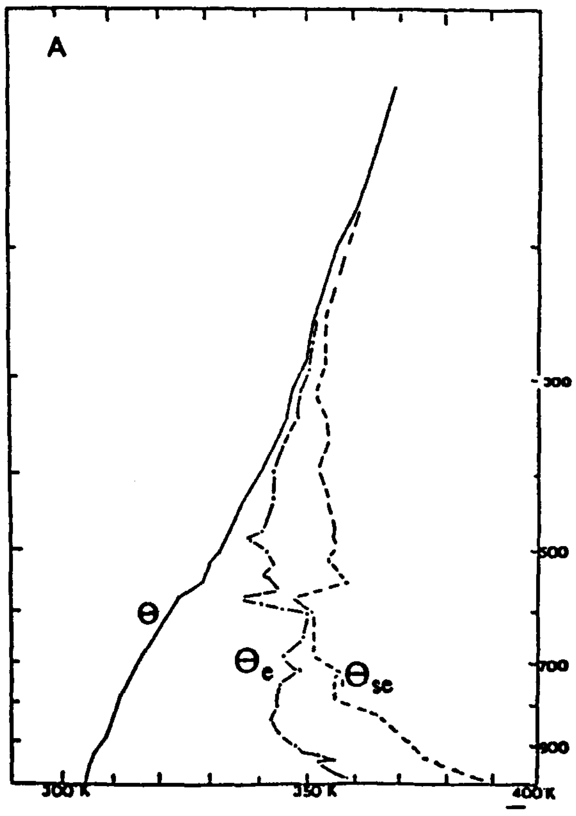

Fig 3.12a Plots of potential temperature (θ), equivalent potential temperature (θ_e), and saturated equivalent potential temperature (θ_{se}) for prefrontal environment, Panchiao, at 20 LST on 24 June 1987.

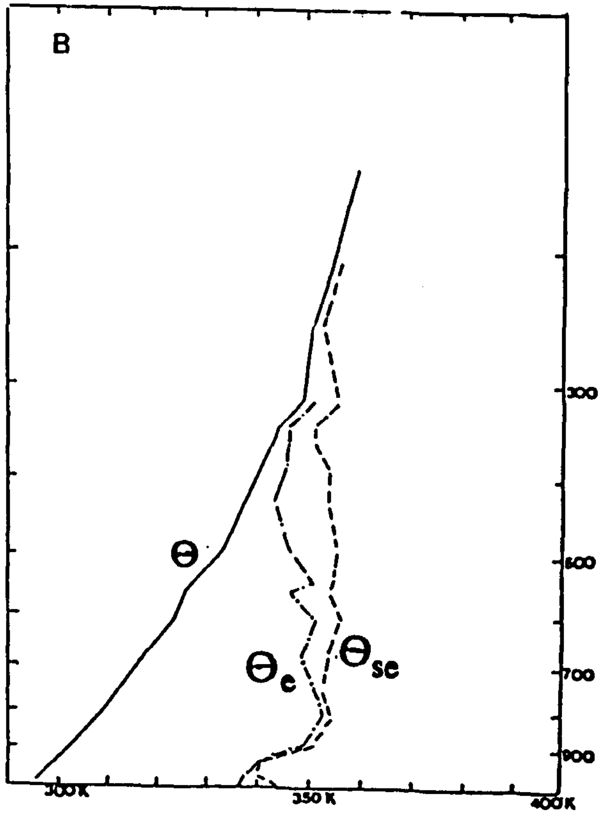

Fig. 3.12b As in Fig 3.12a except for post-frontal environment, Panchiao, at 08 LST on 24 June 1987.

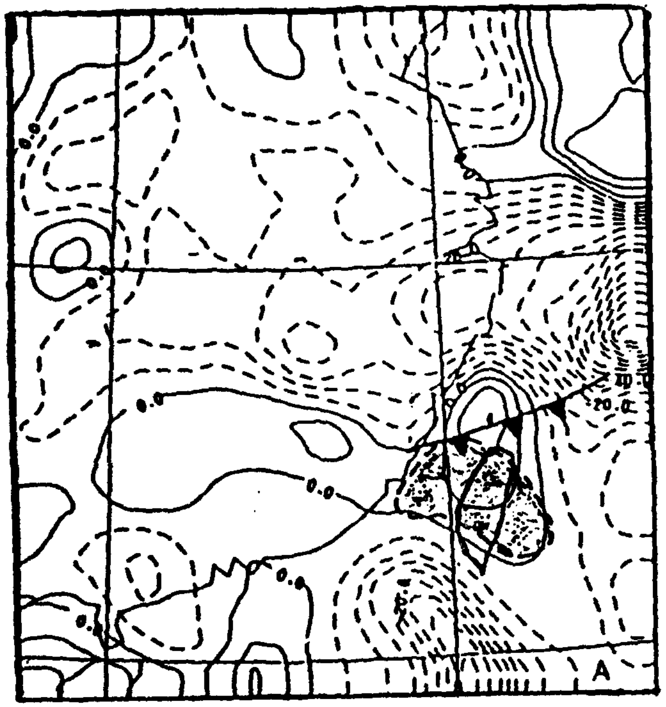

Fig. 3.13a The advection of equivalent potential temperature ($2^{o}C$ per day) at 850 mb, 20 LST on 24 June. Solid lines show warm or positive advection, while dashed lines show just the opposite. Shaded area represents cloud distributions over the next 12 hours (after Chiou, 1990).

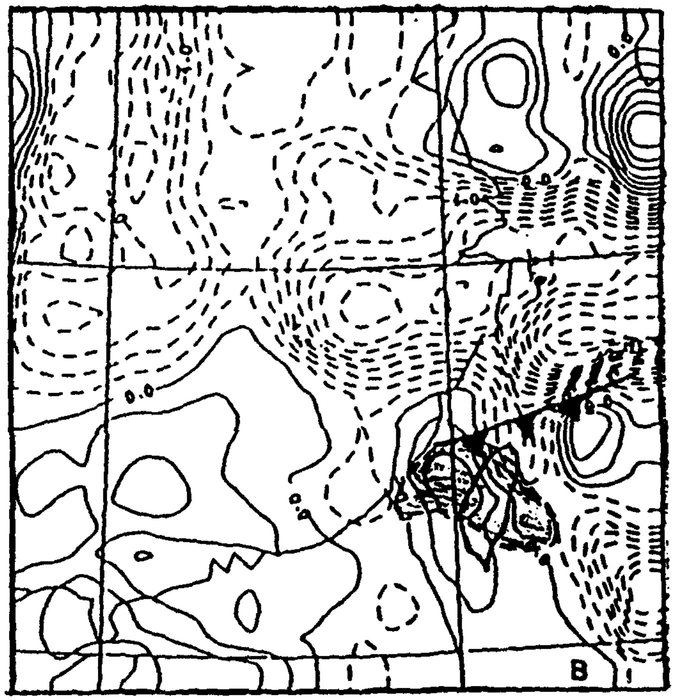

Fig. 3.13b Thermal advection ($2^{o}C$ per day) at 850mb for 20 LST 24 June (after Chiou, 1990).

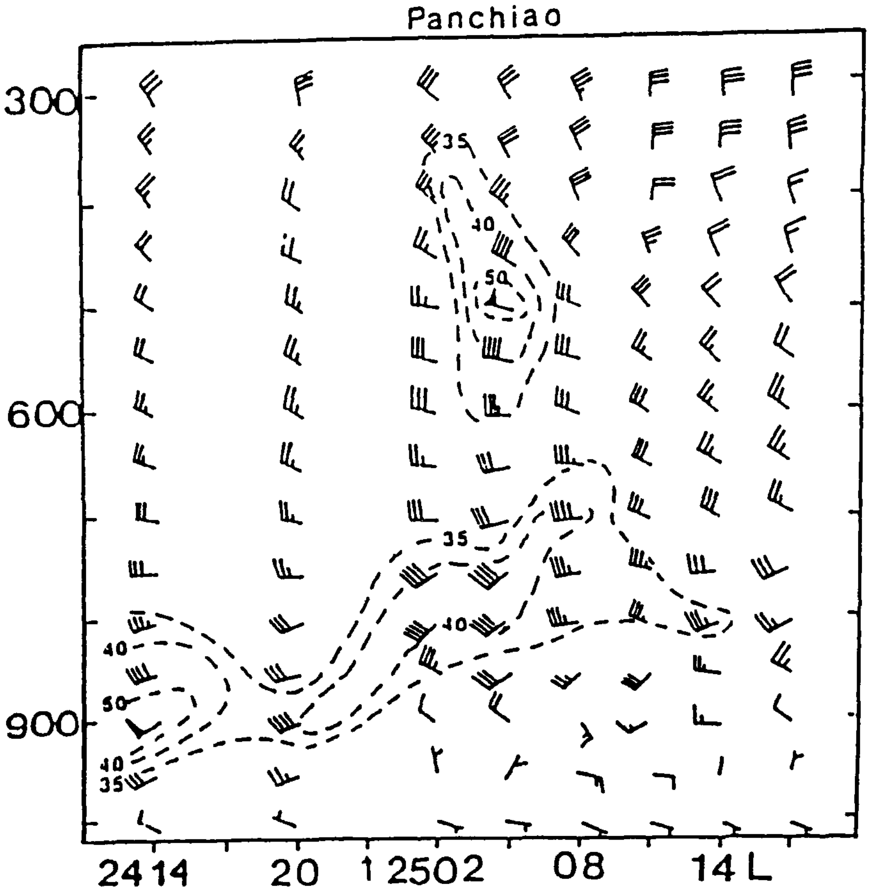

Fig. 3.14 Time-height variations of Panchiao rawinsonde winds on 24/25 June 1987. All times are LST. Isotachs of 35 knots or greater are shown by dashed lines. The arrow points out frontal passage (after Lin et al., 1992).

Studying Fig. 3.14, a low-level jet (LLJ) of 25 m s^{-1} is discovered at 900 mb nine hours before frontal passage at Panchiao. After the front had passed, the LLJ lifted to nearly 700 mb. The mid-level jet (MLJ), not seen before convection, was found at 500 mb with a speed of 25 m s^{-1} at 05 LST 25 June. According to Lin et al., (1992), MLJ development was caused by the vertical transport of horizontal momentum due to convective eddies associated with the rainbands.

The Makung rawinsonde winds (Fig. 3.15) show a situation similar to Panchiao. Prefrontal low-level winds indicated a constant flow of the southwest monsoon. A LLJ of 35 knots (18 m s^{-1}) was found at 930 mb 14 hours before frontal passage at 19 LST. The MLJ (> 20 m s^{-1}) did not form until convection began around 14 LST, the same time when the LLJ was no longer found. The MLJ is evident between 350-500 mb.

3.6 Rainfall Amounts

It has been mentioned that due to the slow movement of the Mei-Yu front and its orientation the heaviest rainfall occurred during IOP-13. The rainfall rate was classified as moderate to strong with a maximum rate of 40 mm/hr (Wang and Lin, 1991). Several plots of horizontal rainfall distribution are presented. First of all, four plots showing three-hourly periods of accumulated rainfall are seen in Fig. 3.16 starting from 04 LST 25 June. As the prefrontal convective rainband initially moved south toward Taiwan the area to the northeast of CP-4 received nearly 2 inches (50 mm) of rain by 0600 LST

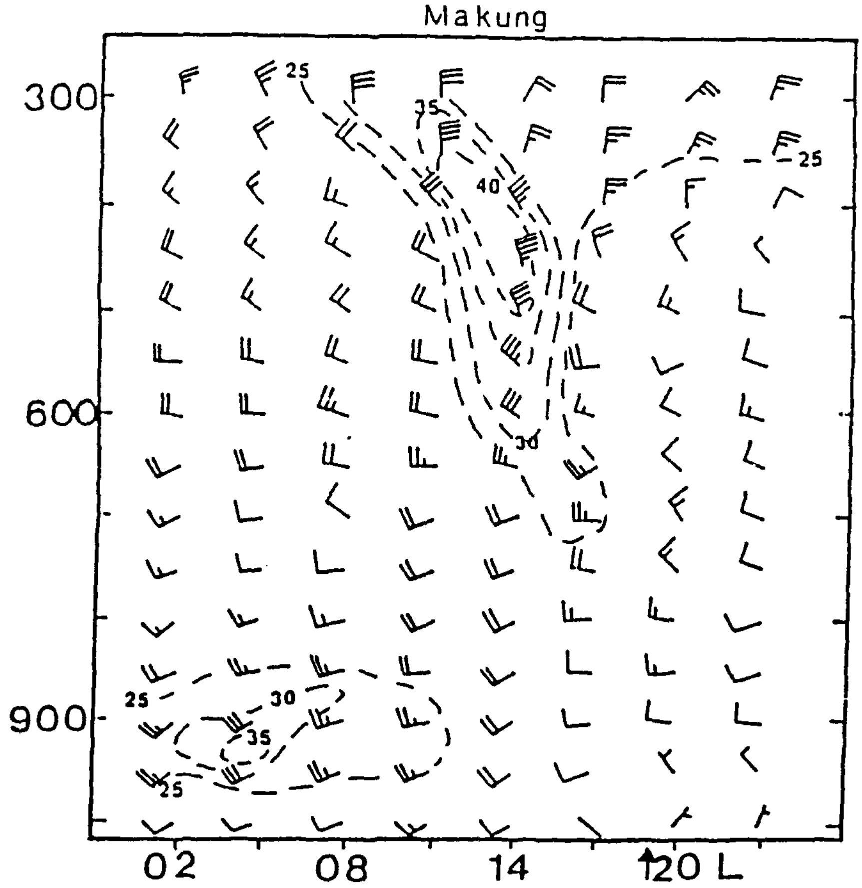

Fig. 3.15 As in Fig. 3.14 except for Makung on 25 June (after Chang, 1992).

(Parsons and Trier, 1989). Examining Fig. 3.16b, the heaviest rainfall (150 mm in 3 hrs) from 07-10 LST occurred in between the CP-4 and TOGA radars as the front sagged slowly to the south and intensified. The system maintained its strength the first nine hours as seen by the 130 mm of rainfall production between 10-13 LST just to the south of TOGA (Fig. 3.16c). After 13 LST (Fig. 3.16d), the system weakened due to the influence of the warm oceanic waters as the front slipped further south at a pace of 2.5 m s^{-1}.

Studying Fig. 3.17, notice that the heaviest rainfall for the two hours is centered between the two Doppler radars. The rainfall doubled in intensity between 07 and 08 LST just to the south of the CP-4 radar. The location of the heaviest rainfall remained nearly stationary over these time periods. The six time periods chosen for this study, 0634-0707 LST coincide with the heaviest rainfall in the area around the two Doppler radars.

Figure 3.18 depicts the 24-hour accumulated rainfall amounts over Taiwan for 25 June 1987. Two areas of over 200 mm (8 inches) of rain fell to the northeast and southwest of the TOGA radar. Notice that the majority of the rain fell on the northwestern windward side of Taiwan (west of the CMR). Also, the system decayed as it moved to the south as most of the heavier rain greater than 40 mm fell in the northwestern sector of Taiwan.

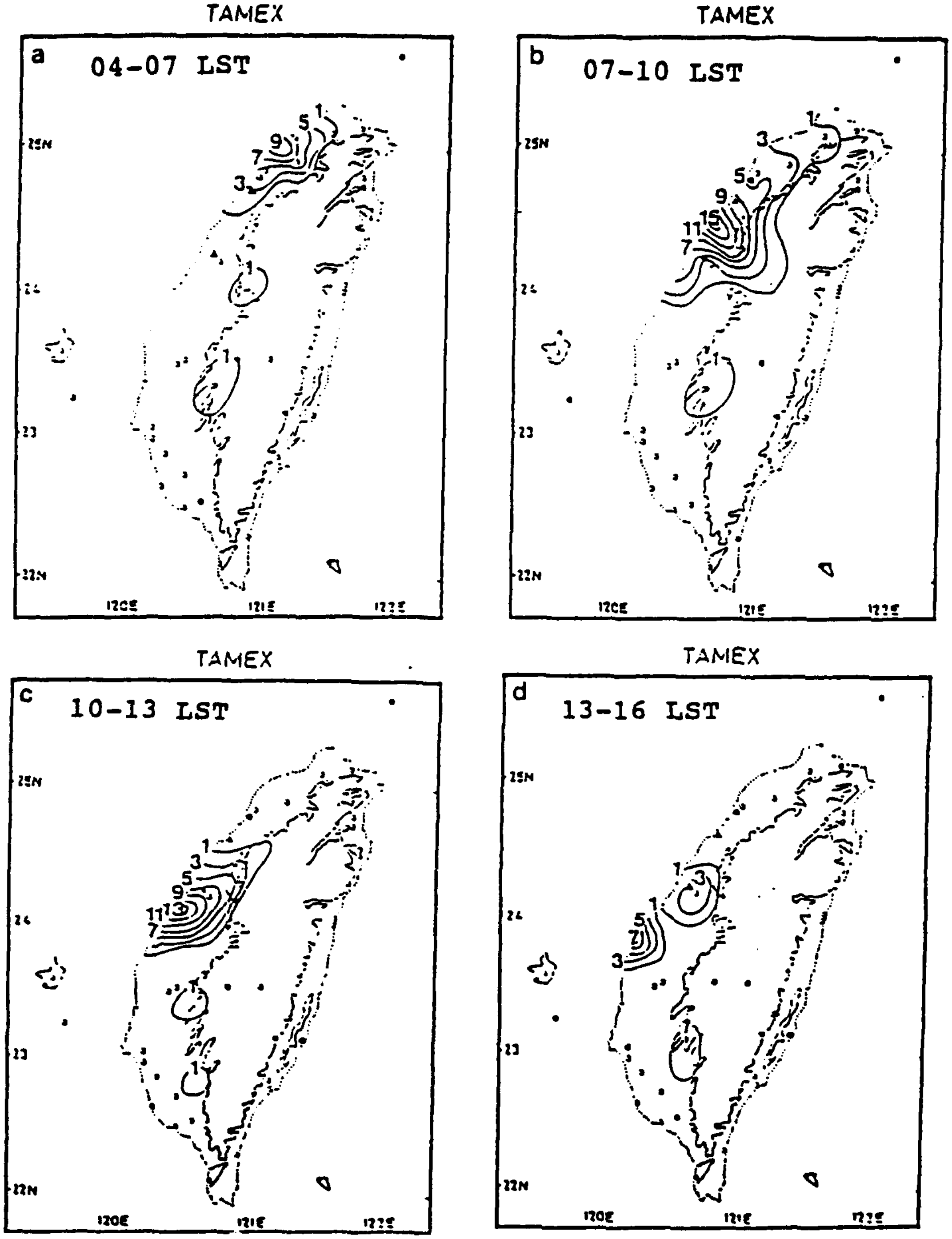

Fig. 3.16 Accumulated rainfall rate for the 3-hourly periods: (a) 04-07, (b) 07-10, (c) 10-13, and (d) 13-16 LST on June 25. The 500 meter contour for the CMR is shown. Units are 10 mm per every 3 hrs. Solid triangles indicate location of CP-4 and TOGA radars (after Chang, 1992).

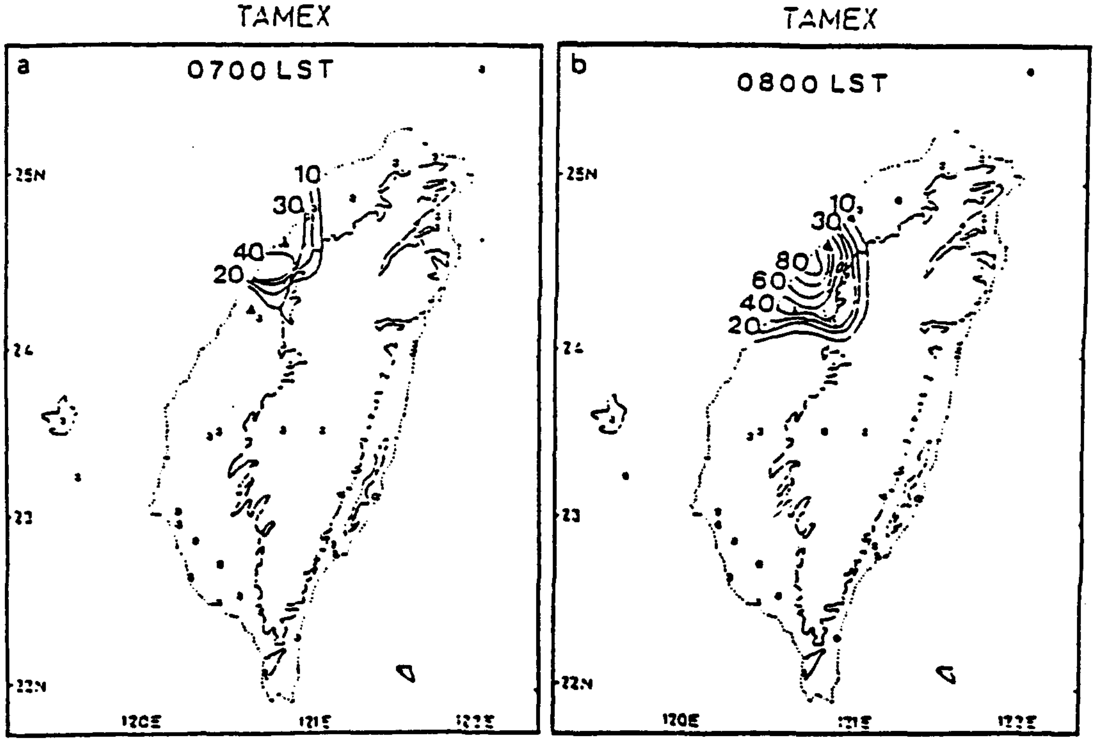

Fig. 3.17 Hourly rainfall rates for (a) 07 and (b) 08 LST on 25 June. Contour interval is 10 mm per hr (after Chang, 1992)

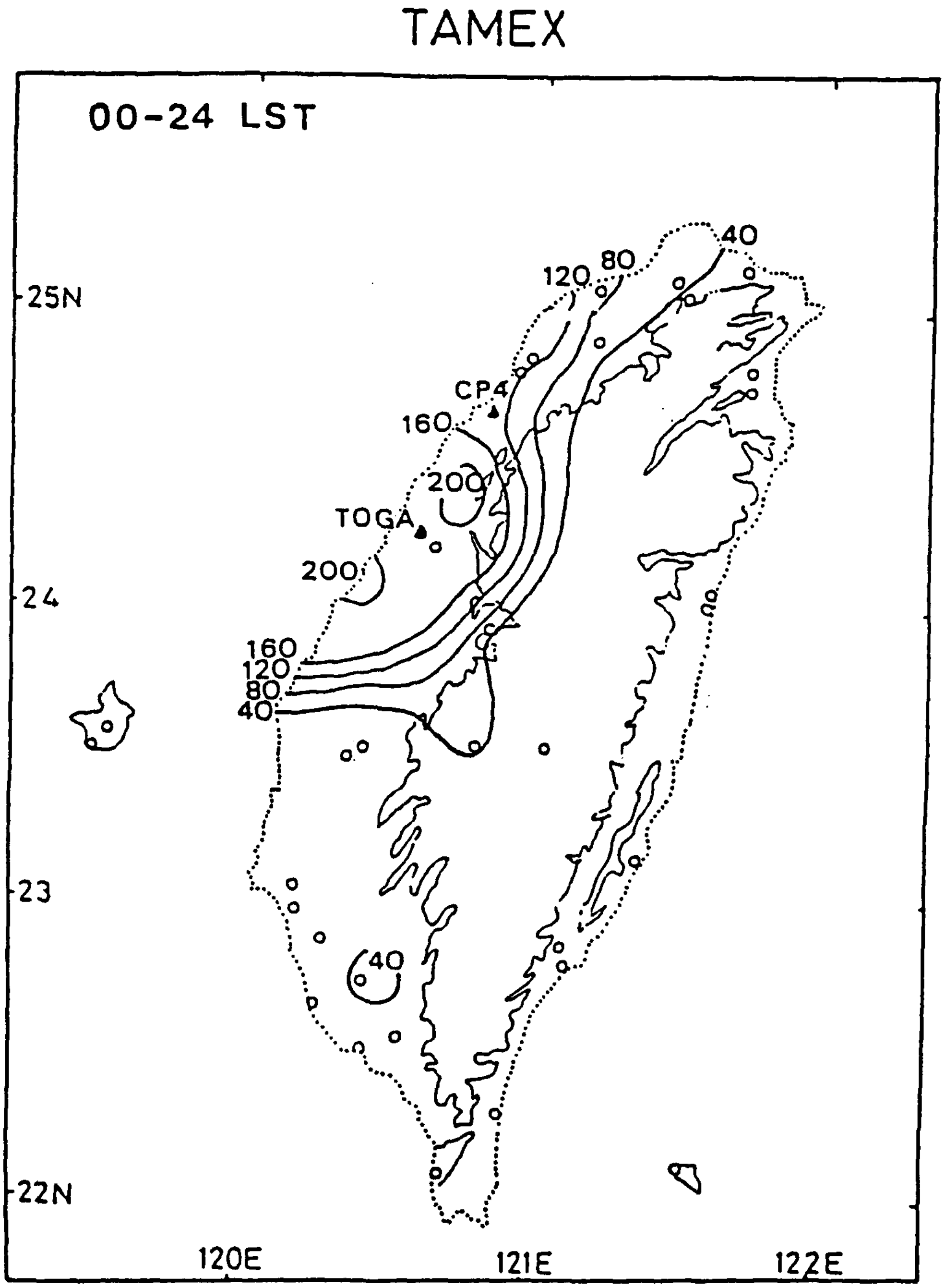

Fig. 3.18 Twenty-four hour accumulated rainfall amount on 25 June over Taiwan. Contour interval is 40 mm per 24 hrs (after Chang, 1992).

CHAPTER 4: Methodology

4.1 Introduction

This study employed a single Doppler radar. As the Mei-Yu front began to approach the Taiwan coast, the only Doppler radar that was active was the CP-4 located at WaiPu Beach. Although the TOGA radar was later turned on to collect dual-Doppler radar scans, the initial stages of the Mei-Yu front were only examined by the CP-4 radar. The lack of dual-Doppler radar data coverage would normally prevent a detailed study of the internal structure of the Mei-Yu front as it reached the Taiwan coast, however, this study takes advantage of the special circumstances that this Mei-Yu front presented to study the internal structure of the front as it approached and reached the Taiwan coast. The Mei-Yu front during the time periods under study was nearly two dimensional. The predominant flow relative to the front was perpendicular to the frontal boundary. Under these special circumstances, it is possible to recover the horizontal and vertical velocities. The techniques discussed in section 3 detail the assumptions and the mathematics used to recover the flow field.

4.2 Other Techniques

Several methods for processing single Doppler radar data have been employed in the past. The simplest technique is a Velocity-Azimuth Display (VAD). VAD scanning requires an azimuthal scan of the storm at an elevation angle that scans the middle layers of the storm. A VAD scan also requires that the scatterers be uniformly sized and have uniform motion through all 360 degrees of the scan. Unfortunately, the Mei-Yu front violates these constraints. Wakimoto (1982) also faced similar problems while examining the structure of the gust front associated with microbursts. Wakimoto limited his study to low elevation angles and assumed that the gust front was two-dimensional in order to perform the analysis. This study uses the same technique and assumptions and it extends the technique to larger elevation angles.

4.3 Data Processing

This study examines the Mei-Yu front at six consecutive time periods starting at 0634 LST on 25 June 1987. The raw CP-4 data in Universal Format were processed using the Saint Louis University DRAS package. The data from IOP-13 were collected in a PPI scan rather than the RHI scan needed for this study, so the data were processed as if it were a dual-Doppler analysis and then a RHI scan was reconstructed from the partially processed PPI data. Once a RHI scan through the storm was reconstructed, the RHI data were gridded with a Barnes (1973) objective analysis. The gridded data were then used to reconstruct the flow field interior to the Mei-Yu front. The horizontal wind field (the radial velocity, V_r) was recovered from:

$$V_r = \overline{V}\cos\phi \qquad (1)$$

This approximation holds provided the elevation angle (ϕ) is relatively small. The techniques for recovering the vertical velocity field are discussed in the next section.

4.4 Vertical Velocity Computations

In a cylindrical coordinate system (r, θ, z, t) with the radar as the origin, the anelastic mass continuity equation can be written as:

$$\frac{\partial \rho_o r V_r}{r \partial r} + \frac{\partial \rho_o V_\theta}{r \partial \theta} + \frac{\partial \rho_o w}{\partial z} = 0 \qquad (2)$$

where V_r = radial velocity, V_θ = = tangential velocity, w = vertical velocity, r = distance from the radar, θ = azimuth angle, and $\rho_o(z)$ = environmental air density determined from observation. As discussed earlier during IOP-13, the Mei-Yu front was nearly quasi-two dimensional. Thus, the flow parallel to the frontal boundary is nearly zero. Equation (2) can be expanded and simplified to give:

$$\rho_o(z) \left| \frac{V_r}{r} + \frac{\partial V_r}{\partial r} \right| + \rho_o \frac{\partial V_\theta}{r \partial \theta} + \rho_o \frac{\partial W}{\partial z} = 0 \qquad (3)$$

A scale analysis for the Mei-Yu front, using the assumption that the front is quasi-two dimensional shows that the second term in (3) is at least an order of magnitude smaller than the other terms. For the RHI analysis presented in this study, the second term has been dropped. The first term is the divergence of the wind field <u>in the plane</u> of the RHI scan.

Equation (3) can be simplified to:

$$D + \rho_o \frac{\partial W}{\partial z} = 0 \qquad (4)$$

Integration of (4) from z_2 to z_1 $(z_2 > z_1)$ yields:

$$(\rho_o W)_{z1} = (\rho_o W)_{z2} + \overline{\rho_o(z)D}[z_2 - z_1] \qquad (5)$$

Equation (5) can be simplified in practice to:

$$W_{z1} = (\frac{\rho_{o2}}{\rho_{o1}})\ W_{z2} + \overline{\rho_o(z)D\delta z} \qquad (6)$$

With downward integration, round-off and other errors accumulate in the lowest layers resulting in vertical velocities that are much larger than the real field. The variational adjustment scheme is applied to correct the vertical velocity field. The adjustment scheme is discussed in detail in Lin et al. (1986).

4.5 Momentum Fluxes

Given the vertical and horizontal velocity fields, the momentum fluxes (u'w') can be computed. In this study there were enough samples in a particular RHI scan to compute a representative mean. The horizontal and vertical means were subtracted from each grid point:

$u' = u - \bar{u} = -V_r$,

$w' = w - \bar{w}$, and

$u'w'$ = local momentum flux.

4.6 TOGA VS Dual-Doppler at 0653 LST

In order to test the single-Doppler analysis method, a single-Doppler analysis using data from the TOGA radar at 0653 LST was compared with the dual-Doppler analysis at the same time. The 310° azimuth from the TOGA was selected as the best match for the dual-Doppler data. The data presented for the dual-Doppler data were selected along a radial at approximately 315° angle from TOGA.

Figure 4.1a shows a TOGA analysis for the approaching front with strong NW winds at the surface, and strong NW winds above the front aloft. A downdraft of winds occurs at $r = 17$ km due to a convective cell with a reflectivity value of 40 dBZ or greater. The front is located at a low-level convergent area of winds at $r = 24$ km. The reflectivity areas in this plot are a few dBZs stronger than for the dual-Doppler analysis in Fig. 4.2a since the single-Doppler data are unfiltered and will present slightly higher reflectivity and velocity values (Beeson, 1991). The front in the dual-Doppler analysis is also located by the convergent winds at $r = 24$ km. The high reflectivity core in the single-Doppler analysis at $r = 17$ km is somewhat lower in height than the core in the dual-Doppler analysis.

The second plot for the single-Doppler analysis (Fig. 4.1b) shows the vertical velocity (w) field. The w field is very close to the dual-Doppler analysis (Fig. 4.2b) except for a few very small bullseyes of -4 m s^{-1} values that are larger than the dual-Doppler analysis. Notice the large downdraft area ahead of the front that matches well in both figures. Also, the 2 areas of updrafts, r = 20, 5 km high, and the area immediately above the slope of the front match very closely.

From this comparison, it demonstrates that the simplified continuity equation, as described earlier, can be used to obtain vertical velocities in a direction nearly normal to the front from a single-Doppler radar that are realistic in value. The single-Doppler analysis can be used in lieu of a more extensive Doppler radar coverage to obtain meteorological significant phenomena, whenever a convective system behaves quasi two-dimensional in character, such as the case being studied.

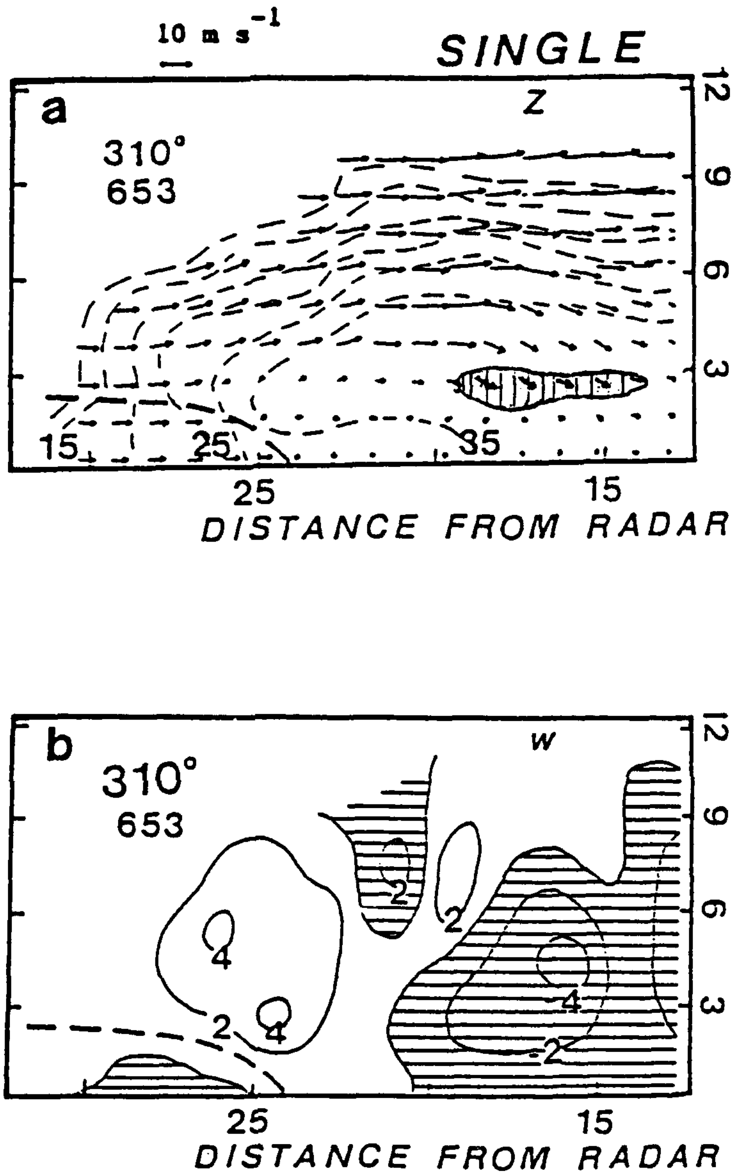

Fig. 4.1 RHI scan at 310° from TOGA radar for (a) reflectivity with winds and (b) vertical velocity (w) for 0653 LST on 25 June 1987. Reflectivity contours are for every 5 dBZ and hatched area > 40 dBZ. W contours are for every 2 m s^{-1} with downward vertical motion denoted by hatched area.

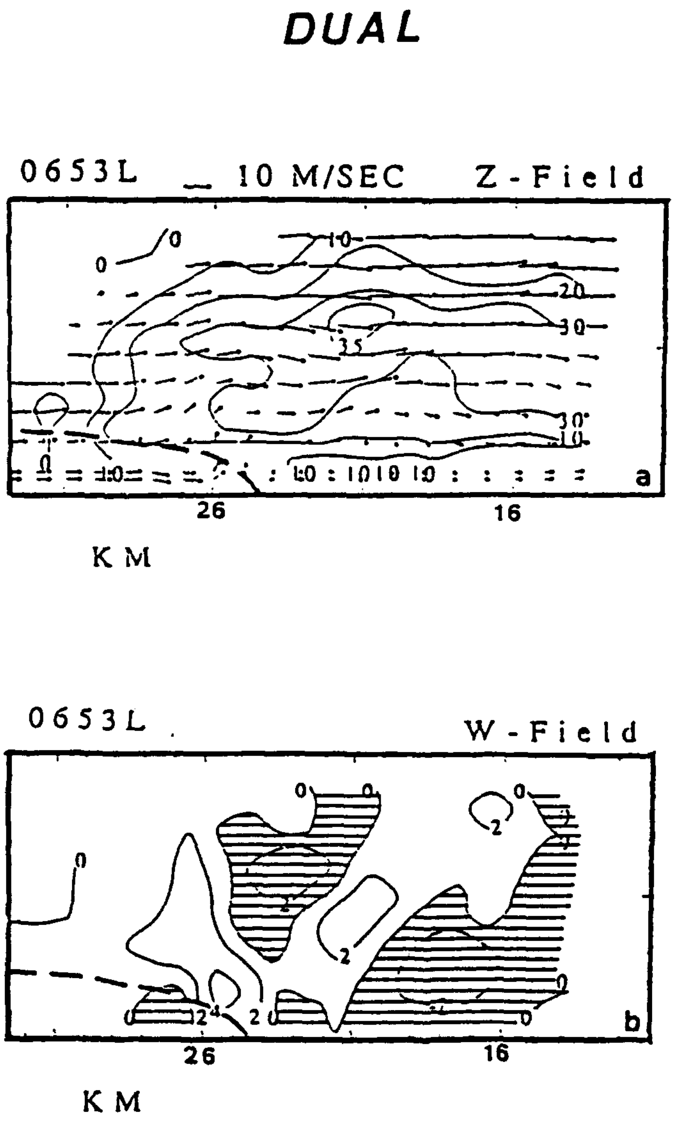

Fig. 4.2 Dual-Doppler RHI scan at nearly a 315° azimuth for (a) reflectivity with winds and (b) vertical velocity (w) for 0653 LST on 25 June 1987. Reflectivity contours are for every 5 dBZ. While w contour interval is for every 2 m s^{-1} with downward vertical motion denoted by hatched area.

Chapter 5: Results

In this study, only the single Doppler data obtained from CP-4 are considered. It is of interest to investigate the system using both PPI and RHI displays at times of interest.

5.1 PPI Scans

CP-4 Doppler data for six time periods starting at 0634 LST and ending at 0706 LST 25 June 1987 were processed. This 40-minute time period was chosen to see the life cycle of a convective cell. Each scan shown encompasses an azimuth from 160° to 60°, or a 260° sector of data. The range markers on all PPI scans from the center of the CP-4, labeled with an N, are at 20 and 40 km. Table 5.1 shows how the CP-4 radar beam elevation angle rises as distance increases from the radar beam. For example, a 0.3° radar elevation angle produces a beam height of 105 m at 20 km away from the radar, and is double that number for 40 km. Finally, the outline of the coast of Taiwan is marked by the dotted N-S line on each PPI plot.

Figure 5.1 shows the reflectivity field at 0.3° for four time periods. A wavy frontal pattern is depicted. Carbone (1982) showed that strong low-level shear of the winds across a cold front can produce small scale vortices on the average of every 13 km along the gust front. For this case, it is seen that the wavelength of these vortices are on the order of

Table 5.1 The height of the radar beam at 20 and 40 km away from the CP-4 radar for five different elevation angles.

CP-4 RADAR ELEVATION ANGLE	DISTANCE FROM RADAR	
	20 km	40 km
0.3°	105 m	210 m
1.8°	628 m	1257 m
3.1°	1083 m	2166 m
6.0°	2094 m	4188 m
9.0°	3141 m	6282 m

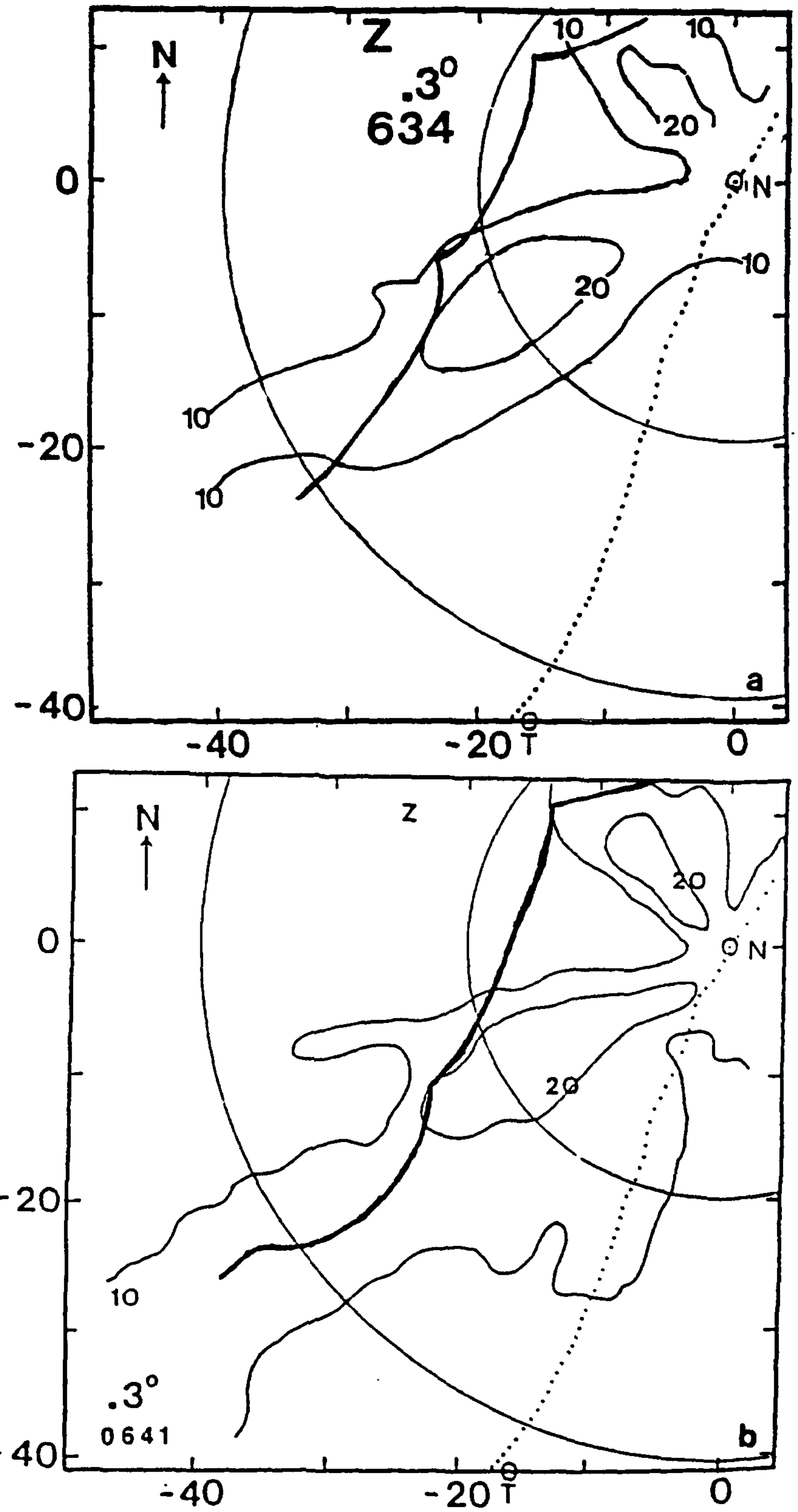

Fig. 5.1 PPI scans for reflectivity field at 0.3° elevation angle from CP-4 radar at (a) 0634 LST and (b) 0641 LST on 25 June 1987. Range markers are at 20 km intervals.

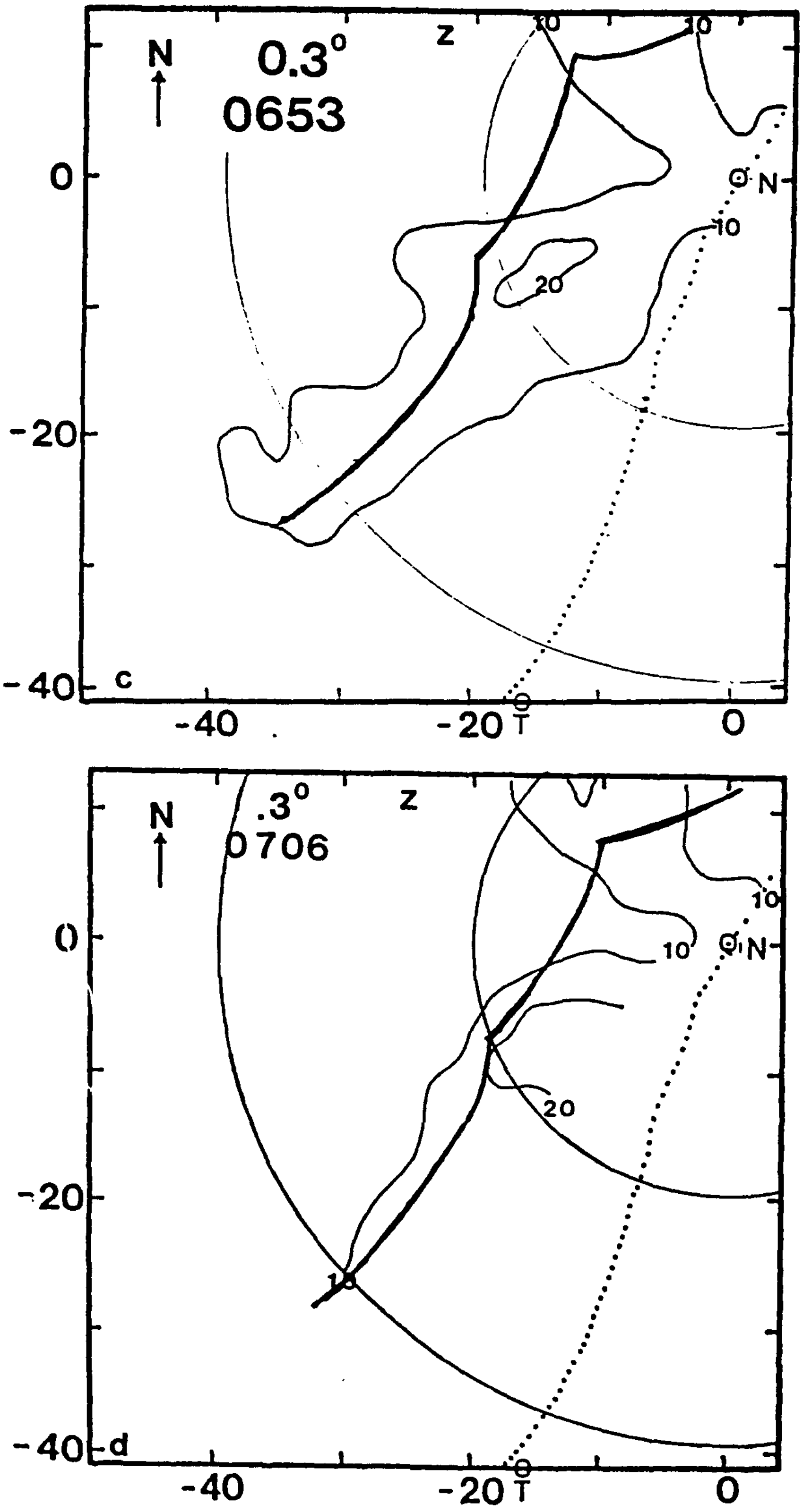

Fig. 5.1 cont. Same as Fig. 5.1 except for (c) 0653 LST and (d) 0706 LST.

15-20 km (Lin et al., 1992). Reflectivity values remain weak throughout the time period with the highest dBZ value only in the low 20s. The V-shaped "notch" is evident in all four time periods behind the front, signifying dry air intrusion from mainland China.

Figure 5.2 (3.1° elevation angle) shows the marked increase in reflectivity values, slightly > 40 dBZ (shaded area), over and around the CP-4 radar during all four time periods, indicative of convective activity. Note that the largest cell moves slightly to the east and closer to the radar with time. A large area of reflectivities > 30 dBZ (hatched area), engulf the area surrounding the radar, indicative of a prefrontal convective rainband on the warm side of the front throughout the 40-minute time span.

The next set of plots, Fig. 5.3, shows the evolution of radar reflectivity values at a 6.0° radar elevation angle. At this angle, a large cell (> 40 dBZ) is found to be on top of the radar site and barely moves in the ensuing 40 minutes. The 9.0° radar elevation angle depicts little movement of the large convective cell over the CP-4 radar (Fig.5.4). A large area of reflectivities > 30 dBZ persists in a semi-circle around the radar site. The trailing region behind the front is mainly a stratiform type precipitation with reflectivities < 30 dBZ. It is noted, however, that the back edge of the 10 dBZ reflectivity contour does move slightly to the east during the 40 minute time period.

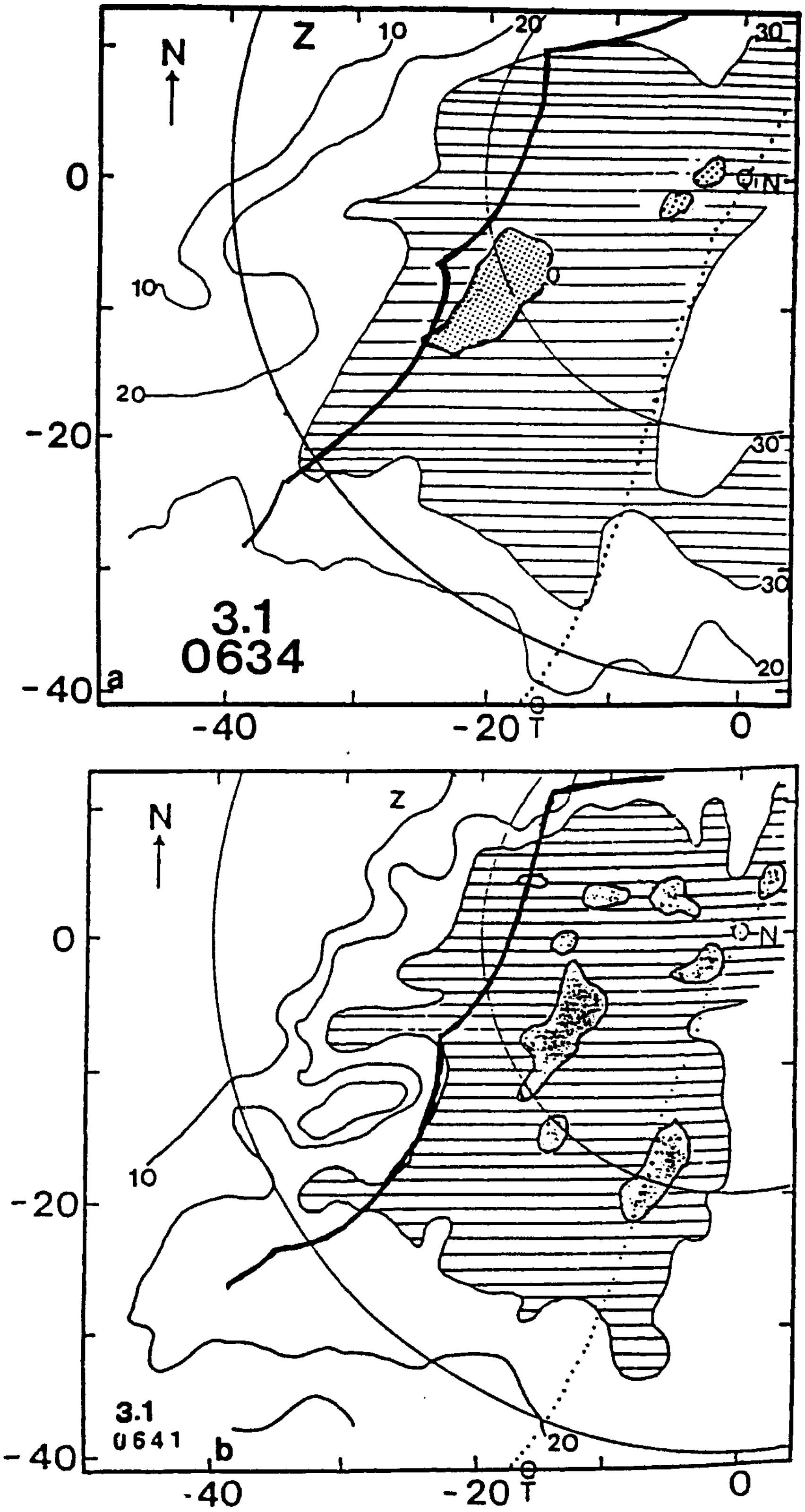

Fig. 5.2 PPI scans for reflectivity field at 3.1° elevation angle from CP-4 radar at (a) 0634 LST and (b) 0641 LST on 25 June 1987.

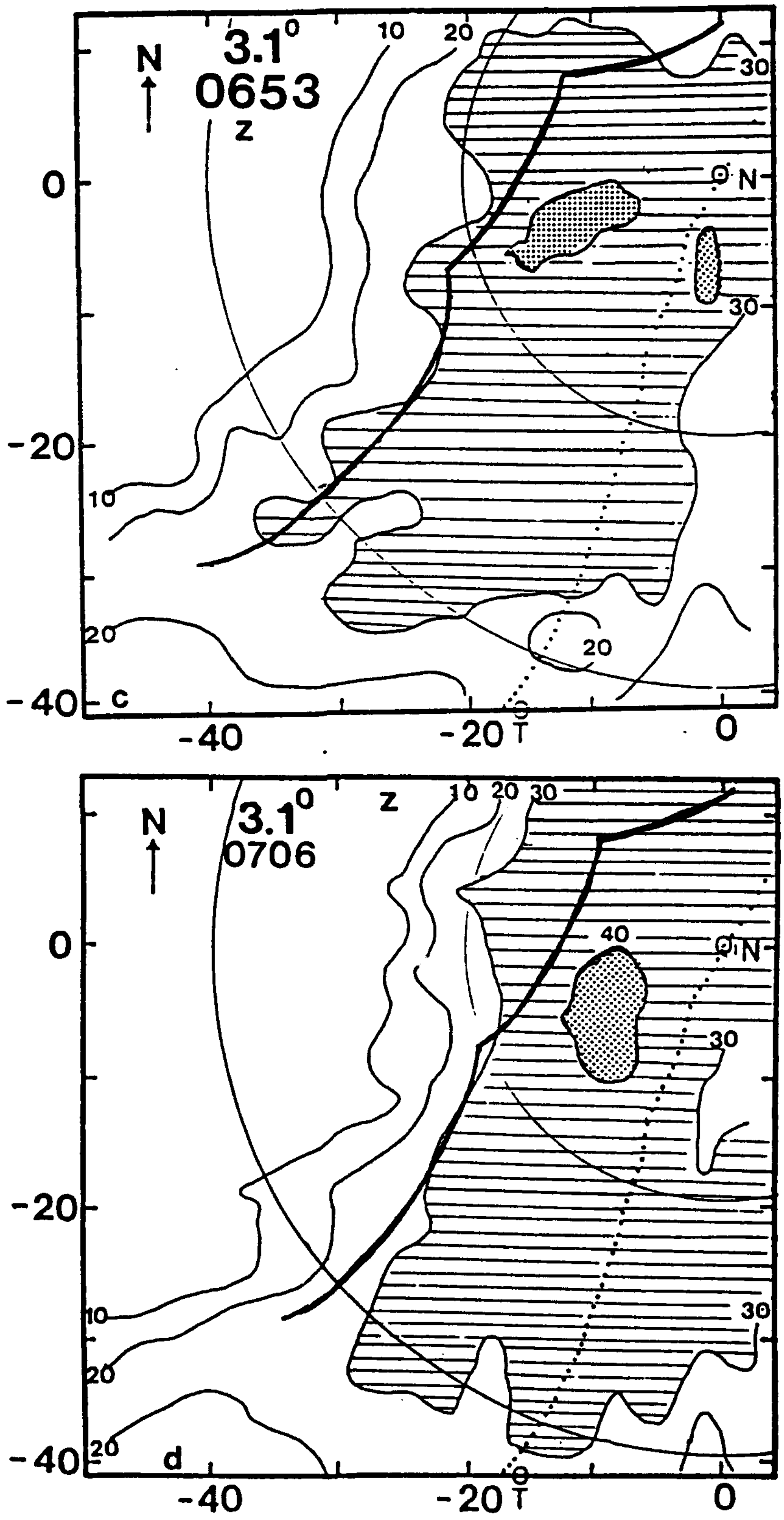

Fig. 5.2 cont. Same as Fig. 5.2 except for (c) 0653 LST and (d) 0706 LST.

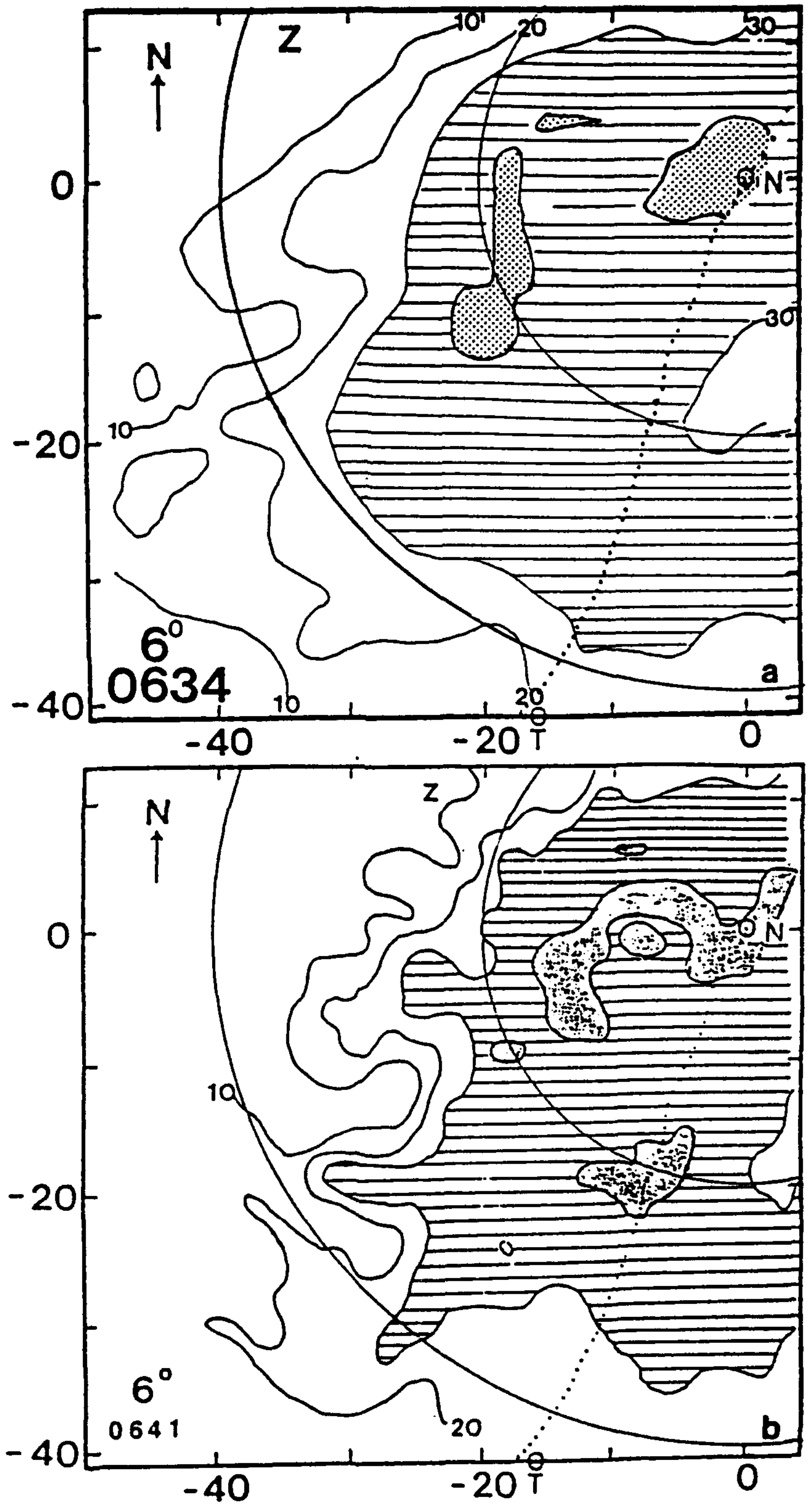

Fig. 5.3 PPI scans for reflectivity field at 6.0° elevation angle from CP-4 radar at (a) 0634 LST and (b) 0641 LST on 25 June 1987.

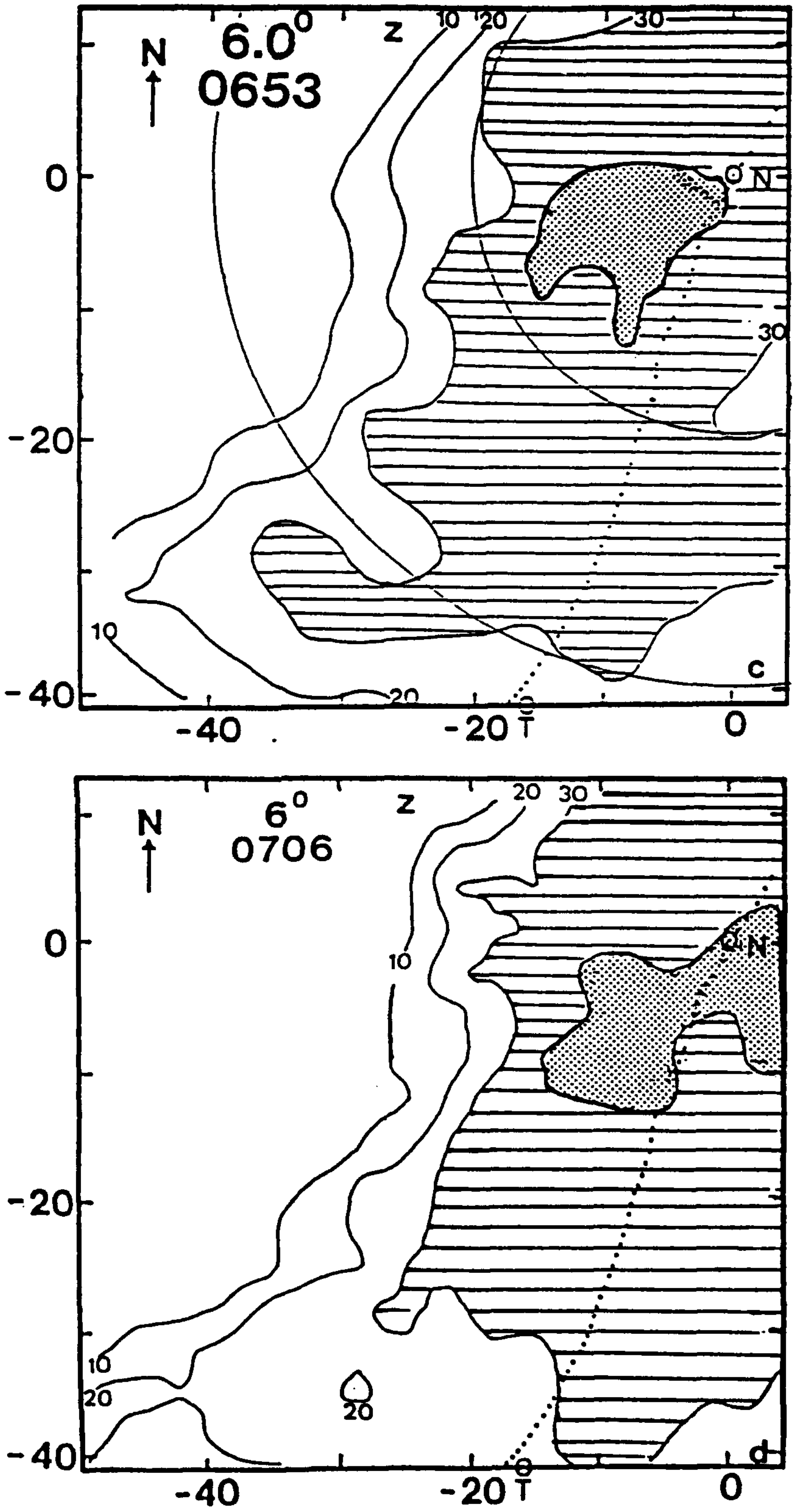

Fig. 5.3 cont. Same as Fig. 5.3 except for (c) 0653 LST and (d) 0706 LST.

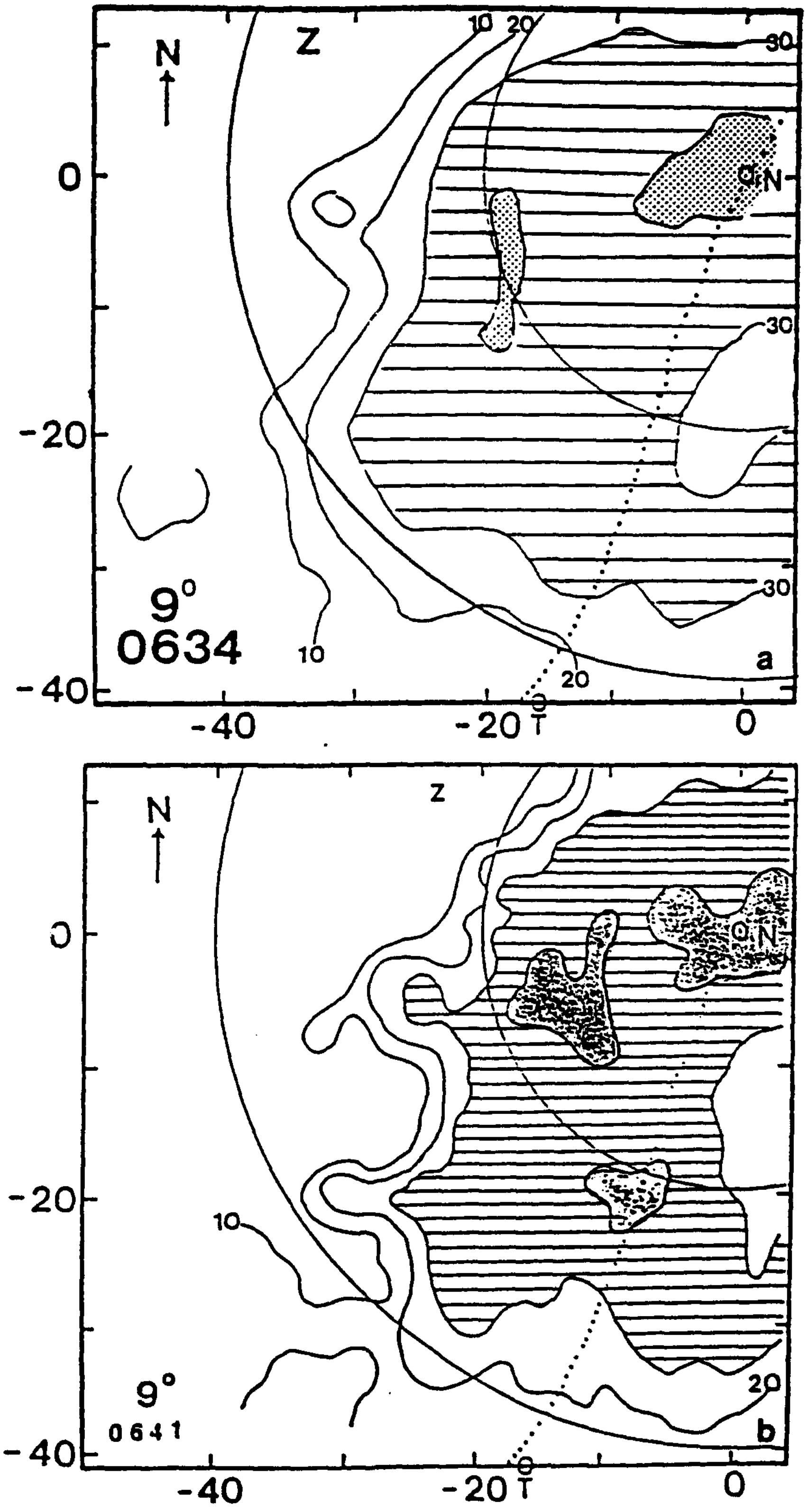

Fig. 5.4 PPI scans for reflectivity field at 9.0° elevation angle from CP-4 radar at (a) 0634 LST and (b) 0641 LST on 25 June 1987.

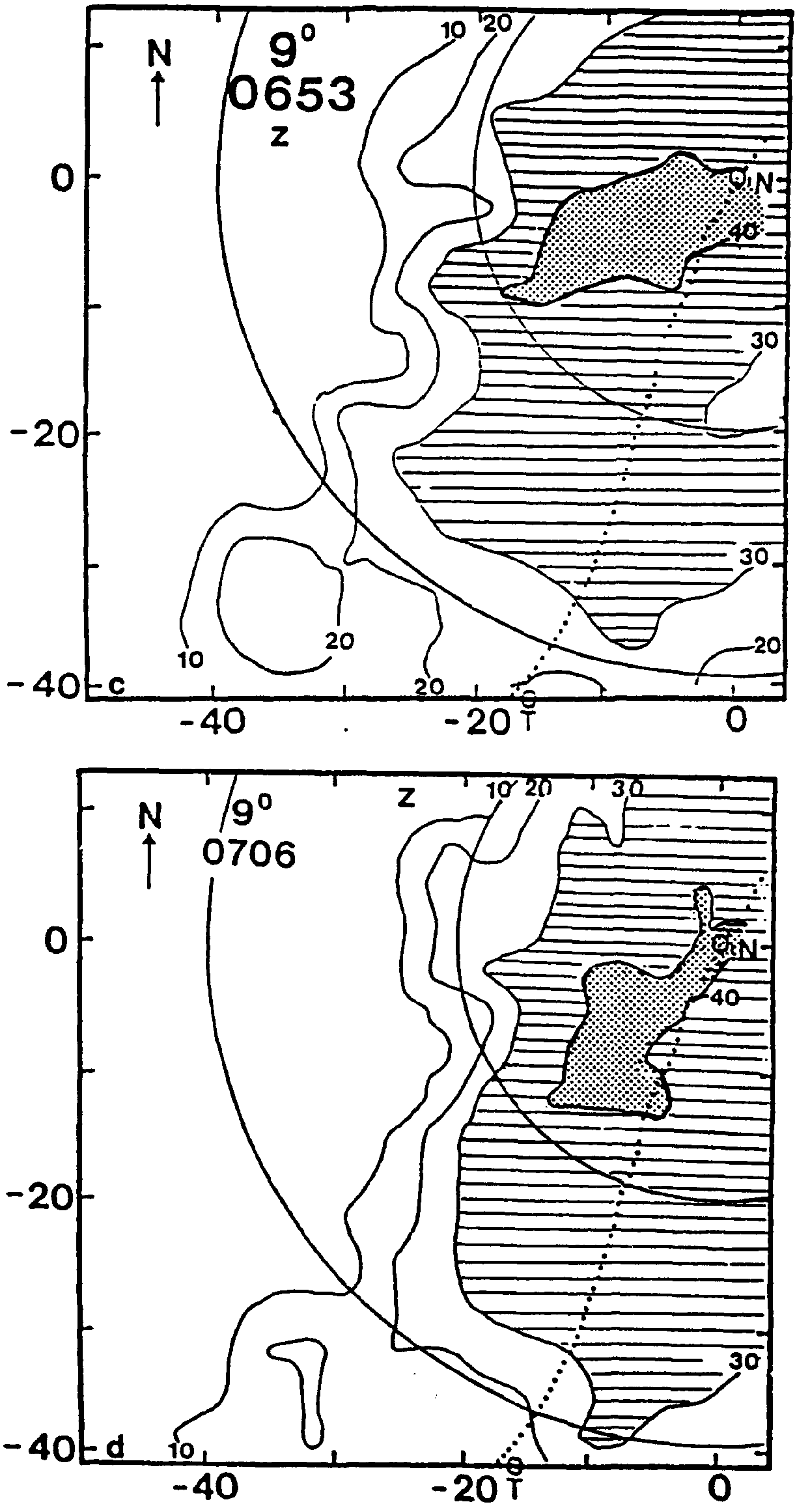

Fig. 5.4 cont. Same as Fig. 5.4 except for (c) 0653 LST and (d) 0706 LST.

The radial velocity (V_r) field at 0.3^o is shown in Fig. 5.5. Remember, the radar beam only rises from the surface to 210 m at a distance of 40 km away from the radar. Positive radial velocities (shaded area) indicate flow away from the radar. In all four time periods this area is found almost exclusively on an E-W band whose southern boundary hugs the CP-4 radar. The negative radial velocity values point out the strong southwesterly flow field to the south of the radar. The compact V_r gradient indicates the shearline (heavy dashed line) moves very little during observation. Notice the small $-V_r$ area to the northwest of the radar on the first three time periods, indicating cooler, northwesterly flow behind the front.

Figure 5.6 shows V_r from a 1.8^o radar elevation angle. Not much has changed from the previous lower angle. The wind flow is predominantly out of the southwest with values > 15 m s^{-1}. The zero-velocity line in Figs. 5.5 and 5.6, (line where winds are normal to the radar beam), is found to be nearly E-W and borders on the CP-4 radar.

The 3.1^o elevation angle for V_r, Fig. 5.7, indicates that the flow is strongest at this level, with some areas of flow seen to be > -18 m s^{-1}, toward the radar.

At 6.0^o (Fig. 5.8), the V_r zero-line begins at the radar site and now stretches to the northwest, instead of the previous E-W line. This indicates veering of the flow field with

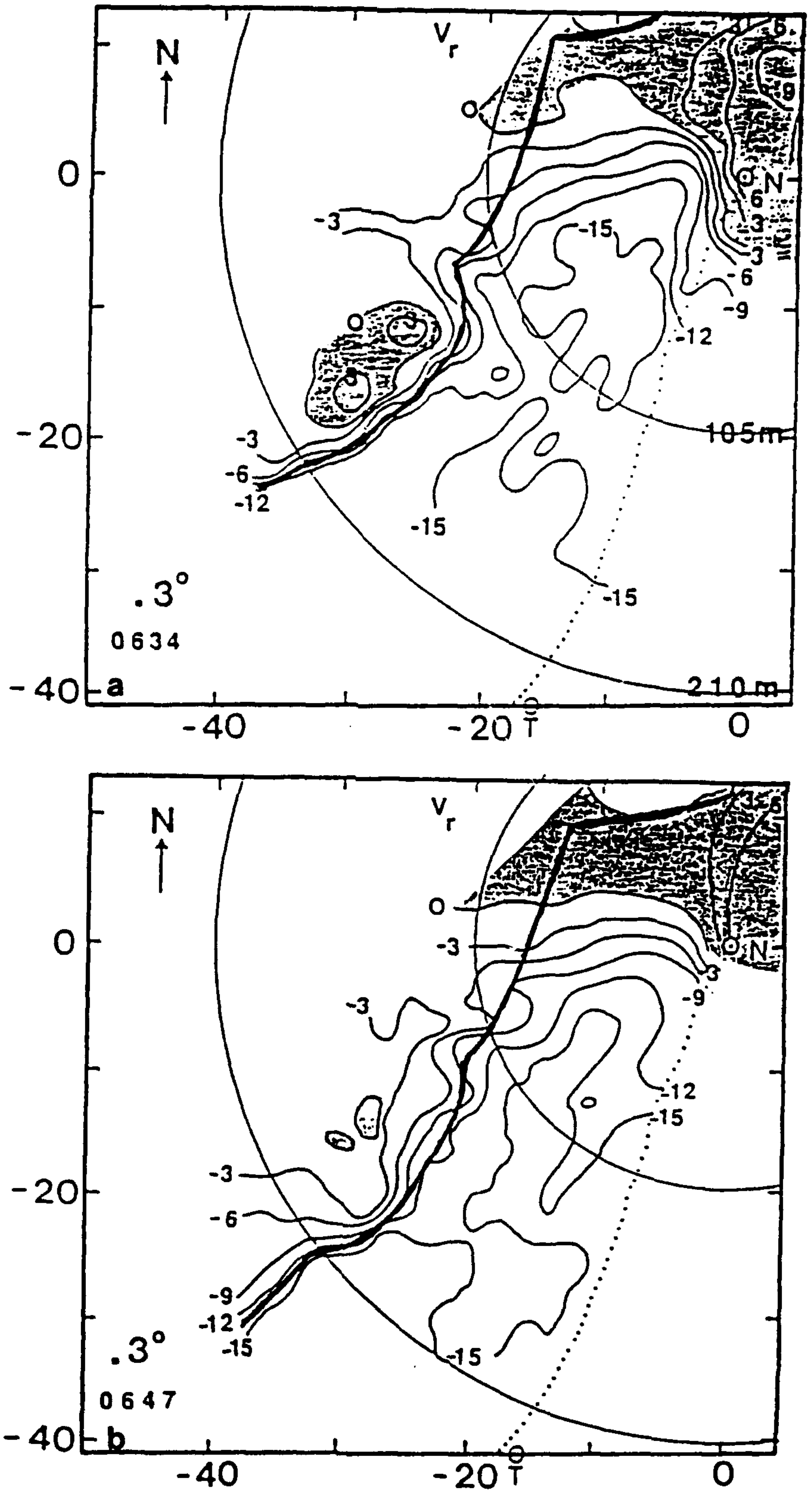

Fig. 5.5 Radial velocity field for 0.3° elevation angle from CP-4 radar at (a) 0634 LST and (b) 0647 LST on 25 June 1987.

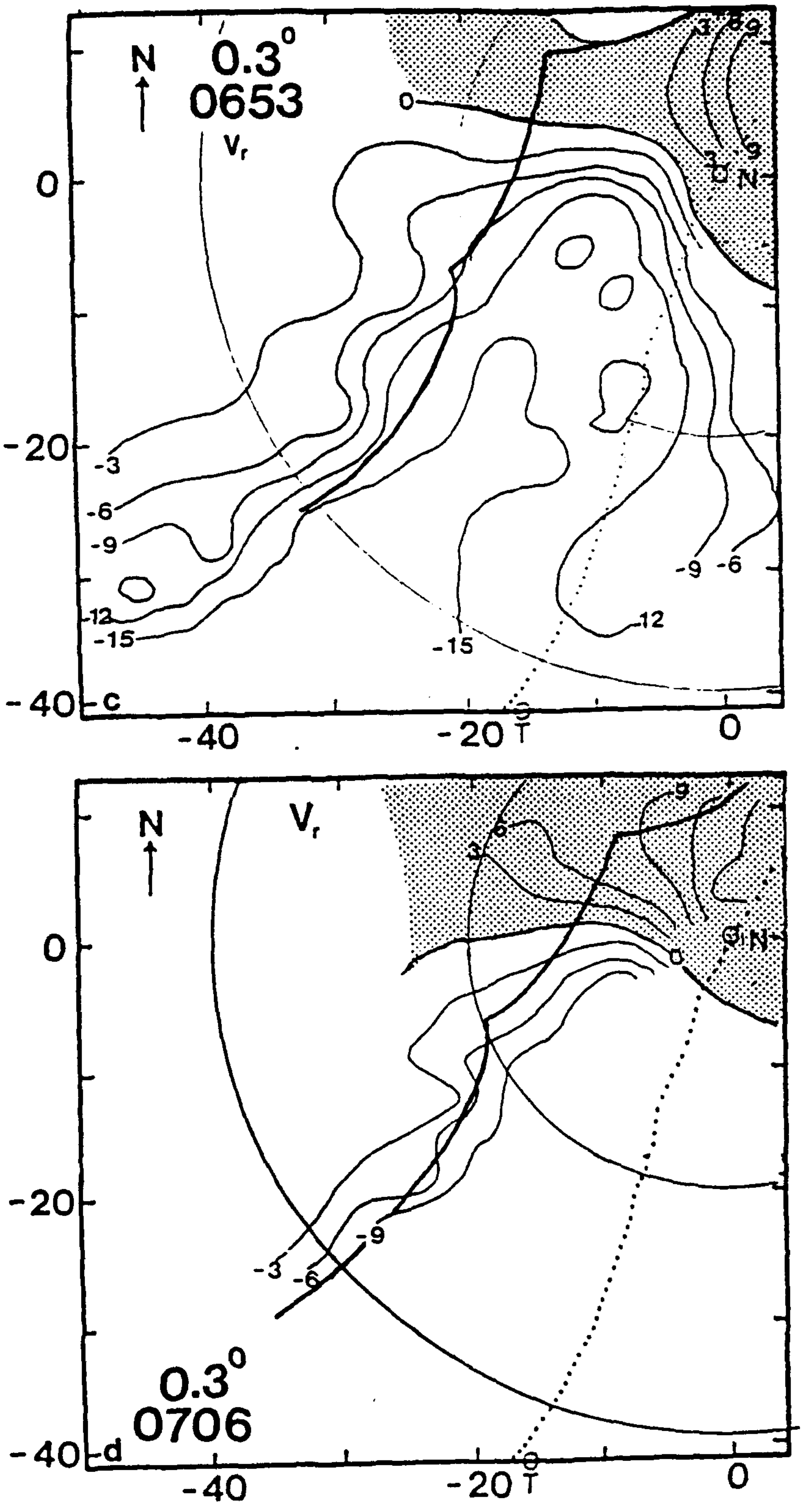

Fig. 5.5 cont. Same as Fig. 5.5 except for (c) 0653 LST and (d) 0706 LST.

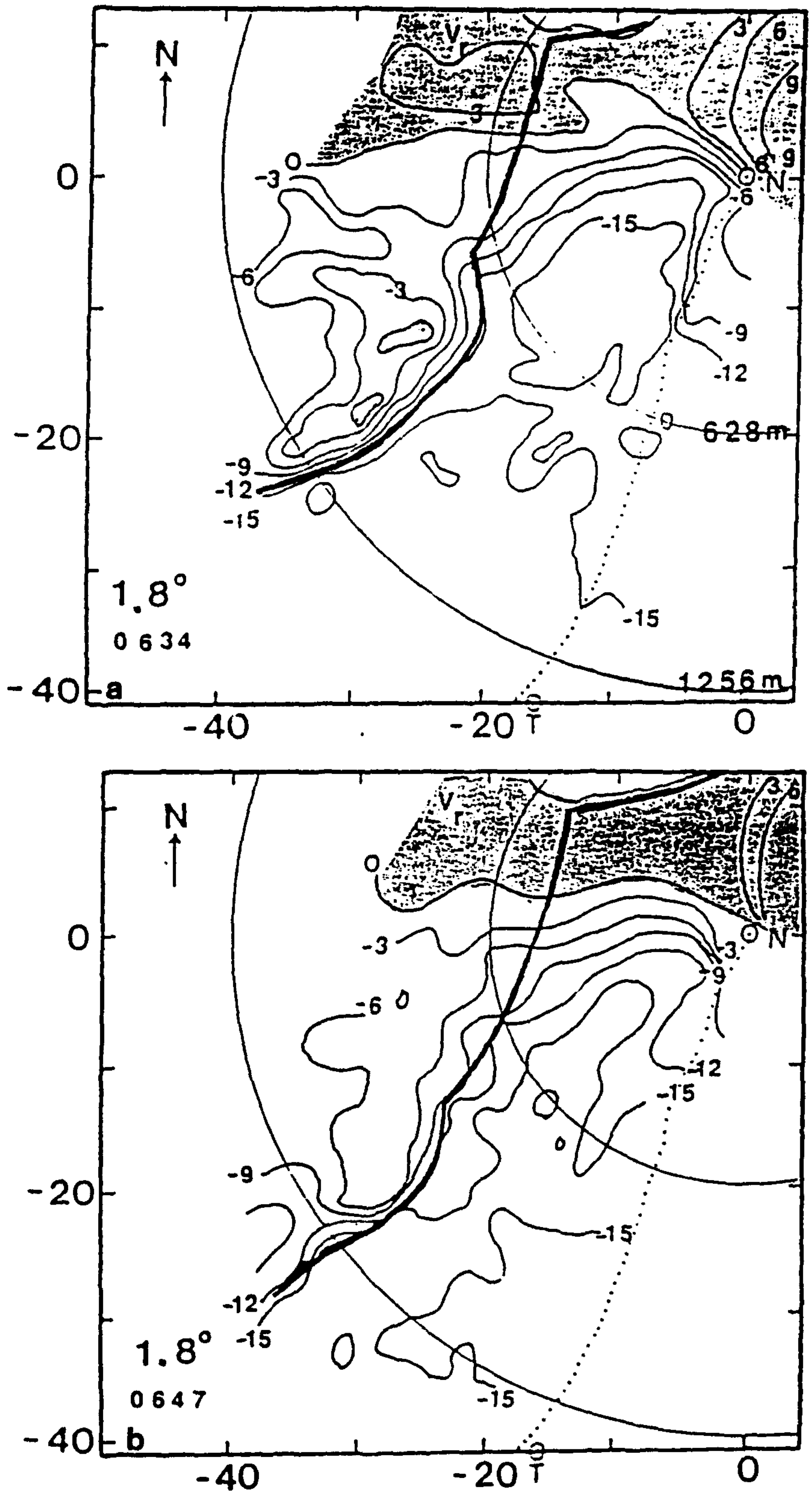

Fig. 5.6 Radial velocity field for 1.8° elevation angle from CP-4 radar at (a) 0634 LST and (b) 0647 LST on 25 June 1987.

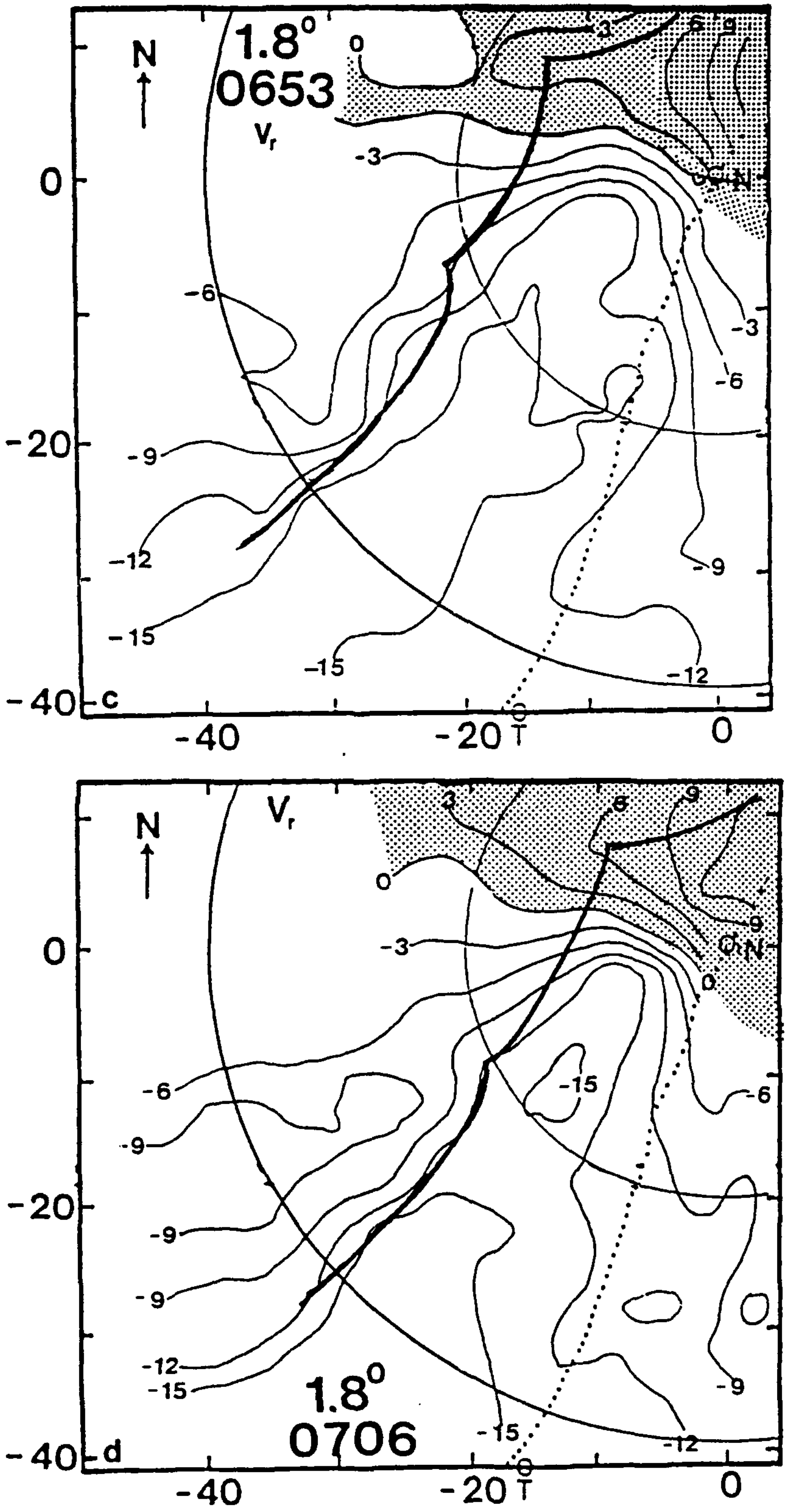

Fig. 5.6 cont. Same as Fig. 5.6 except for (c) 0653 LST and (d) 0706 LST.

height and points out the winds are becoming predominantly northwesterly in the NW quadrant of the plot. Remember, at 20 km away from the radar the beam is 2.1 km high, or just above the height of the shallow approaching cold front, and at 40 km it is 4.2 km high.

Finally, the 9.0° elevation angle (Fig. 5.9), shows V_r is almost entirely negative, except in the NE quadrant that abutts the radar site. This is further evidence of the southwesterly monsoon flow in the warm sector, while the flow behind the surface front veers to the NW pulling in cooler, drier air from the mainland of China.

5.2 RHI Scans at 300° Radial

RHI data are presented for six-consecutive time periods, same as the PPI data, from the CP-4 radar. The first set of plots involves RHI displays along a 300° azimuth and the second set along a 330° azimuth. These azimuths were selected as they both slice across the Mei-Yu front at nearly 90° angles. The plots presented are displayed in four panels for each time period to include: (1) Reflectivity with winds; (2) Radial velocity; (3) Vertical velocity, and (4) Divergence. Contours for reflectivity are displayed in 5 dBZ intervals. Radial velocity values are presented using 2 $m\ s^{-1}$ intervals, while vertical velocity is shown using 1 $m\ s^{-1}$ contours. Divergence is displayed for the first 3 time periods with intervals of $0.5 \times 10^{-3}\ s^{-1}$, while the last 3 time

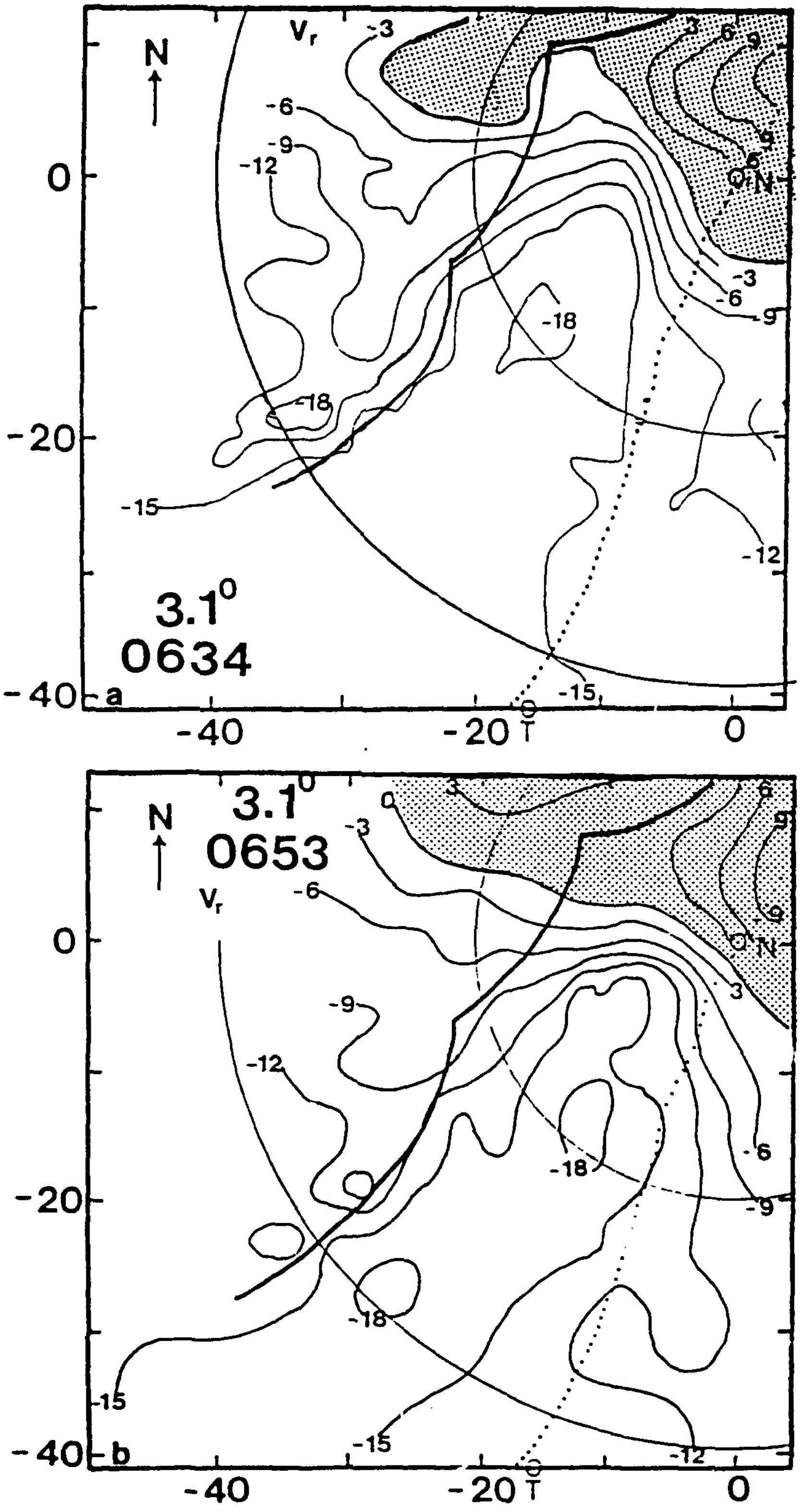

Fig. 5.7 Radial velocity field for 3.1° elevation angle from CP-4 radar at (a) 0634 LST and (b) 0653 LST on 25 June 1987.

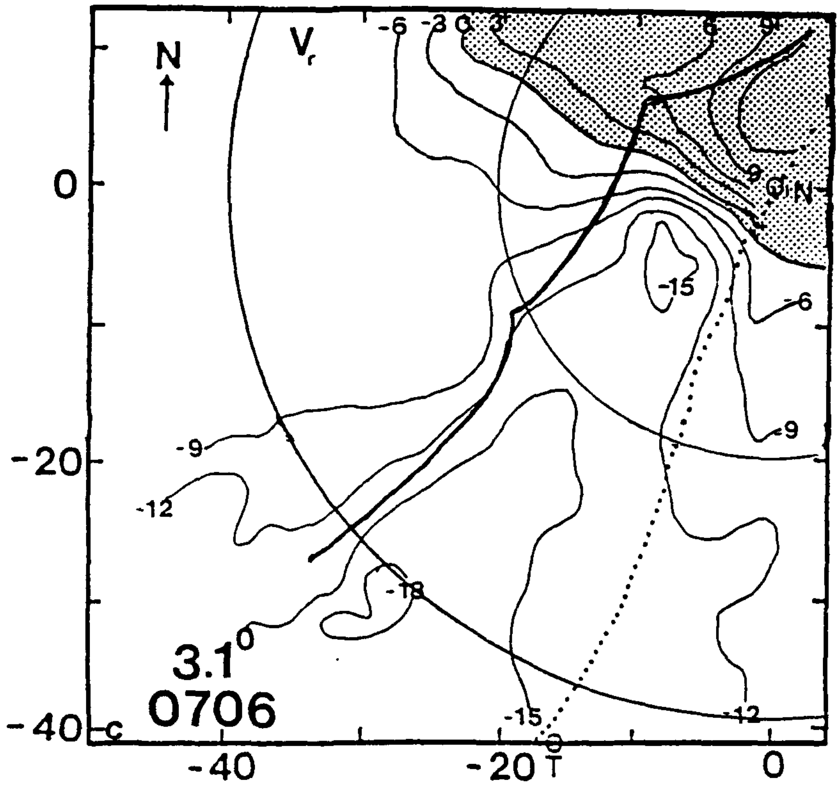

Fig. 5.7 cont. Same as Fig. 5.7 except (c) 0706 LST.

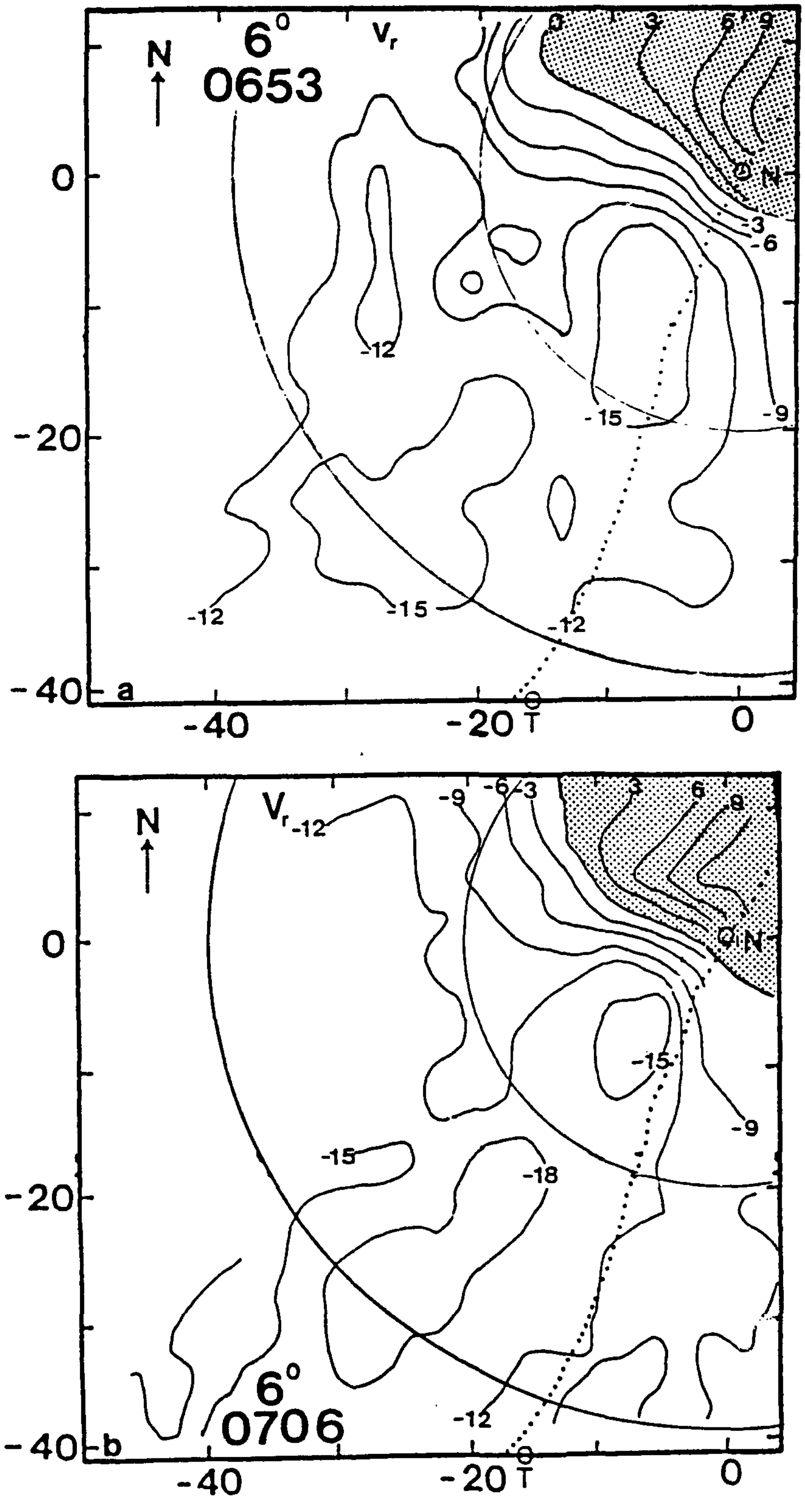

Fig. 5.8 Radial velocity field for 6.0° elevation angle from CP-4 radar at (a) 0653 LST and (b) 0706 LST.

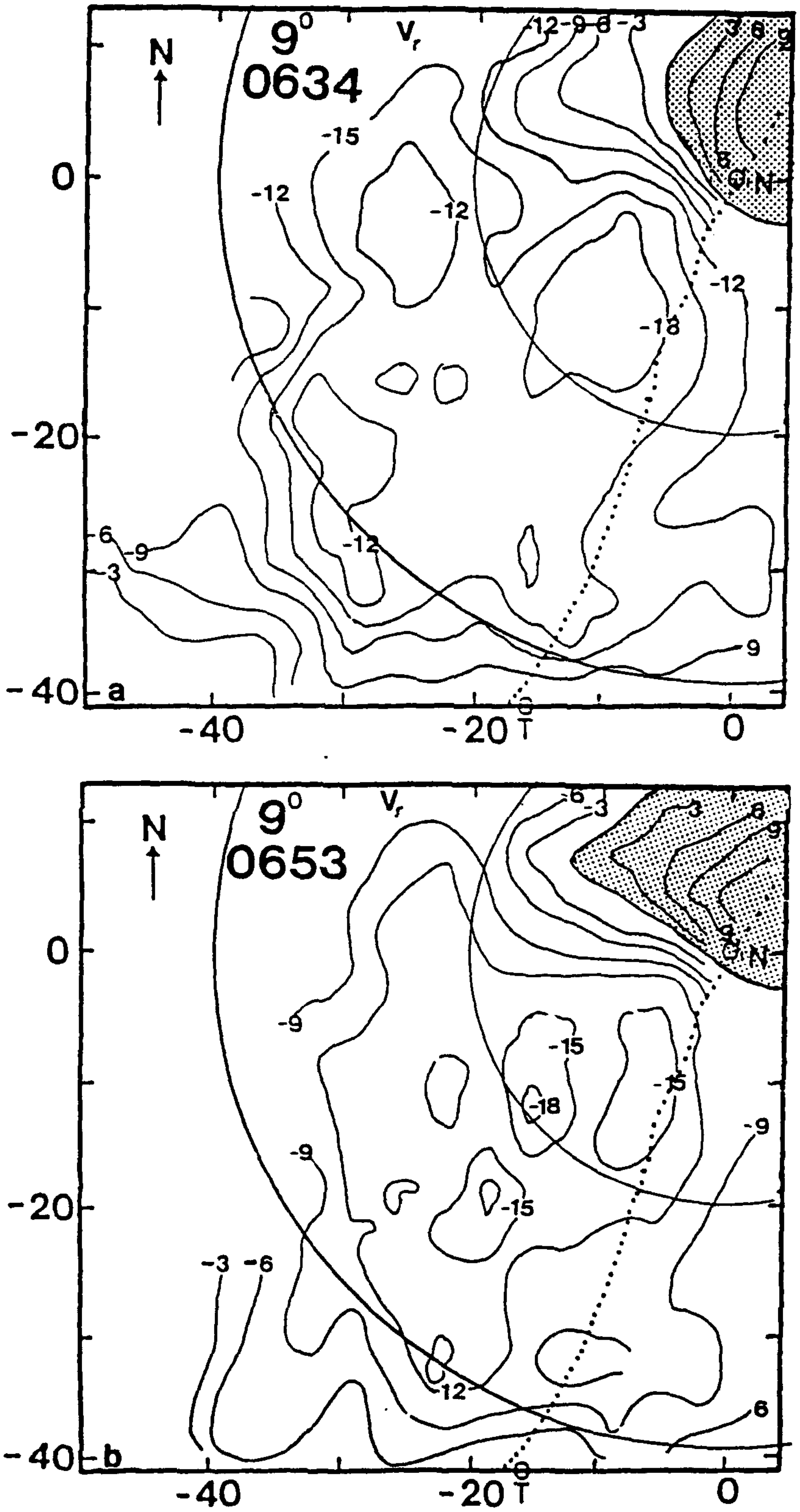

Fig. 5.9 Radial velocity field for 9.0° elevation angle from CP-4 radar at (a) 0634 LST and (b) 0653 LST on 25 June 1987.

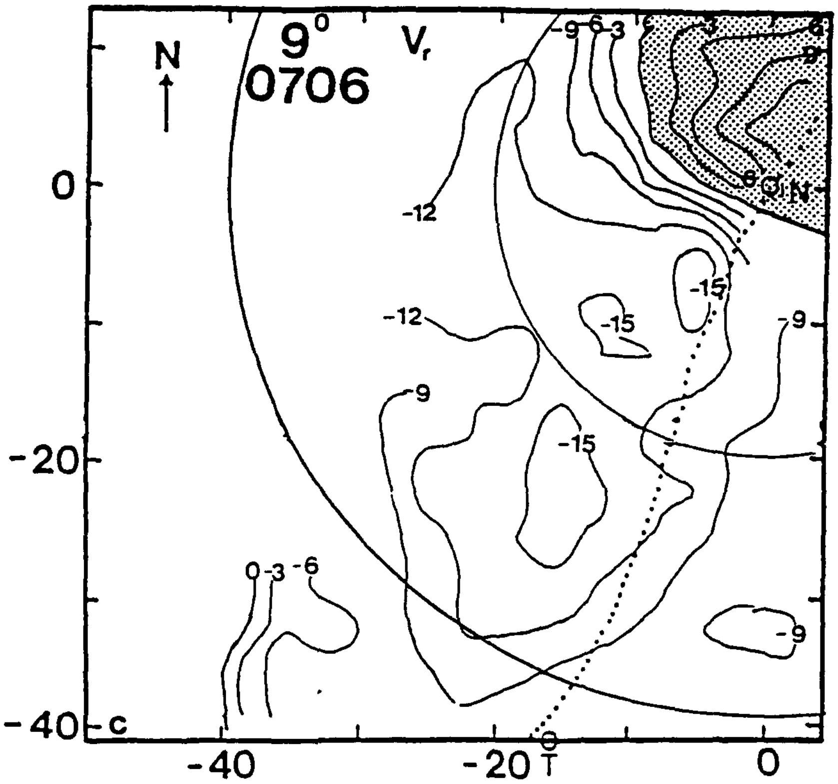

Fig. 5.9 cont. Same as Fig. 5.9 except for (c) 0706 LST.

periods use a contour of 1.0×10^{-3} s^{-1}.

At 0634 LST (Fig. 5.10), the reflectivity field shows two maximum cores (shaded) centered at r = 13 and 17 km, 3 km high. The intersection of the Mei-Yu front and the surface is at 17.5 km away from the radar in an area of low level weak winds. Positive radial velocities are found in a shallow layer (surface to 3 km) mainly in the cold air behind the front indicating a northeasterly component. From earlier dual-Doppler studies the cold air was seen to be confined to the lowest two kilometers above the surface (Lin et al., 1990; Pasken and Lin, 1991). In the middle layer, the strongest winds behind the front are seen to flow into the rainband, showing the prevailing northwesterly flow. Weak negative vertical velocities at the front and ahead of the front appear to be caused by precipitation loading in the high reflectivity regions. A 2 m s^{-1} upward velocity maximum is found at r = 23 km due to the release of latent heat by condensation creating buoyant parcels. There is slight convergence at the surface in association with the front. An area of weak divergence is found in the prefrontal region due to falling precipitation particles from the thunderstorm that contact the surface and spread out horizontally.

Figure 5.11 refers to the same four panels as before except for 0641 LST. The Mei-Yu front is now located at r = 17 km. A high reflectivity core (> 35 dBZ), found in the first time period, has shifted closer to the radar and lower to the

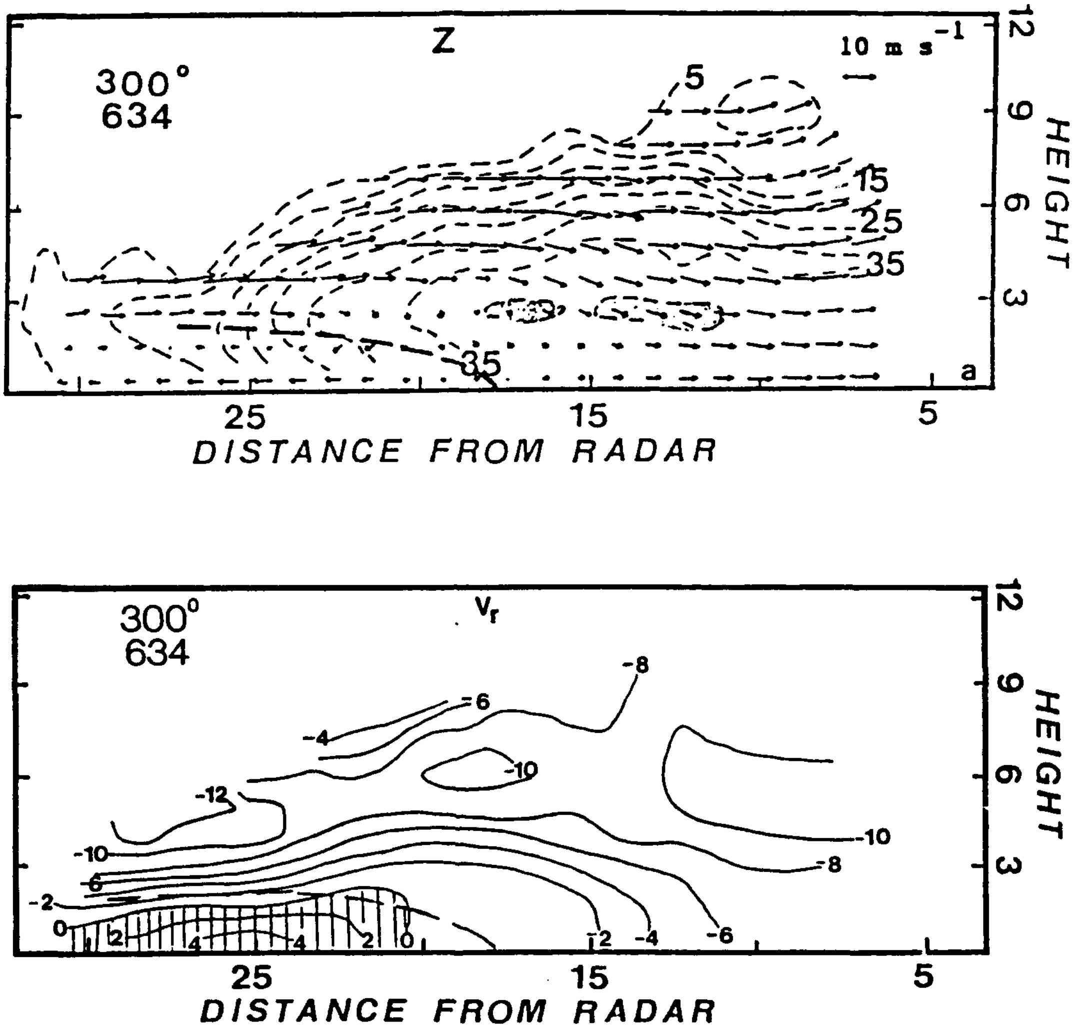

Fig. 5.10 RHI scan at 300° from CP-4 radar for (a) reflectivity with winds and (b) radial velocity for 0634 LST. Reflectivity contours every 5 dBZ and shaded area > 40 dBZ. Radial velocity contour every 2 m s^{-1} with positive areas (away from radar) denoted by hatching.

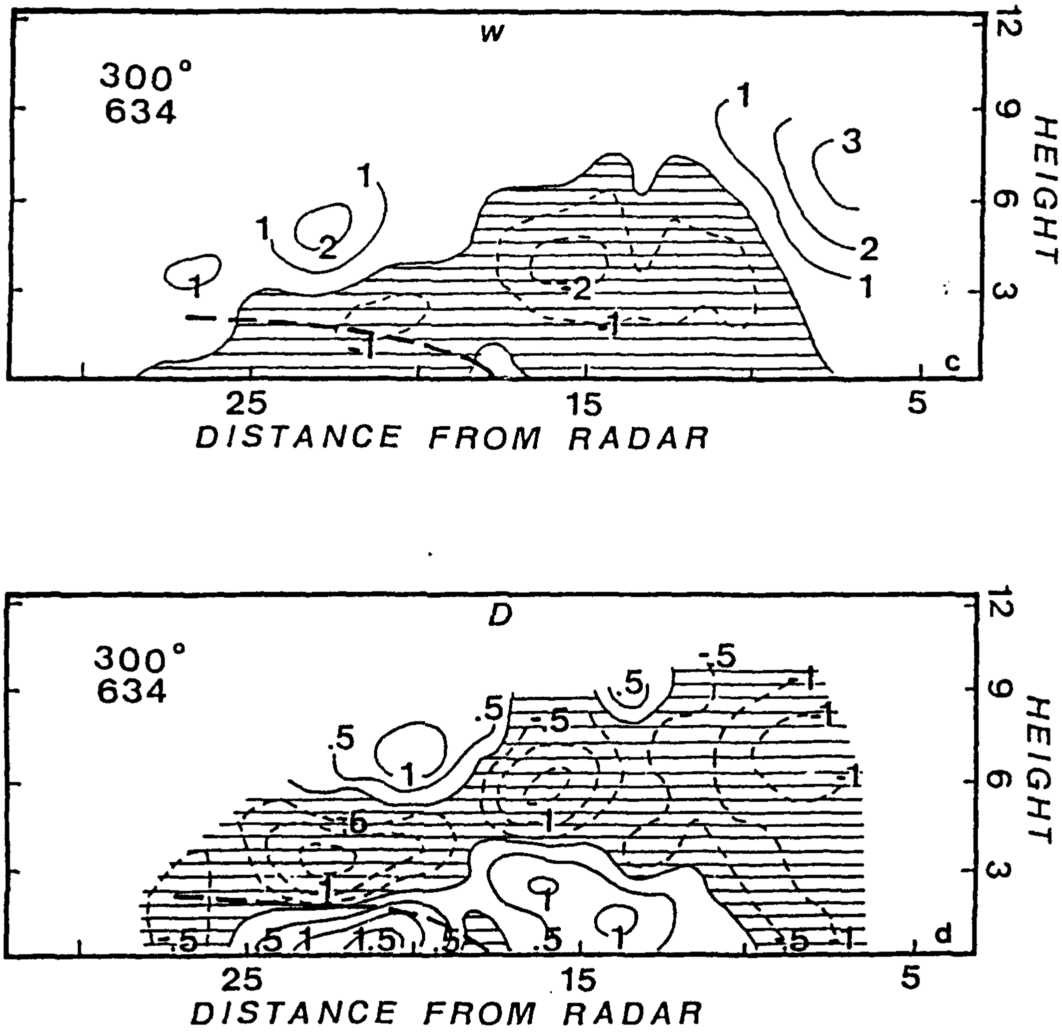

Fig. 5.10 cont. RHI scan at 300° from CP-4 radar for (c) vertical velocity (w) and (d) divergence. W contour interval every 1 m s^{-1} with downward vertical motion denoted by hatched area. Divergence contour for every 0.5 x 10^{-3} s^{-1} with convergence shown by hatched area.

ground due to precipitation drag centered at r = 10 km. The prefrontal downdraft has strengthened with a maximum of -3 m s^{-1} in an elongated core at r = 13 km. A cell > 40 dBZ (shaded) is beginning to strengthen at r = 8 km, 5 km high, and is associated with an area of maximum upward vertical velocity. Slight convergence at the surface surrounded by divergence values denotes the frontal boundary.

Figure 5.12 shows the same fields as Fig. 5.11, but 7 minutes later. A large area or core of reflectivity > 35 dBZ still exists above and in the prefrontal region. The maximum height of the 5 dBZ contour has decreased by nearly 3 km and there are no cells > 40 dBZ to be found. Radial velocities are positive underneath the front with a maximum of 4 m s^{-1}. This still indicates northeasterly flow of cooler air in the lowest 2 km behind the front at r = 16 km. Of interest is the decrease of the negative V_r area as the cell began to collapse. The contour of zero vertical velocities has fallen nearly 3 km in 7 minutes to a level of 6 km. At the same time, a notch of upward vertical velocities is found at r = 15 km, 3-8 km high. Divergence at the surface dominates in both postfrontal and prefrontal areas which may be due to heavy precipitation.

Figure 5.13 is the same as Fig 5.12 except for 0653 LST. The front is located at r = 15 km. The large high reflectivity core (> 35 dBZ) has shifted further ESE toward the radar. A small reflectivity core > 35 dBZ behind the front at

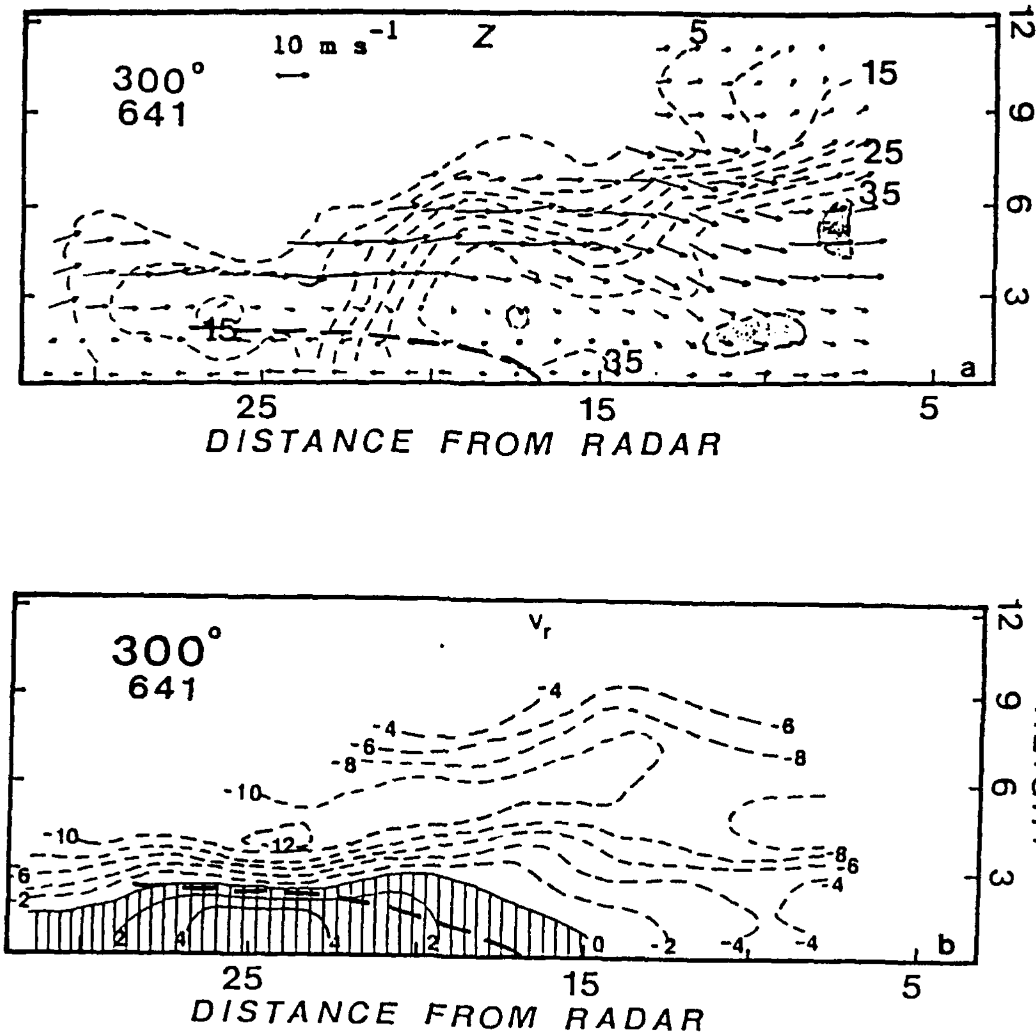

Fig. 5.11 Same as Fig. 5.10 a,b except for 0641 LST.

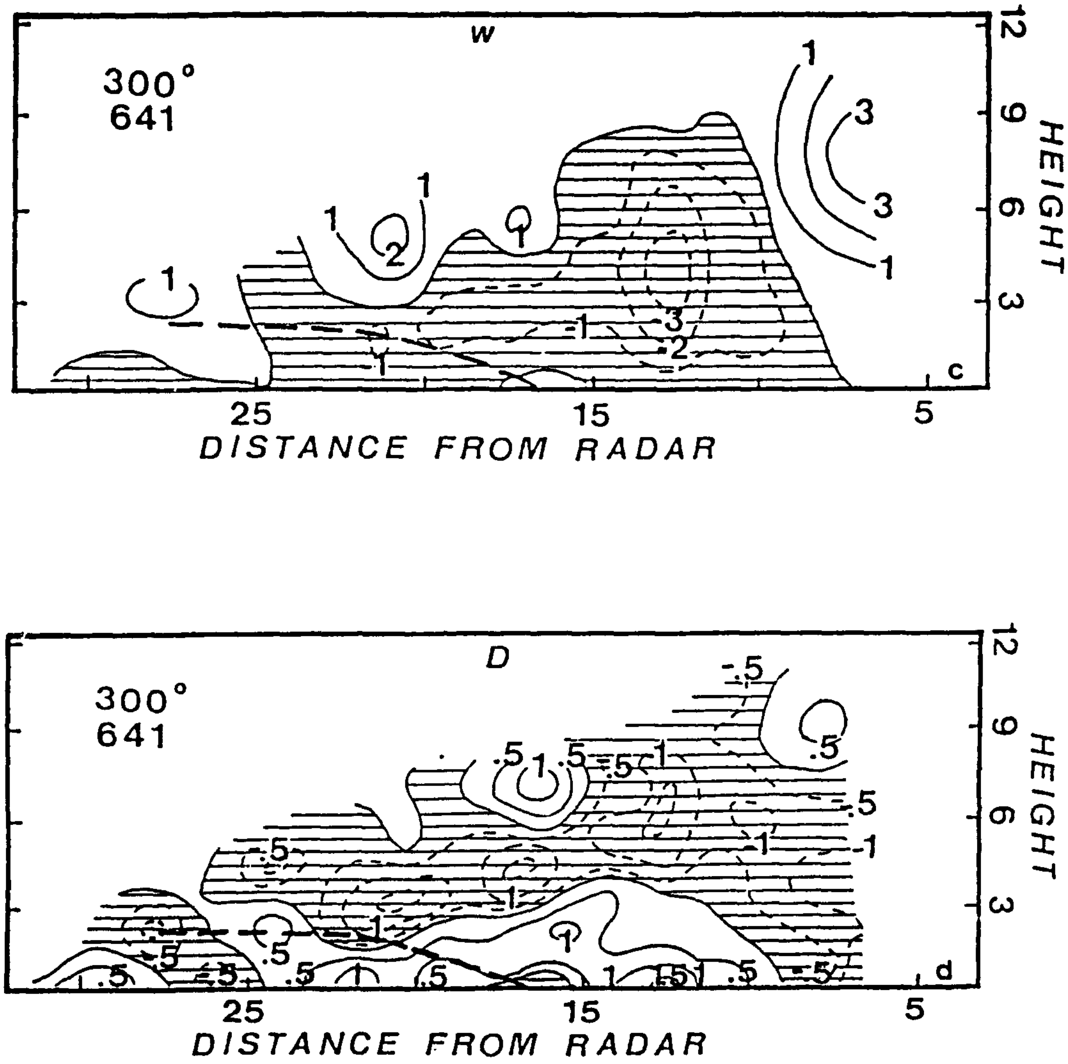

Fig. 5.11 cont. Same as Fig. 5.10 c,d except for 0641 LST.

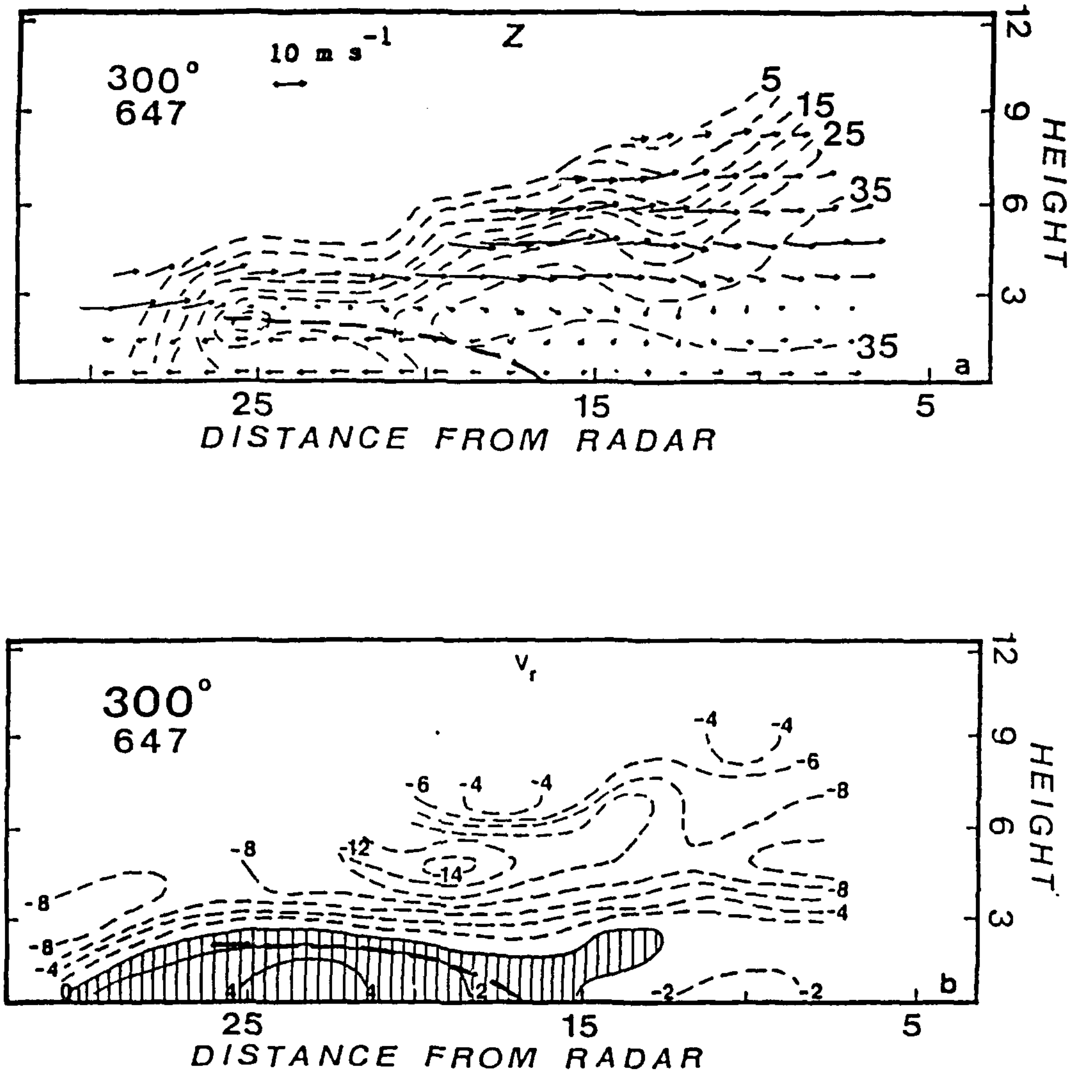

Fig. 5.12 Same as Fig. 5.10 a,b except for 0647 LST.

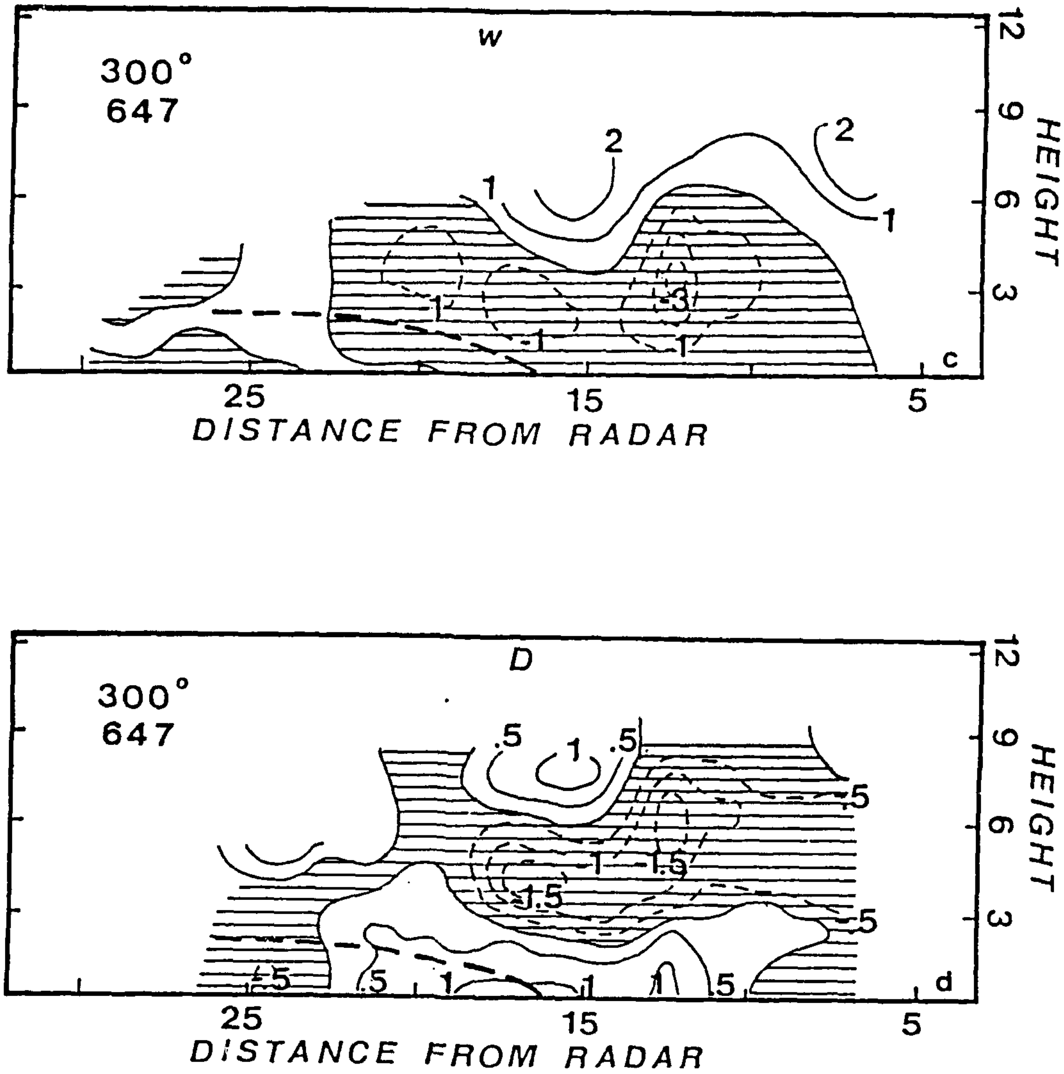

Fig. 5.12 cont. Same as Fig. 5.10 c,d except for 0647 LST.

r = 20 km, 3 km high, indicates the development of a new cell. Positive radial velocities dominate underneath the surface front as cool northeasterly air from northern China flows across northern Taiwan. The downward air flow and negative vertical velocities ahead of the front in mid to low-levels still support the idea that precipitation drag is the dominant force associated with the highest reflectivity cores. Slight divergence at the surface can not be used to pinpoint the frontal location due to the obscuring rainfall.

The time period of 0700 LST, (not shown), depicts a continued strengthening of a cell at a location near 3 km high, r = 17.5 km. Radial velocities are similar to prior time periods. Upward vertical velocities of 2 m s^{-1} are found in the vicinity of the developing cell, while slightly negative velocities are found over the entire lowest 2 km near the surface. The front has moved slightly closer to the radar and is found at r = 14.5 km. The wind field shows a situation similar to the previous time periods with strong postfrontal flow nearly perpendicular to the front, while prefrontal low-level winds are very weak indicating winds blowing parallel to the front.

The final time period (0706 LST) is shown in Figure 5.14. It is interesting to note that the developing cell at r = 17 is in the same position, but has been elongated along the radar. These elongated contours are indicative of the northwesterly airflow. The frontal position has moved 3.5 km closer to the radar from its starting position in the initial

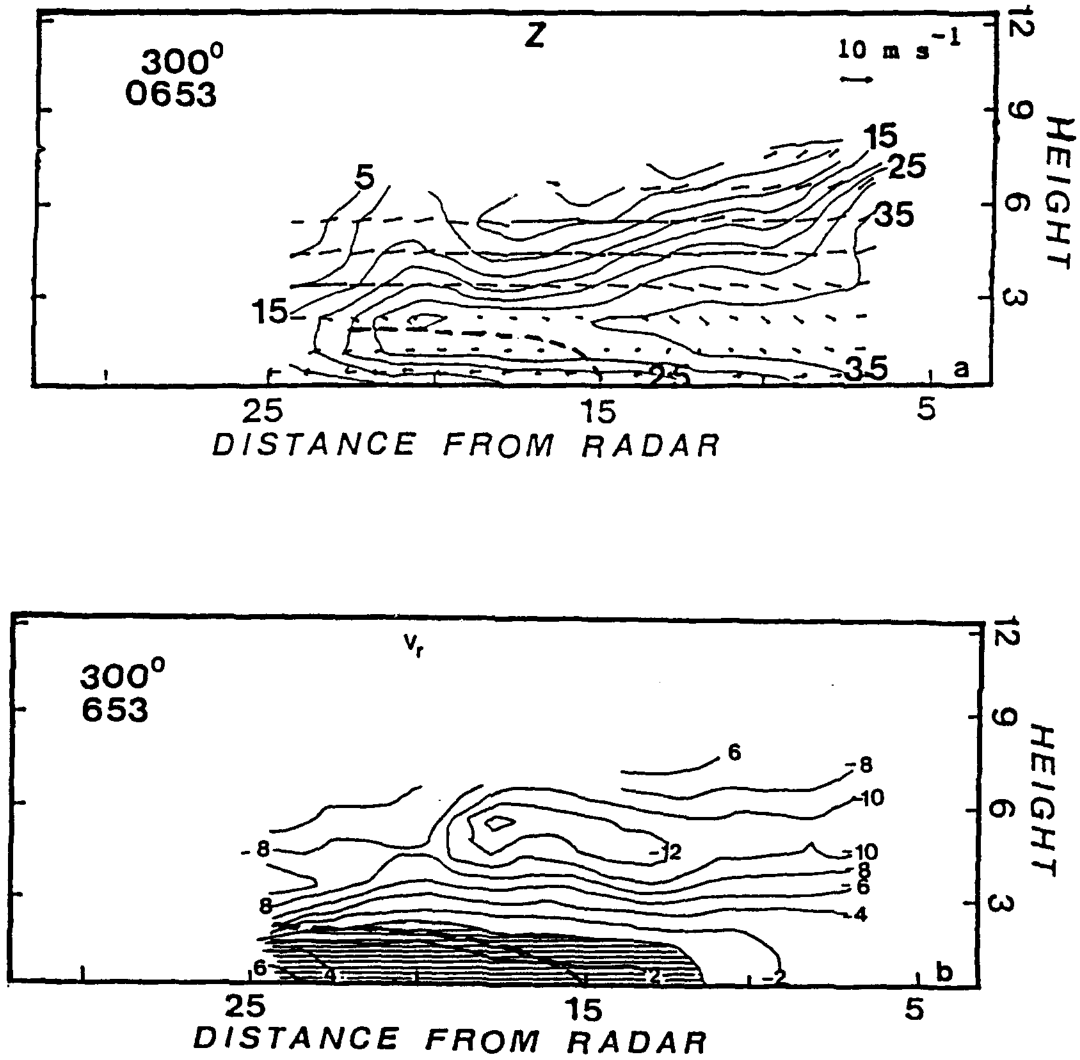

Fig. 5.13 Same as Fig. 5.10 a,b except for 0653 LST.

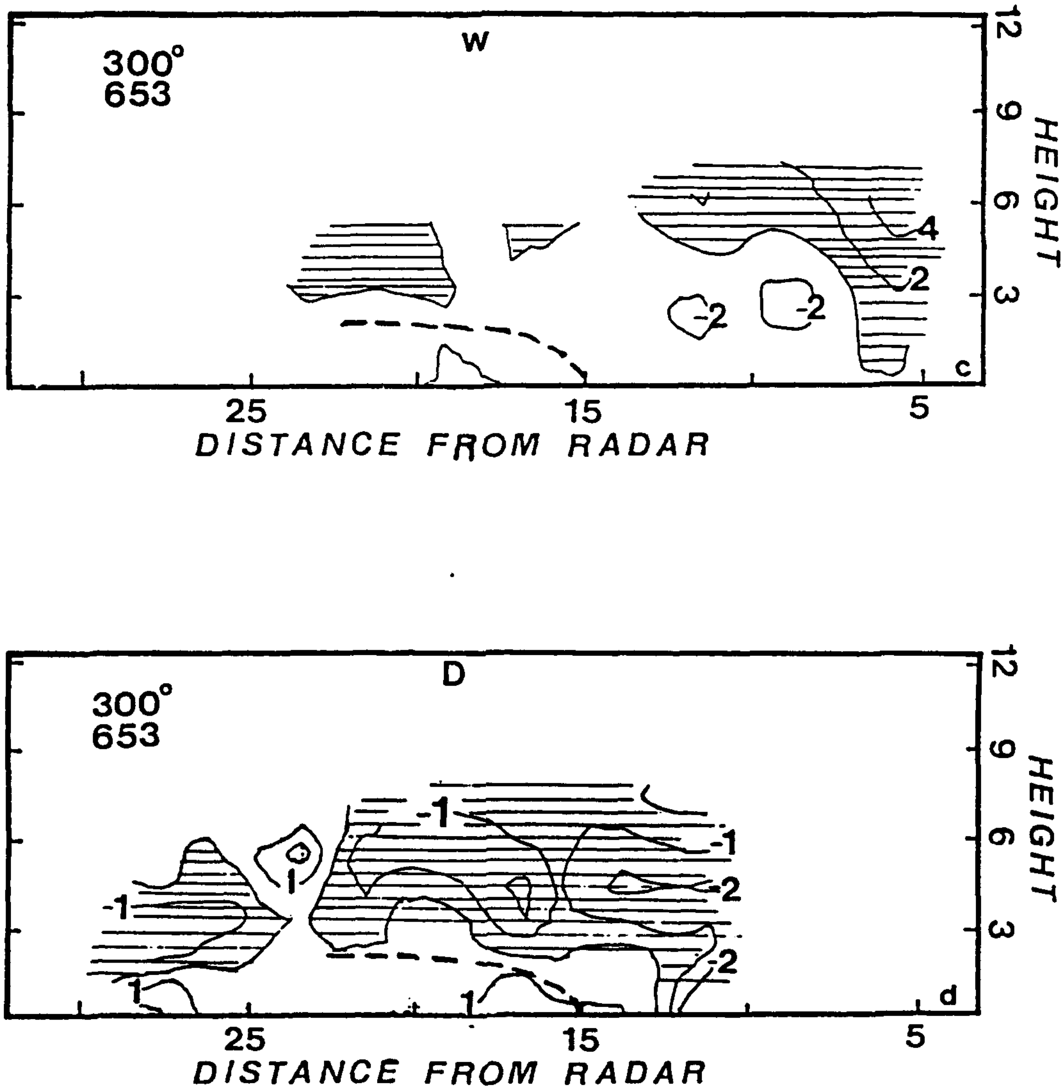

Fig. 5.13 cont. RHI scan at 300° from CP-4 radar for (c) vertical velocity and (d) divergence with interval of 1.0 x 10^{-3} s^{-1} and hatched area indicative of convergence. Contour interval for w is 1 m s^{-1}, but note that hatched area denotes upward vertical velocity.

time period. The V_r field is still similar to past times with a core of maximum negative values (flow toward the radar) centered nearly at mid-levels above the leading edge of the front. Minimum convergence occurs just behind the front in the postfrontal area from $r = 15.2$ to 18 km.

Throughout the 40 minute depiction of the meteorological fields for the 300° azimuth, it is seen that the front moves quite slowly (2.5 m s^{-1}). An existing cell decayed in the initial 20 minutes, but a second convective cell developed above the slight convergence caused by the lifting of the front as it moved ENE. Air flow from the rear of the front causes an elongation of the reflectivity cores southeastward that release precipitation into the warm region ahead of the front. This sustains continuing precipitation as the southwest monsoon advects warm, moist air in the lower layer into the area ahead of the front. Divergence at the surface occurs due to falling rain particles that spread out horizontally, and thus begin to create new convective cells.

5.3 RHI Scans at 330° Radial

The same six time periods used in the first RHI sequence are shown except with an azimuth angle of 330° from the CP-4 radar. The PPI plots shown earlier show a kink in the front in this direction allowing a second slice through the approaching Mei-Yu front. This PHI section encompasses the prefrontal convective area along with the postfrontal

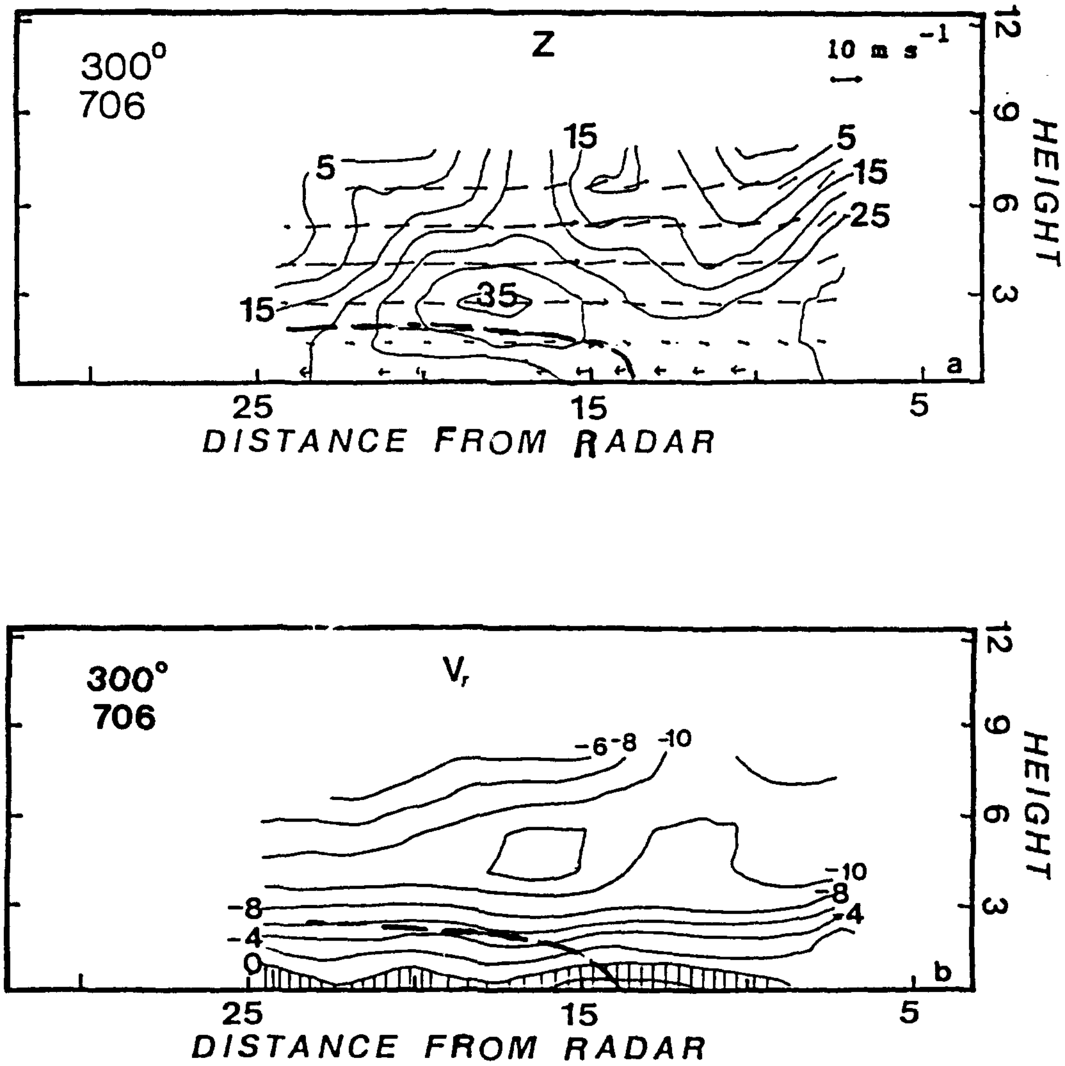

Fig. 5.14 Same as Fig. 5.10 a,b except for 0706 LST.

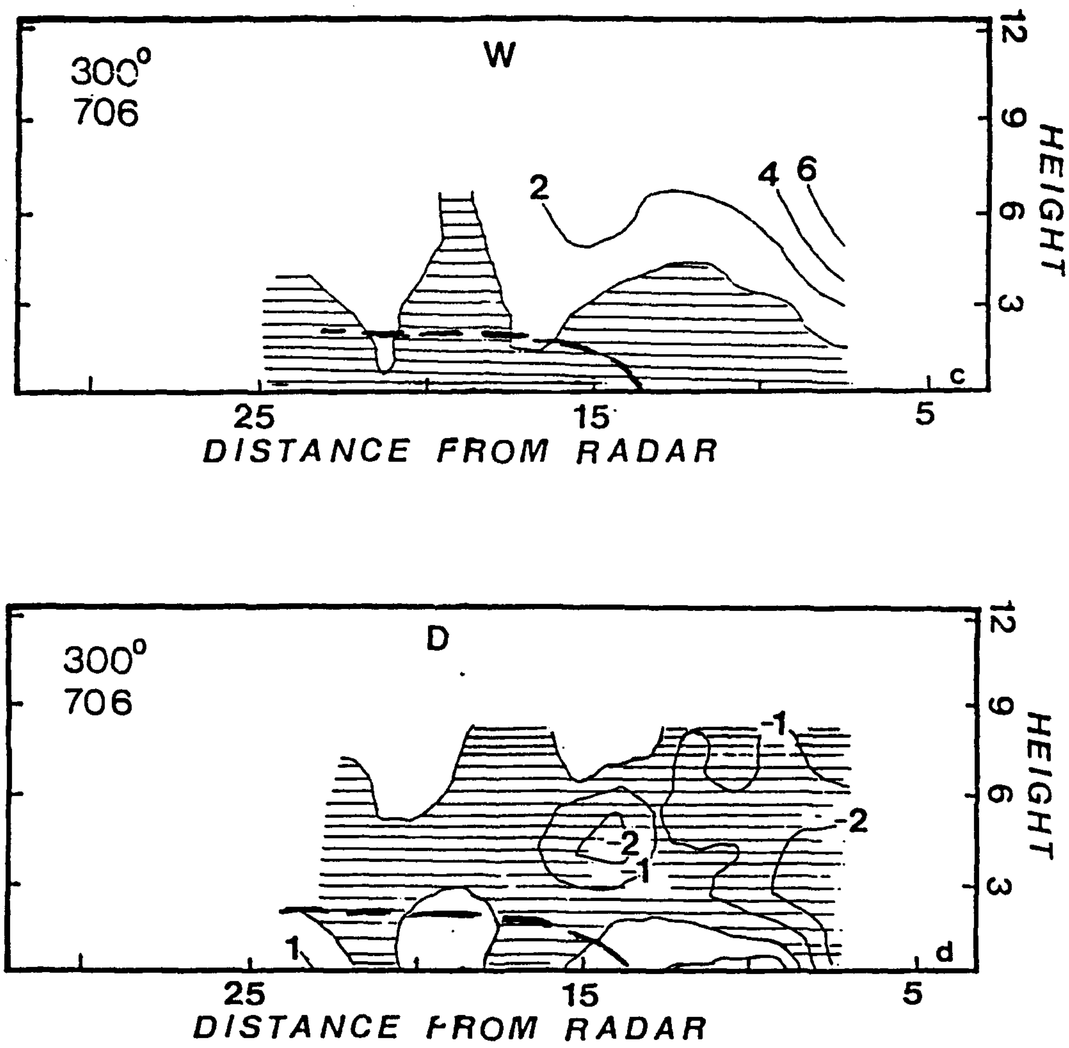

Fig. 5.14 cont. Same as Fig. 5.13 c,d except for 0706 LST.

stratiform region of light precipitation.

Figure 5.15 is the 330° RHI section at 0634 LST that shows the surface frontal position nearly 18 km away from the radar. The reflectivity field in comparison with Fig. 5.10 is not quite as strong. The wind field flow is seen to be strong and from the northwest behind the front. There is predominant weak downward vertical velocity in the postfrontal and prefrontal low-level to mid-level areas. Slight upward motion (< 1 m s^{-1}) in conjunction with very weak convergence is found at the frontal leading edge.

Six minutes later (Fig. 5.16), the front has moved about 1 km closer to the radar. A 40 dBZ cell has developed near r = 8 km, at about the 4 km level. This cell is in an area of downward vertical motion. A region of positive radial velocities (flow away from the radar) exists in front of the Mei-Yu front. Ahead of the front, at mid-levels, there is a strong downdraft (-3 m s^{-1}) associated with a collapsing convective area. Immediately below that area at the surface, relatively strong divergence (10^{-3} s^{-1}) is found. This strong divergence enhances the flow towards the approaching Mei-Yu front.

The 0647 LST time frame (Fig. 5.17) shows the gradual movement of the front to about r = 16 km. The strongest reflectivity cell from the prior time period has diminished in an area (r = 5 km) of moderate downward vertical velocities (-2 m s^{-1}) and convergence. The region of positive radial veloci-

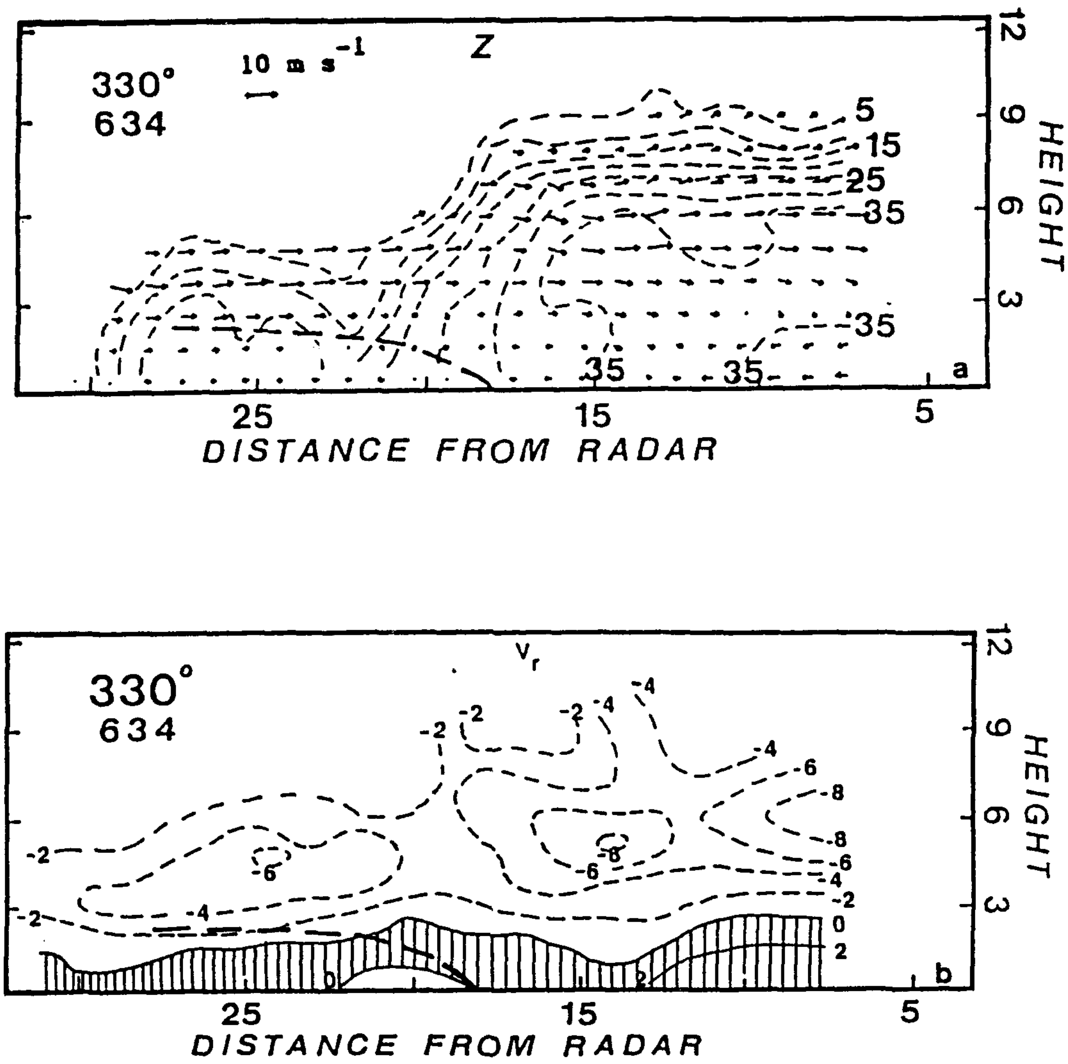

Fig. 5.15 RHI scan at 330° from CP-4 radar for (a) reflectivity with winds and (b) radial velocity for 0634 LST. Reflectivity contours are for every 5 dBZ and shaded area > 40 dBZ. Radial velocity contour for every 2 m s^{-1} with positive areas (away from radar) denoted by hatching.

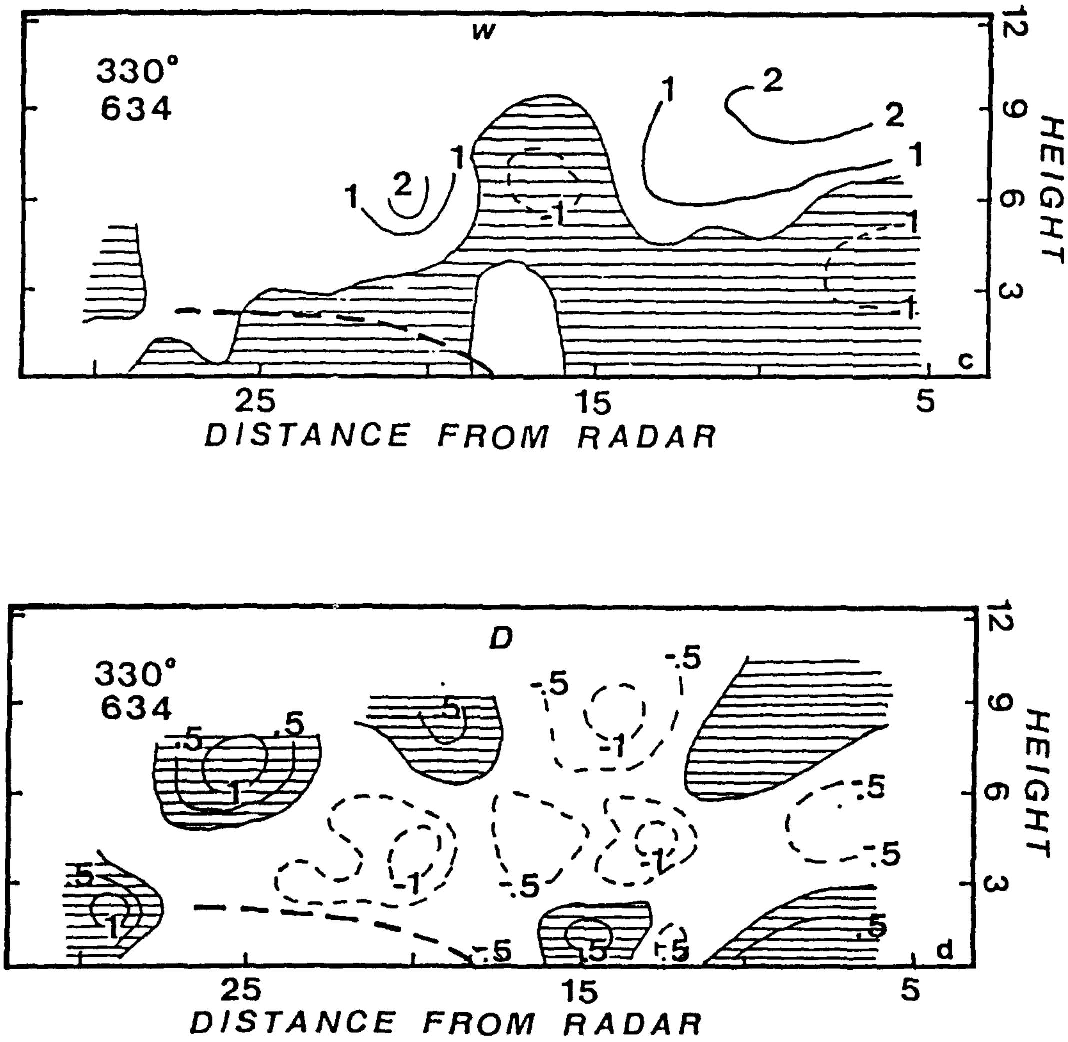

Fig. 5.15 cont. RHI scan at 330° from CP-4 for (c) vertical velocity and (d) divergence. W contour interval every 1 m s^{-1} with downward vertical motion denoted by hatched area. Divergence contour for every 0.5 x 10^{-3} s^{-1} with positive areas (divergence) shown by hatched area.

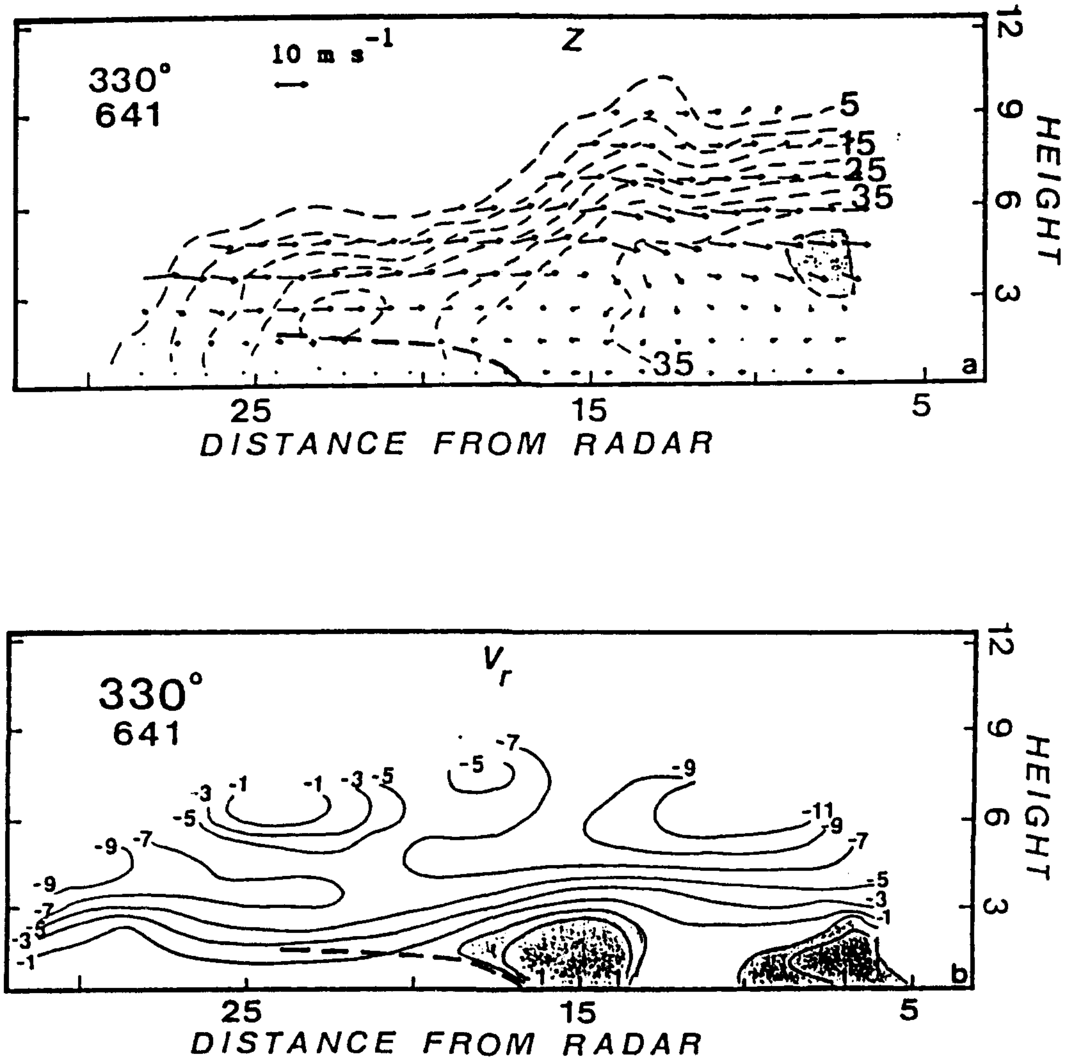

Fig. 5.16 Same as Fig. 5.15 a,b except for 0641 LST.

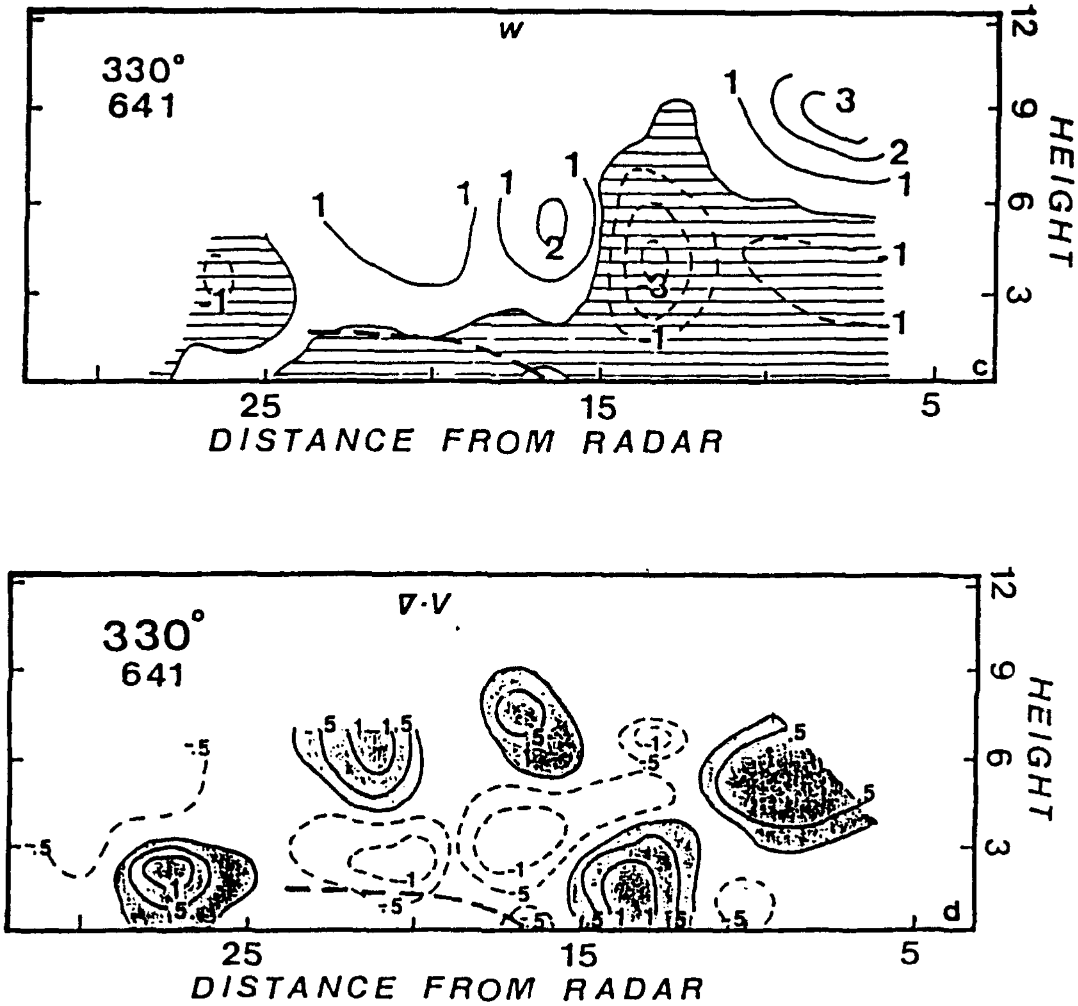

Fig. 5.16 cont. Same as Fig. 5.15 c,d except for 0641 LST.

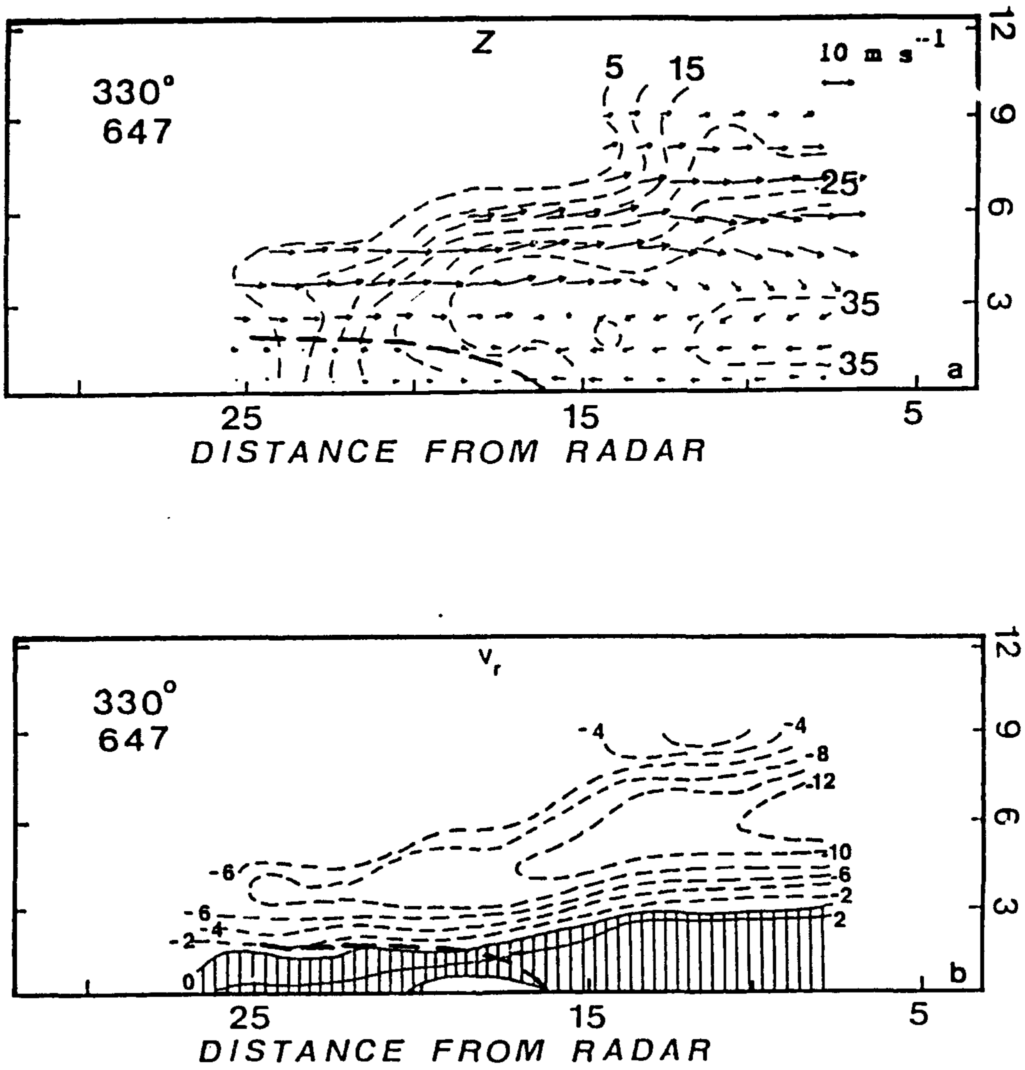

Fig. 5.17 Same as Fig. 5.15 a,b except for 0647 LST.

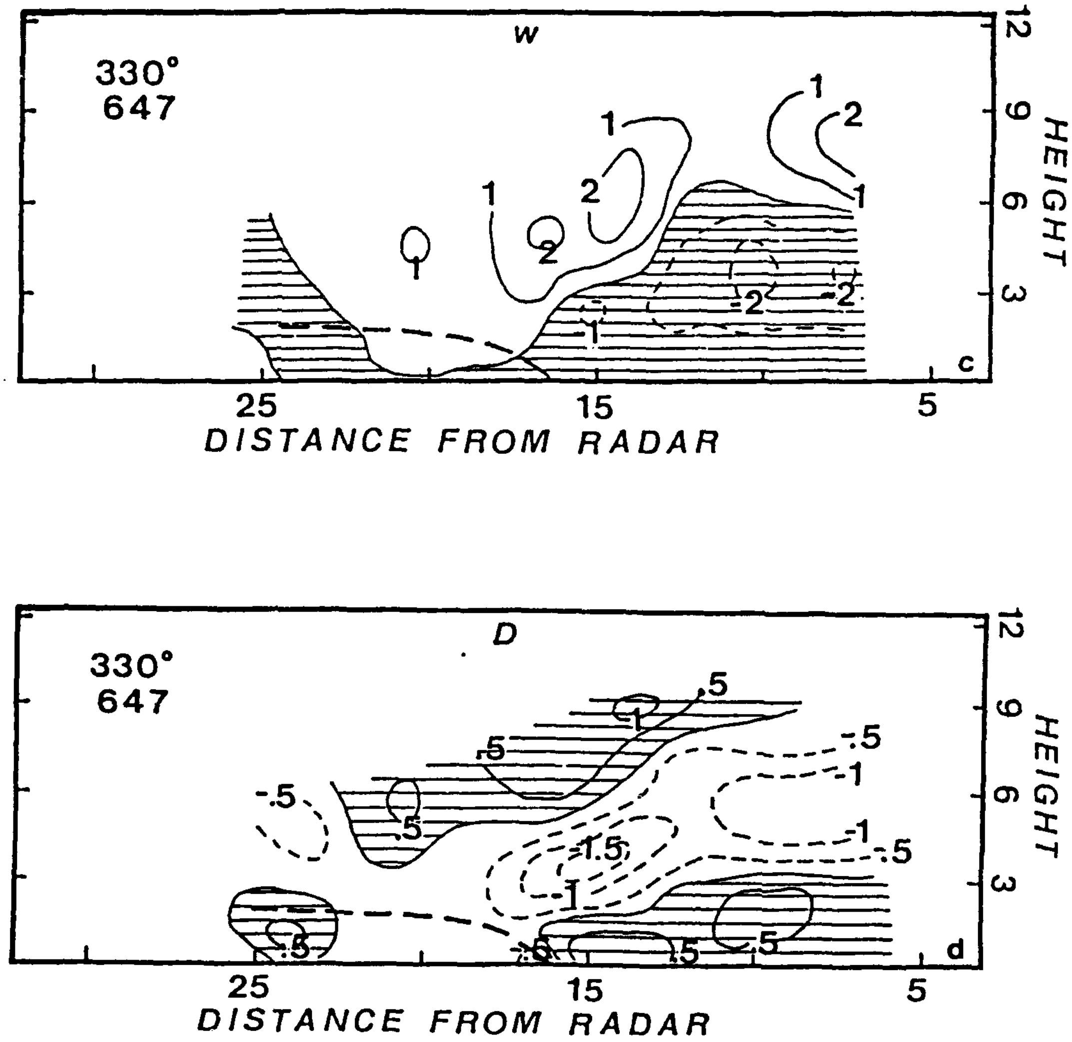

Fig. 5.17 cont. Same as Fig. 5.15 c,d except for 0647 LST.

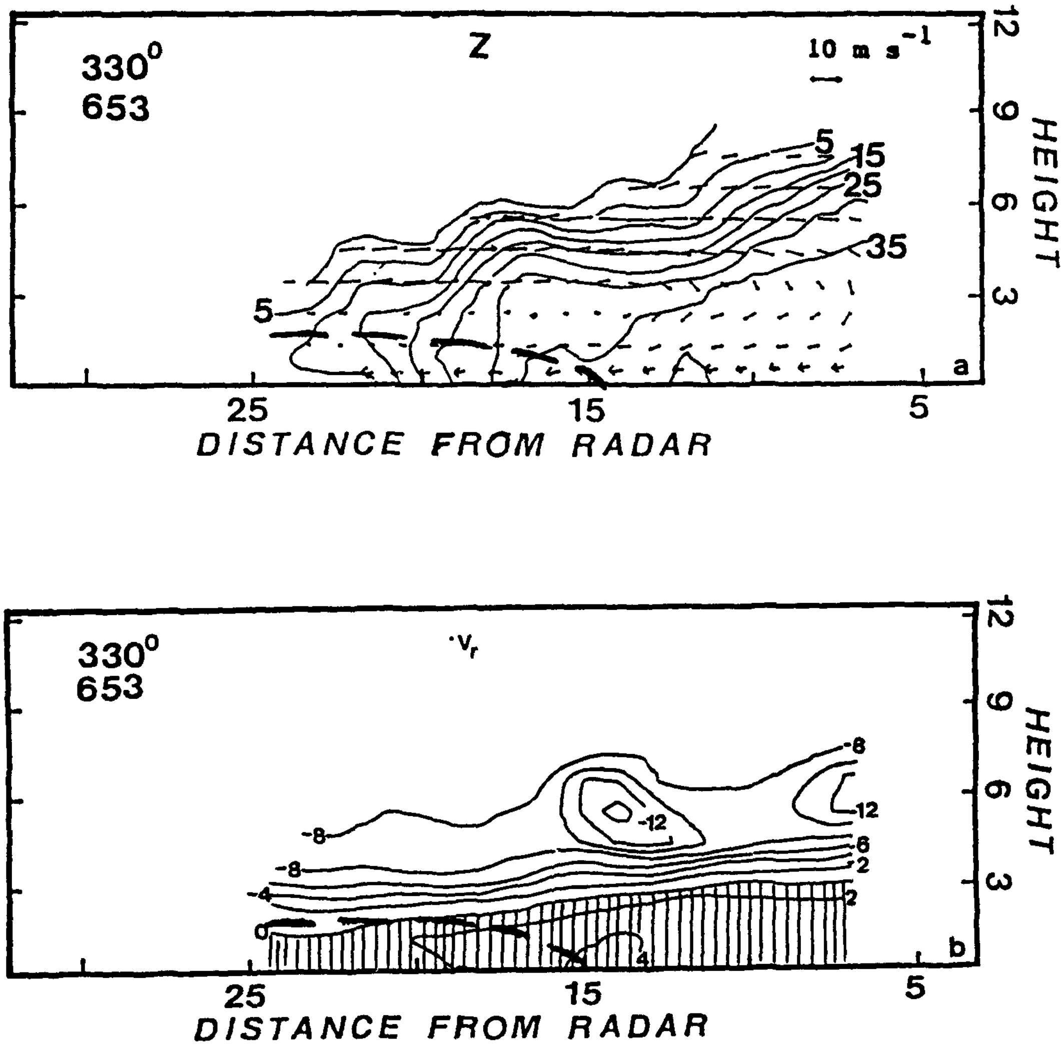

Fig. 5.18 Same as Fig. 5.15 a,b except for 0653 LST.

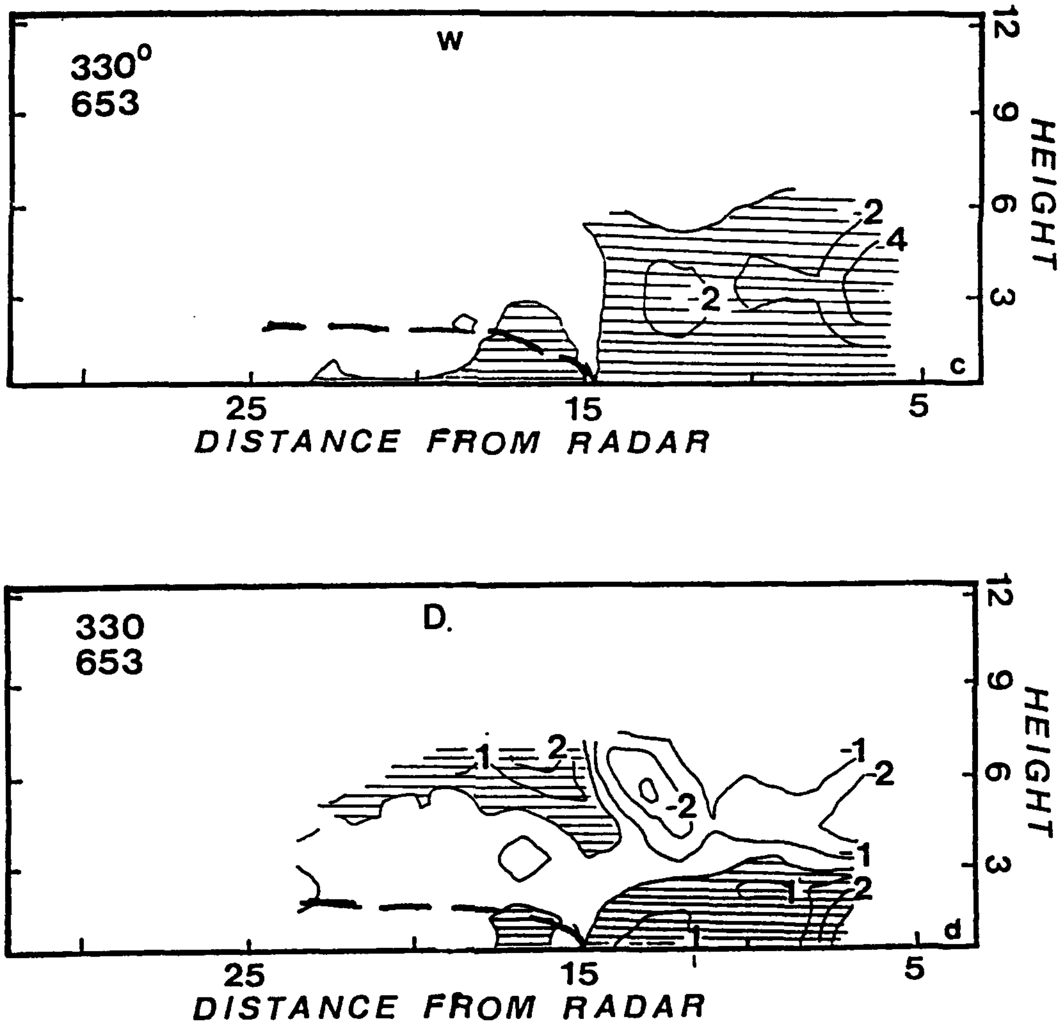

Fig. 5.18 cont. Same as Fig. 5.15 c,d except for 0653 LST.

ties (flow away from the radar) are due to the downward vertical motion near 10 km. The downward motion causes a large region of divergences ahead of the front. The frontal boundary is marked by the convergence. Mid-level positive upward velocities are found above the front, due to a combination of a weak upward push by the front and release of latent heat by the precipitation particles. A swath of weak convergence values is now organized at mid-levels above the front as flow from the rear collides with the flow of the decaying cell at $r = 15$ km.

The fourth consecutive time period (Fig. 5.18) is similar to the last time frame except that stronger downward vertical velocities prevail within 6 km of the radar as the high reflectivity core (> 35 dBZ) begins to collapse. The front (at $r = 15$ km) has moved slowly closer to the radar as marked by the small zone of convergence at $r = 15$ km. Wind flow seems to have shifted more to the NW as a core of radial velocities (-12 m s^{-1}) is found at $r = 14$ km.

At 0700 LST (not shown), the structural feature is nearly identical to 0653 LST in Fig. 5.18. Wind flow fields look very similar as the front is now found at $r = 14$ km. The only difference is that the area of highest reflectivities is forming at $r = 20$ km behind the front in an area of 2 m s^{-1} upward vertical velocity.

The final time frame (Fig. 5.19) at 0706 LST shows the

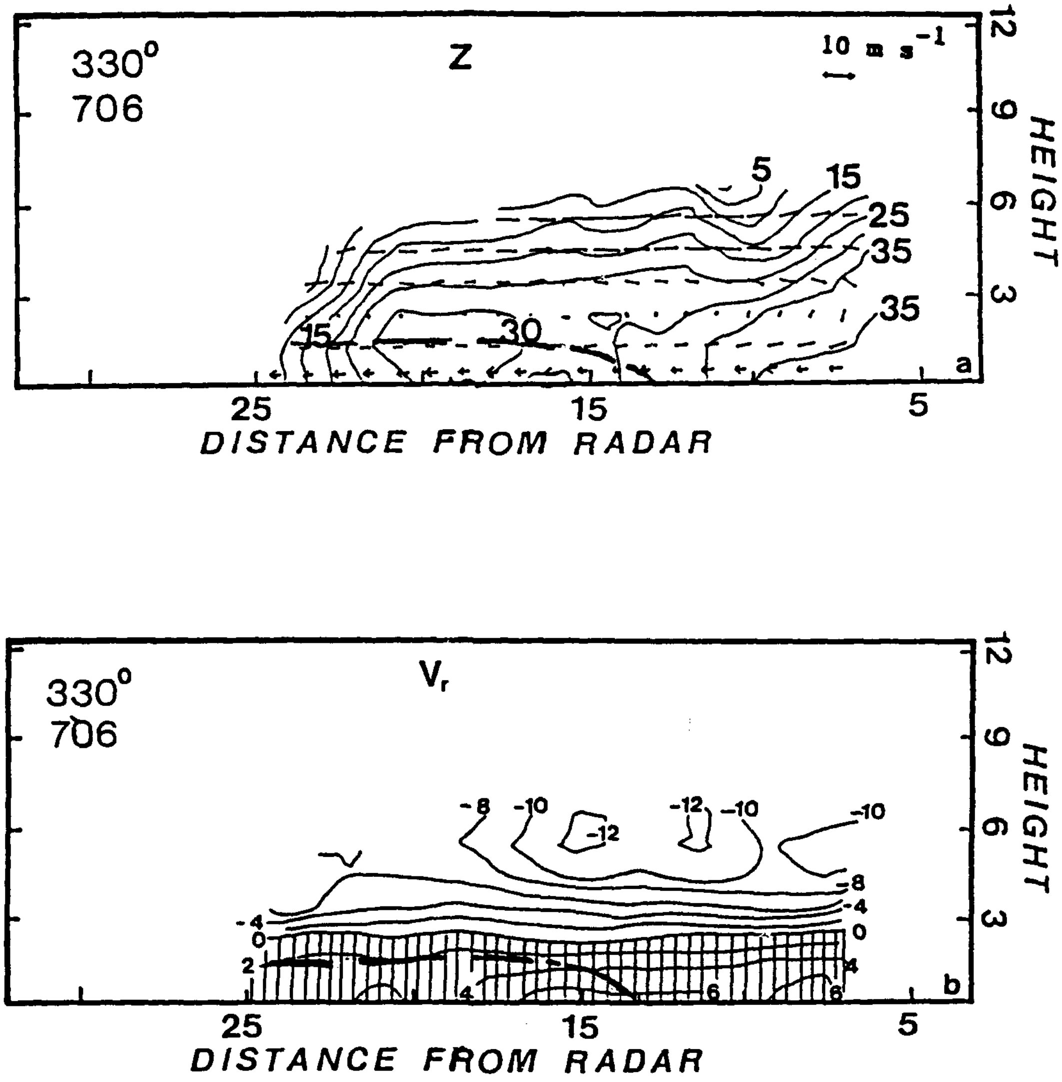

Fig. 5.19 Same as Fig. 5.15 a,b except for 0706 LST.

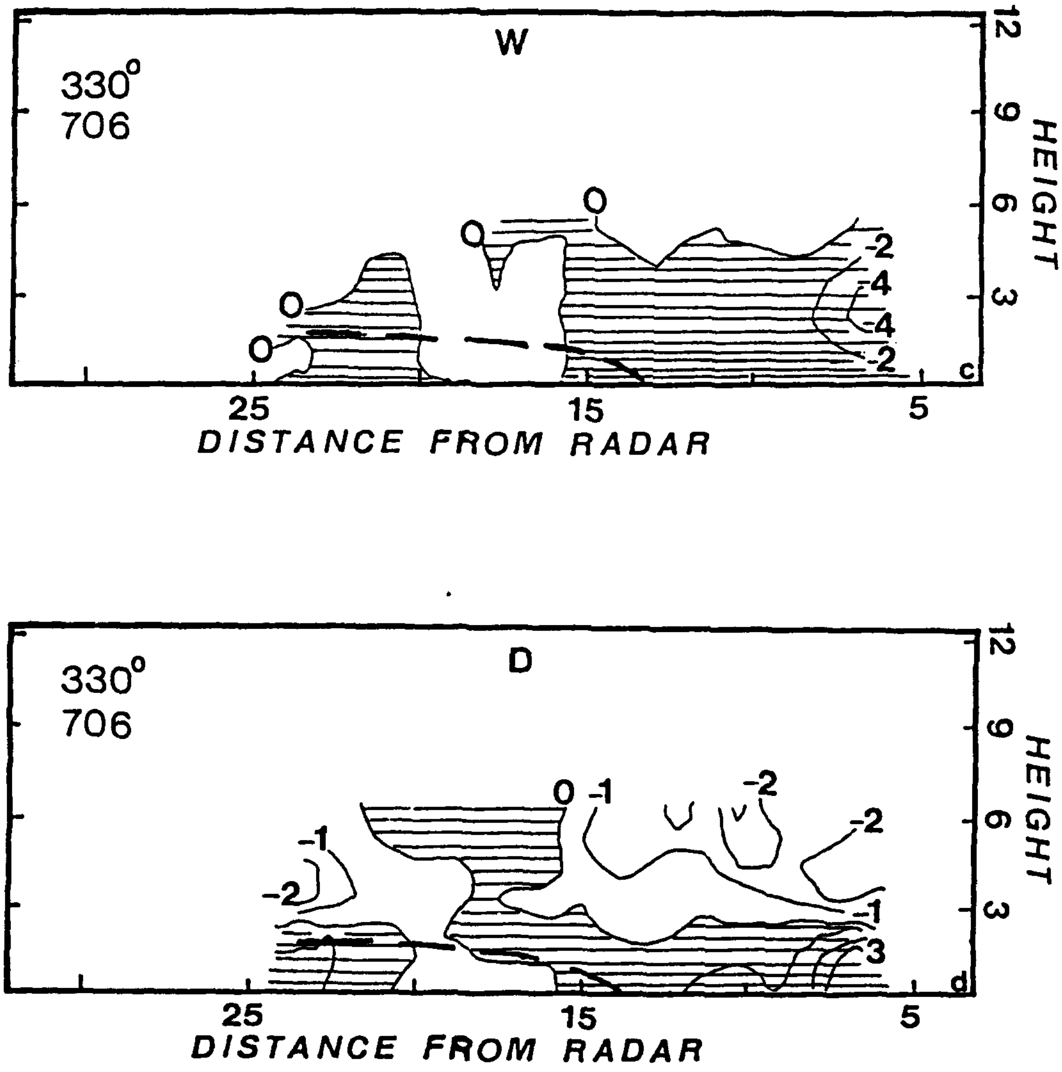

Fig. 5.19 cont. Same as Fig. 5.15 c,d except for 0706 LST.

decrease in the strength of the cell in the prefrontal region into a small area of reflectivities (> 35 dBZ) exists. The frontal boundary is found at 13.5 km. There is an area of convection with a core of strong reflectivities (> 30 dBZ) organized behind the front that can be tied to a weak convergent area. Downward vertical velocity is still prevailant nearest the radar at the low and mid-levels. Some of the strongest positive radial velocities (> 6 m s^{-1}) yet seen, exist below and ahead of the front near the surface, indicating a gradual bending of the low-level wind field that is northeasterly behind the front. Divergence is again dominant ahead of the front due to precipitation obscuring the capabilities of the radar to discern divergent/convergent values.

This 40 minute time period along the 330° azimuth showed the decay and birth of convective cells. These slices once again depicted the convective areas concentrated ahead of the front with stratiform precipitation in the postfrontal region. Falling rain, although not conducive to providing an aid to upward vertical motion, creates convergence at surface areas as the downrush of air and precipitation particles spread out, triggering more convective cells.

5.4 Momentum Flux

It is of interest to study the vertical fluxes of horizontal momentum to see the interaction between convective rainbands and the surrounding area. In this study, the vertical

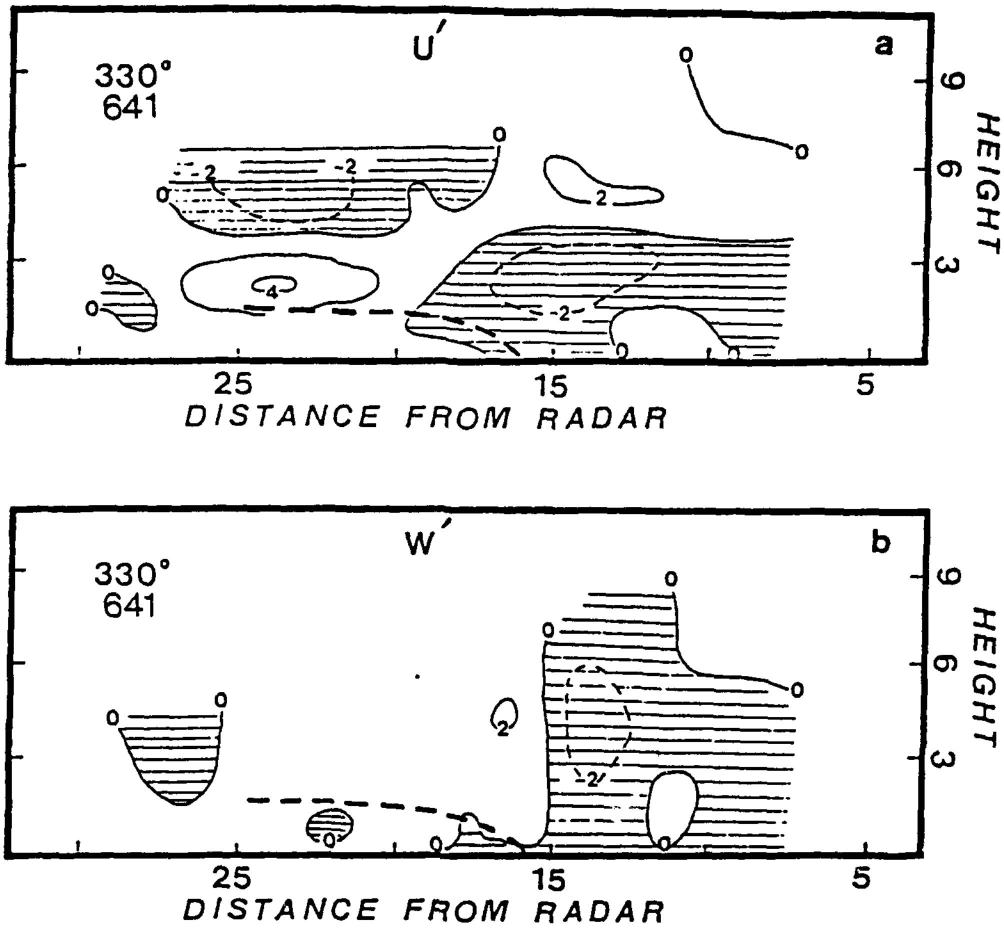

Fig. 5.20 (a) Deviation from mean wind (eddy) using u' = $-V_r$. Hatched area represents negative area (away from radar) with contour interval every 2 m s^{-1}. (b) W' or deviation from vertical motion. Downward motion denoted by hatched area and contour interval every 2 m s^{-1}. Both plots are for 0641 LST on 25 June 1987 from a 330° azimuth from the CP-4 radar.

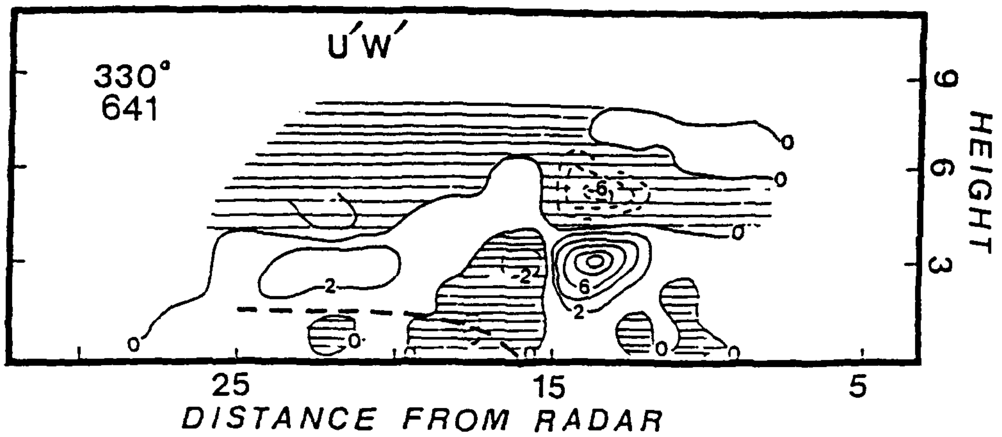

Fig. 5.21 Local momentum flux (u'w') for 0641 LST on 25 June 1987 at a 330° azimuth from the CP-4 radar. Downward flux denoted by hatched areas with contour interval for every 2 m s^{-1}.

momentum flux (u'w') is computed. The horizontal ($\bar{u}$) and vertical ($\bar{w}$) means were computed for each time period and radial independently.

Figure 5.20 presents the deviation from the mean for u and w for 0641 LST at a 330° radial. These eddies, as explained by Sutton (1953), behave similar to molecules by carrying momentum and heat from one layer to another through mixing. Note that u' has a large negative area (-2 m s^{-1}) at the front and ahead of the front up to around 4 km high indicating the velocities ahead of the front are lower than the mean. This can be attributed to the fact that there is a northwestward wind component in that area at low levels, see Fig. 5.17 for illustration. A small positive area centered at $r = 24$ km shows a southeastward component just above the front. Just above that positive area a larger negative u' area exists that can be explained due to a smaller value of negative radial velocities compared to a larger mean V_r value. This means a more northerly component of V_r at that level, indicative of the ushering in of northerly winds due to veering behind the front.

W' in Fig. 5.20b shows a predominance of negative values at the leading edge of the front and in the entire prefrontal region. This is due to the downward motion in this area as a result of precipitation drag associated with the convective cell ahead of the front.

Figure 5.21 shows the local momentum flux of (u'w') for

330^0 azimuth at 0641 LST. The small bullseye ahead of the front at 3 km indicates the strongest upward momentum flux values due to downward vertical motion and a negative u' component. Immediately above that bullseye, negative areas (u'w' < 0) dominate.

From a development of the mixing length theory according to Sutton (1953) and as expressed in Chang (1992), the eddy momentum flux, $\overline{u'w'}$, can be expressed as:

$$\overline{u'w'} = -K\frac{\partial \bar{u}}{\partial z}$$

where K is the eddy viscosity coefficient. From Chang (1992), for downgradient (countergradient) transportation of horizontal momentum, K is positive (negative).

The averaged momentum flux ($\overline{u'w'}$) for 0641 LST at 330^o is presented in Fig. 5.22. Note that $\overline{u'w'} > 0$ up to 3.5 km indicating upward transport of u-momentum by eddies. The vertical shear of the environmental wind in the surface to 3.5 km layer (see Fig. 14 in Lin et al., 1992) in a direction normal to the line is positive, indicative of the upgradient transport of horizontal momentum in violation of the mixing length theory. Above that level to 5 km, downward transport of horizontal u-momentum is indicated ($\overline{u'w'} < 0$). The layer from 3.5 to 5 km heights has positive vertical shear, resulting in a downgradient transfer of u-momentum. So the vertical transport of u-momentum at heights below 3.5 km is countergradient, similar to findings in Chang (1992) and for a tropical convective line

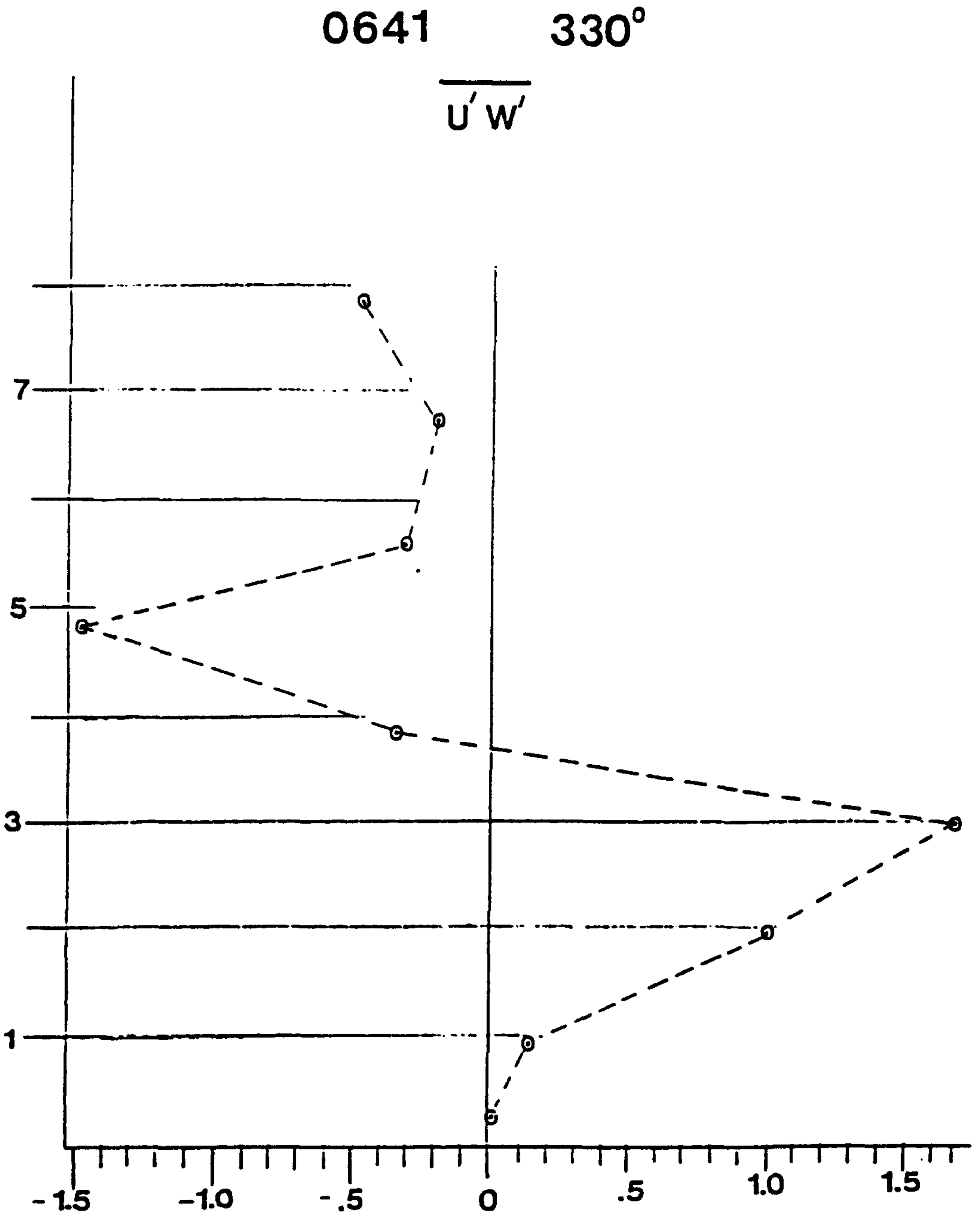

Fig. 5.22 Eddy momentum flux ($\overline{u'w'}$) for 0641 LST on 25 June 1987 at a 330° azimuth from CP-4 radar. P-4 radar.

in GATE that was examined by LeMone (1983).

Chapter 6: Conclusion

A subtropical prefrontal convective rainband on 25 June 1987 in association with the Mei-Yu front was investigated using TAMEX IOP-13 data. This rainband moved very slowly SSE through northwestern and western Taiwan. With the aid of single-Doppler radar data obtained from CP-4 on the northwestern coast of Taiwan, the kinematic structure of this rainband was analyzed. Fields of reflectivity, radial velocity, vertical velocity, and horizontal divergence along two radials nearly perpendicular to the front were investigated over a 40-minute time period.

Results show that: (1) the depth of the cool air behind the front is relatively shallow and less than 2.2 km in depth; (2) convection was moderate in the warm sector ahead of the front; (3) the front moved very slowly (2.5 m s^{-1}) due to its ENE-WSW orientation in relation to the topography of Taiwan resulting in heavy precipitation on the west coast of the island; (4) convective cells were seen to grow and dissipate within the period under observation; (5) postfrontal rear-to-front northwesterly mid-level winds caused an elongation of reflectivity cores which dropped precipitation into the southeast warm sector ahead of the front; (6) low level winds due to the southwest monsoon advected warm, moist air into the area ahead of the front (a mechanism that sustained long-lived convection); (7) collapsing convective cells cause surface divergence as the rain particles spread out horizontally and causes other pockets of surface convergence that create the formation of new convective cells; (8) moderate convection (w_{max} updraft < 8 m s^{-1}) with isolated, scattered cells > 40 dBZ occurred in a broad area ahead of the front with a narrow, postfrontal stratiform region behind; (9) a predominance of downward vertical velocities in the prefrontal region at low to mid-levels are seen due to precipitation drag in association with the elongated high reflectivity cores; and (10) from a comparision of single versus dual-Doppler radar analysis, the simplified continuity equation can be used to obtain realistic vertical velocities of a quasi two-dimensional convective rainband when only single Doppler radar data are available.

BIBLIOGRAPHY

Batten, L.J., 1973: Radar Observation of the Atmosphere. University of Chicago Press, Chicago. 324 pages.

Bell, G.D., and L.F. Bosart, 1988: Appalachian Cold-Air Damming. Mon. Wea. Rev., 116, 137-161.

Beeson, M.R., 1991: An Observational Study of a Prefrontal Convective Rainband using TAMEX Single- and Dual-Doppler Data. Master Thesis, Saint Louis University.

Browning, K.A., and T.W. Harrold, 1970: Air Motion and Precipitation Growth at a Cold Front. Quart. J. R. Met. Soc., 96, 369-389.

Carbone, R.E., 1982: A Severe Frontal Rainband. Part 1: Storm Wide Hydrodynamic Structure. J. Atmos. Sci., 39, 258-279.

Chiou, T.K., 1990: Forecasting of Mesoscale Convective System over Southern China During the Mei-Yu Period. Proceedings, Workshop on TAMEX Scientific Results, 24-26 September 1990, Boulder, CO., 95-102.

Chang, H.W., 1992: Dynamic and Thermodynamic Characteristics of a Prefrontal Convective Rainband in Northern Taiwan Determined from TAMEX Data. Ph.D Thesis, Saint Louis University.

Chen, G.T.-J.,1978: On the Mesoscale Systems for the Mei-Yu Regime in Taiwan. Proceedings, Conference on Severe Weather in the Taiwan Area, 27-28 May 1978, National Science Council, Taipei, Taiwan, 150-157.

Chen, G.T.-J, 1977: A Synoptic Case Study on Mean Structure of Mei-Yu in Taiwan. Atmos. Sci., 4, 38-47.

Chen, G.T.-J, and Y.-H. Kuo, 1991: The Scientific Results of TAMEX. Proceedings, International Conference on Mesoscale Meteorology and TAMEX. 3-6 December 1991, Taipei. 7-15.

Chen, G.T.-J, and C.Y. Tsay, 1978: A Synoptic Case Study of Mei-Yu near Taiwan. Pap. Meteor. Res., 1, 25-36.

Chen, G.T.-J, 1980: Mesoscale Analyses for a Mei-Yu case over Taiwan. Pap. Meteor. Res., 2, 63-74.

Chen, G.T.-J, and C.-P. Chang, 1980: The Structure and Vorticity Budget of an Early Summer Monsoon Trough (Mei-Yu) over Southeastern China and Japan. Mon. Wea. Rev., 108, 942-953.

Chen, G.T.-J., and S.-S. Chi, 1980: On the Frequency and Speed of Mei-Yu Fronts Over Southern China and the Adjacent Seas. Pap. Meteor. Res., 1, 25-36.

Chen, G.T.-J., 1983: Observational Aspects of the Mei-Yu Phenomenon in Subtropical China. J. Meteor. Soc. Japan, 61, 306-312.

Chen, G.T.-J., and C.C. Yu, 1988: Study of Low Level Jet and Extremely Heavy Rainfall over Northern Taiwan in the Mei-Yu Season. Mon. Wea. Rev., 116, 884-891.

Chi, S.-S., and R.A. Scoffield, 1991: Study of the Mesoscale Convective Systems (MCSs) Propagation Characteristics over Subtropical China During Taiwan Mei-Yu Season. Proceedings, Workshop on TAMEX Scientific Results, Taipei, 3-6 Dec 1991, 32-41.

Forbes, G.S., R.A. Anthes, and D.W. Thompson, 1987: Synoptic and Mesoscale Aspects of an Apppalachian Ice Storm Associated with Cold-Air Damming. Mon. Wea. Rev., 115, 564-591.

Frank, W.M., 1978: The Life Cycles of GATE Convective Systems. J. Atmos. Sci., 35, 1256-1264.

Houze, R.A., S.A. Rutledge, M.I. Biggerstaff, and B.F. Smull, 1989: Interpretation of Doppler Weather Displays of Midlatitude Mesoscale Convective Systems. Bull. Amer. Meteor. Soc., 70, 608-619.

Jou, B.J., and S.M. Deng, 1990: Mesoscale Characteristics of Mei-Yu Front: A TAMEX Case Study. Proceedings, Workshop on TAMEX Scientific Results, 24-26 September 1990, Boulder, 150-157.

Jou, B.J., and S.M. Deng, 1991: Structure of Low-Level Jet and Its Role in Triggering and Organizing Moist Convection over Taiwan: A TAMEX Study. Proceedings, Workshop on TAMEX Scientific Results, Taipei, 3-6 December 1991.

Kuo, Y.-H., and R.A. Anthes, 1982: Numerical Simulation of a Mei-Yu System over Southeastern Asia. Paper Meteor. Res., 5, 15-36.

Parsons, D.B., and S.B. Trier, 1989: TAMEX Doppler Radar Operations Summary NCAR/TN-315+STR. 59 pages.

Kuo, R.A., and G.T.-J. Chen, 1990: The Taiwan Area Mesoscale Experiment (TAMEX): An Overview. Bull. Amer. Meteor. Soc., 71, 488-503.

LeMone, M.A., 1983: Momentum Transport by a Line of Cumulonimbus. J. Atmos. Soc., 40, 1815-1834.

Lin, P.L., T.-C.C. Wang, C.-C. Yeh,1990: The Internal Structure of a Long Lived Rainband Revealed from Dual-Doppler Analysis in TAMEX IOP-13. Proceedings, Workshop on TAMEX Scientific Results, 24-26 September 1990, Boulder, CO., 26-33.

Lin, M.S., and S.M. Lin, 1990: The Comparison of Environmental Conditions Among Selected Mesoscale Convective Systems During TAMEX Period. Proceedings, Workshop on TAMEX Scientific Results, 24-26 September 1990, Boulder, Co., 103-108.

Lin, Y.J., T.C. Wang, and J.H. Lin, 1986: Pressure and Temperature Perturbations Within a Squall Line Thunderstorm Derived from SESAME Dual-Doppler Data. J. Atmos. Sci., 43, 2302-2327.

Lin, Y.J., R.W. Pasken, and H.W. Chang, 1990: An Investigation of a Prefrontal Convective Rainband in IOP-13 Using Dual-Doppler Data. Proceedings, Workshop on TAMEX Scientific Results, 24-26 September 1990, Boulder, CO., 34-41.

Lin, Y.J., R.W. Pasken, and H.W. Chang, 1992: The Structure of a Subtropical Prefrontal Convectuve Rainband. Part I: Mesoscale Kinematic Structure determined from Dual-Doppler Measurements. Accepted for publication in Mon. Wea. Rev..

Lin, Y.J., H.Shen, R.W. Pasken, 1991: Kinematic Energy Budgets of a Subtropical Squall Line Determined from TAMEX dual-Doppler Measurements. Mon. Wea. Rev., 2654-2663.

Lin, Y.J., H.W. Chang, R.W. Pasken, and M.R. Beeson, 1991: An Investigation of Prefrontal Convective Rainbands in IOP-13 Using Dual-Doppler. Proceedings, Workshop on TAMEX Scientific Results, 24-26 September 1990, Boulder, CO., 121-126.

Lin, Y.J., T.C.C. Wang, R.W. Pasken, H. Shen, and Z.S. Deng, 1990: Characteristics of a Subtropical Squall Line Determined from TAMEX Dual-Doppler Data. Part II: Dynamic and Thermodynamic Structures and Momentum Budgets. J. Atmos. Sci., 47, 2382-2399.

Mannouji, N., and K. Kurihara, 1990: A Numerical Experiment of TAMEX IOP#13 by the Spectral Limited Area Model of JMA. Proceedings, Workshop on TAMEX Scientific Results, 24-26 September 1990, Boulder, CO., 121-126.

Pasken, R.W., and Y.J. Lin, 1991: Mesoscale Structure of a Mei-Yu Front During IOP-13 Based on Single Doppler Measurements. Proceedings, Workshop on TAMEX Scientific Results , 3-6 December 1991, 76-84.

Sutton, O.G., 1953; Micrometeorology. McGraw-Hill Co., 333 pages.

Tao, S.-S., and Y.-H. Ding, 1981: Observational Evidence of the Influence of the Qinghai-Xizhang(Tibet) Plateau on the Occurrence of Heavy Rain and Severe Convective Storms in China. *Bull. Amer. Meteor. Soc.*, *62*, 23-30.

Trier, S.B., and D.B. Parsons, 1990: Numerical Simulation of a Prefrontal Squall Line observed During TAMEX IOP-8. Proceedings, *Workshop on TAMEX Scientific Results*, 24-26 September 1990, Boulder, CO., 62-67.

Tsay, C.-Y., and G.T.-J. Chen, 1980: Dynamic Processes for Vertical Motion in a Mei-Yu System. *Paper Meteor. Res.*, *3*, 67-77.

Wakimoto, R.M., 1982: The Life Cycle of Thunderstorm Gust Fronts as Viewed with Doppler Radar and Rawinsonde Data. *Mon. Wea. Rev.*, 1060-1082.

Wang, T.C.C, Y.J. Lin, R.W. Pasken, and H. Shen, 1990: Characteristics of a Subtropical Squall Line Determined from TAMEX Dual-Doppler Data. Part 1: Kinematic Structure. *J. Atmos. Sci.*, *47*, 2357-2390.

Wang, S.-T., 1986: Observational Analysis of the Interaction Between Fronts and Orography in Taiwan During the Late Winter Monsoon Season. Preprints, *International Conference on Monsoon and Mesoscale Meteorology*, November, 1986, Taipei, 123-135.

Wang, T.C.C, and P.J. Lin, 1991: The Radar Characteristics of Mei-Yu Season Precipitation Systems in Taiwan Area. *International Conference on Mesoscale Meteorology and TAMEX*. 3-6 December 1991, Taipei. 97-106.

BIOGRAPHY OF THE AUTHOR

Michael Joseph Miglioranzi was born on January 14, 1960, and spent his first nine years living in Buffalo, New York. The next nine years he resided in Cincinnati, Ohio. After graduation from Anderson High School in 1978, he attended Miami University of Ohio and graduated with a B.S. degree in Aeronautics. In 1984 he attended the Air Force Officer's Training School in San Antonio, Texas, and received a Commission as an Air Force Officer.

His first assignment was attending one year of school at St. Louis University in the Basic Meteorology Program. Upon graduation, he was assigned as a Wing Weather Officer at MacDill Air Force Base, Florida for two years. The following three years he was a Wing Weather Officer for the F-117A Stealth Fighter Program based at the Tonopah Test Range, Nevada. In 1990, he was offered an assignment through the Air Force Institute of Technology to pursue a Master of Science degree in Meteorology at St. Louis University, which he gratefully accepted.